University of **Valladolid**

PhD Program in Biomedical Research

DOCTORAL THESIS

Hepatic insulin-degrading enzyme regulation and its role on glucagon signaling

Submitted by Carlos Manuel González Casimiro to the
Doctoral Theses Commission as partial fulfillment of
the requirements for the Doctor of Philosophy Degree
by the University of Valladolid

Thesis advisors:

Irene Cózar Castellano, PhD

Germán Perdomo Hernández, PhD

Valladolid, Spain

2022

"Do not conform to the pattern of this world, but be transformed by the renewing of your mind…"

Romans 12:2 RVR60

Acknowledgements

Institutional support and funding.

Summary

Insulin-degrading enzyme (IDE) is a highly conserved and ubiquitously expressed Zn^{2+}-metalloendopeptidase that degrades insulin and glucagon among other substrates. By decades, its main function has been attributed to hepatic insulin clearance, a process that regulates availability of circulating insulin levels, but recent studies performed by our group indicate a more important role of this protein regulating hepatic insulin sensitivity and glucose homeostasis. However, its regulation in response to nutritional state and the fasting-to-postprandial transition is poorly understood and much less attention has been dedicated to its role on regulating glucagon signal transduction and mitochondrial function in hepatocytes. In this thesis, we studied the regulation of IDE mRNA and protein levels as well as its proteolytic activity in the liver under fasting (18 h) and refeeding (30 min and 3 h) conditions, in mice fed a standard (SD) or high-fat (HFD) diets. Likewise, we aim to elucidate the role of IDE on glucagon signaling and its impact on energy metabolism in hepatocytes using a loss-of-function approach. Livers from L-IDE-KO and WT mice were used to obtain tissue extracts and primary hepatocytes for culture. The mouse hepatocyte cell line (AML12) was transduced with an shRNA targeting *Ide* mRNA by means of a lentiviral vector and obtaining a stable line (AML12-shRNA-IDE). L-IDE-KO primary hepatocytes and AML12-shRNA-IDE with their respective controls were stimulated with glucagon and the signaling pathway was analyzed by western blot and ELISA. Mitochondrial function and energy metabolism of AML12-shRNA-IDE and control cells were assessed by Seahorse XFe24 Analyzer with a Mito Stress Assay. In the liver of mice fed a HFD, fasting reduced IDE protein levels (~30%); whereas refeeding increased its activity (~45%) in both mice fed an SD and HFD. Circulating lactate concentrations directly correlated with hepatic IDE

activity and protein levels. Of note, L-lactate in liver lysates augmented IDE activity in a concentration-dependent manner. Additionally, IDE protein levels in liver, but not its activity, inversely correlated (R^2 = 0.3734, p < 0.01) with a surrogate marker of insulin resistance (HOMA index). Liver extracts and primary hepatocytes from L-IDE-KO mice, compared to WT, showed decreased expression of glucagon receptor (~60%), CREB protein (~40%), and diminished phosphorylation of CREB (~50%) upon glucagon stimulation. *Ide* expression and IDE protein levels were reduced by ~50% in AML12-shRNA-IDE cells. At basal state, glucagon receptor, FoxO1 and CREB protein were significantly lower in AML12-shRNA-IDE cells than in control cells, (~40%, ~75% and ~75%, respectively). Glucagon stimulation resulted in less (~30%) cAMP levels and changes in the kinetic of glucagon-mediated phosphorylation of CREB and other PKA substrates in AML12-shRNA-IDE. Seahorse analyses showed that both oxygen consumption and extracellular acidification rates increased 2-fold in AML12-shRNA-IDE with a 2-fold increment of mitochondrial and glycolytic adenosine triphosphate (ATP) production. Finally, we generated, using homology modeling by satisfaction of spatial restrains technique, complete 3D structures of human and murine IDE isoforms with 15a and 15b exons. Our results highlight that the nutritional regulation of IDE in liver is more complex than previously expected in mice. Reduced IDE expression in mouse hepatocytes has a deleterious effect on glucagon signaling, affecting this intracellular pathway in parallel with a shift to a more energetic phenotype. These findings suggest that IDE is necessary for proper glucagon signal transduction and regulation of the energy production in hepatocytes.

VIII

Abbreviations

Abbreviation	Meaning
%	Percentage
1D	Unidimensional
3D	Tridimensional
AD	Alzheimer's Disease
ADP	Adenosine Diphosphate
Alb-Cre	Albumin-Cre
AMPK	AMP-activated protein kinase
ANOVA	Analysis of Variance
ATP	Adenosine Triphosphate
AUC	Area Under Curve
cAMP	Cyclic Adenosine Monophosphate
CBP	CREB-binding protein
cDNA	Complementary Deoxyribonucleic Acid
CEACAM1	Carcinoembryonic Antigen-Related Cell Adhesion Molecule1
ChREBP	Carbohydrate-Responsive Element-Binding Protein
c-Myc	Proto-oncogene of the *Myc* family
CREB	cAMP Response Element-Binding Protein
CRTC2	CREB regulated transcription coactivator 2
CRISPR	Clustered regularly interspaced short palindromic repeats
DAG	Diacylglycerols
DNA	Deoxyribonucleic Acid
Drp1	Dynamin-1-like protein
EASD	European Association for the Study of Diabetes
ECAR	Extracellular acidification rate
EDTA	Ethylenediaminetetraacetic Acid
EGTA	Ethylene Glycol-bis(β-aminoethyl ether)-Tetraacetic Acid
ELISA	Enzyme-Linked Immunosorbent Assay
ER	Endoplasmic reticulum

ERMES	Endoplasmic reticulum-mitochondria encounter structures
ERRγ	Estrogen-related receptor gamma
Fis1	Mitochondrial fission 1 protein
FoxOs	Forkhead Box O proteins
FoxO1	Forkhead Box O1
Fxn	Frataxin
g	Gravities
G6PC	Glucose-6-phosphatase
GAPDH	Glyceraldehyde-3-Phosphate Dehydrogenase
GCGR	Glucagon Receptor
GLUT1	Glucose Transporter 1
GLUT2	Glucose Transporter 2
GS	Glycogen Synthase
GSK3	Glycogen Synthase Kinase 3
h	Hour(s)
HFD	High-Fat Diet
Hmox1	Heme oxygenase 1 gene
HNF-4	Hepatocyte Nuclear Factor 4
HOMA	Homeostatic Model Assessment
HT	Heterozygous
IDE	Insulin-degrading Enzyme
IDF	International Diabetes Federation
IGF-1	Insulin-like Growth Factor I
ipGTT	Intraperitoneal Glucose Tolerance Test
IR	Insulin Receptor
IRβ	Insulin Receptor β-Subunit
KAT2B	Lysine (K) acetyltransferase 2B
KO	Knockout
LDH	Lactate Dehydrogenase

L-IDE-KO	Liver IDE knockout mouse
LSB	Loading (Laemmli) Sample Buffer
MAPK	Mitogen Activated Protein Kinase
MCP-1	Monocyte Chemoattractant Protein-1
Mfn1	Mitofusin-1
Mfn2	Mitofusin-2
Mief2	Mitochondrial elongation factor 2
min	Minute(s)
mRNA	Messenger Ribonucleic Acid
MT-CO1	Mitochondrially encoded cytochrome c oxidase I
mTORC1	Mammalian Target of Rapamycin Complex-1
mTORC2	Mammalian Target of Rapamycin Complex-2
NEFA	Non-Esterified Fatty Acids
NAD	Nicotinamide adenine dinucleotide
ºC	Celsius Degree
OCR	Oxygen consumption rate
p300	Histone acetyltransferase p300
PCK1	Phosphoenolpyruvate Carboxykinase 1
PCR	Polymerase Chain Reaction
PDK1	3-Phophoinositide-Dependent Kinase-1
PGC-1α	Peroxisome proliferator-activated receptor γ coactivator 1-α
PGC1A	PPARGC1A, PGC-1α gene
PIP2	Phosphatidylinositol-4,5-Biphosphate
PKA	Protein Kinase A
PKB	Protein Kinase B 1
PKB2	Protein Kinase B 2
PKC	Protein Kinase C
PVDF	Polyvinylidene Difluoride
RNA	Ribonucleic Acid

RT-qPCR	Real-Time (Reverse Transcription) Quantitative Polymerase Chain Reaction
SD	Standard Diet
SDS	Sodium Dodecyl Sulfate
SEM	Standard Error of the Mean
shRNA	Short Hairpin Ribonucleic Acid
siRNA	Silencing Ribonucleic Acid
SIRT1	Sirtuin-1
SIRT4	Sirtuin-4
SREBP	Sterol Regulatory Element Binding Protein
T1DM	Type 1 Diabetes Mellitus
T2DM	Type 2 Diabetes Mellitus
Tfam	Mitochondrial transcription factor A
UQCRC1	Cytochrome b-c1 complex subunit 1, mitochondrial
Urod	Uroporphyrinogen III decarboxylase
UV	Ultra-Violet
WHO	World Health Organization
WT	Wild Type
XBP-1	X-box binding protein 1

FoldX Parameters

Abbreviation	Meaning
Electro	Contribution of electrostatic interactions.
Helix_dipole	Contribution of helix dipoles.
Mainc_Hbond	Contribution of hydrogen bonds between atoms of the peptide backbone.
Sidec_Hbond	Contribution of hydrogen bridges between side chain atoms and between side chain atoms and peptide backbone atoms.
Energy_SolvH	Contribution of hydrophobic groups.
Partial_covalent	Contribution of partial covalent bonds due to interactions with bonded metal atoms.
Energy_VdW	Contribution of van der Waals interactions.
Energy_Ion	Penalization for ionization energy.
Energy_SolvP	Penalization by coated polar groups.
Entropy_sidec	Penalization for entropic cost of side chains.
Entropy_mainc	Penalization for entropic cost of the peptide backbone.
Energy_vdwclash	Penalization for intrarresidual van der Waals repulsions.
Cis_bond	Penalization for peptide bonds in cis conformation.
Energy_torsion	Penalization for torsions due to intrarresidual van der Waals repulsions.
Manc_vdwclash	Penalization for van der Waals repulsions between atoms of the peptide skeleton.

Table of contents

XX

I. Introduction

I.1. Diabetes Mellitus: a worldwide health problem.

I.1.1. Diabetes and glucose homeostasis.

The term diabetes mellitus (DM) comprises a number of diverse and chronic nosological entities that have in common an alteration in the metabolism of carbohydrates, lipids and proteins [1].

Under physiological conditions and after meals ingestion and digestion, and the subsequent absorption of nutrients including glucose and other monosaccharides, blood glucose levels reach a threshold at which it stimulates the secretion of the hormone insulin by the β-cells of the endocrine pancreas. The sensitivity of pancreatic β-cells to hyperglycemia is determined by the absolute predominance in the plasma membrane of these cells of the glucose transporter 2 (GLUT2) which has a low affinity for the solute and therefore incorporates it at high concentration levels.

The secreted insulin, via the bloodstream, is directed to its target organs, e.g., liver, muscle, adipose tissue and brain, stimulating several metabolic processes in them, including the storage of glucose in the form of glycogen, i.e., glycogenesis, and the glycolysis or glucose breakdown. This ultimately leads to an increase in blood glucose uptake and its utilization by the cells involved with a resulting decrease in blood glucose (**Fig. 1**).

Under fasting conditions, blood glucose levels are lower than under prandial conditions leading to stimulation of pancreatic α-cells, where the high affinity glucose transporter 1 (GLUT1) is highly expressed. Pancreatic α-cells are responsible for the synthesis and secretion into the blood of glucagon, an insulin counter-regulatory hormone of peptidic nature, which results in the stimulation of its target tissues, leading the liver metabolism to the production of glucose from stored glycogen and later to the *de novo* glucose production from other substrates such as pyruvate, thus producing an increase in glycemia and restoring glucose homeostasis (**Fig. 1**).
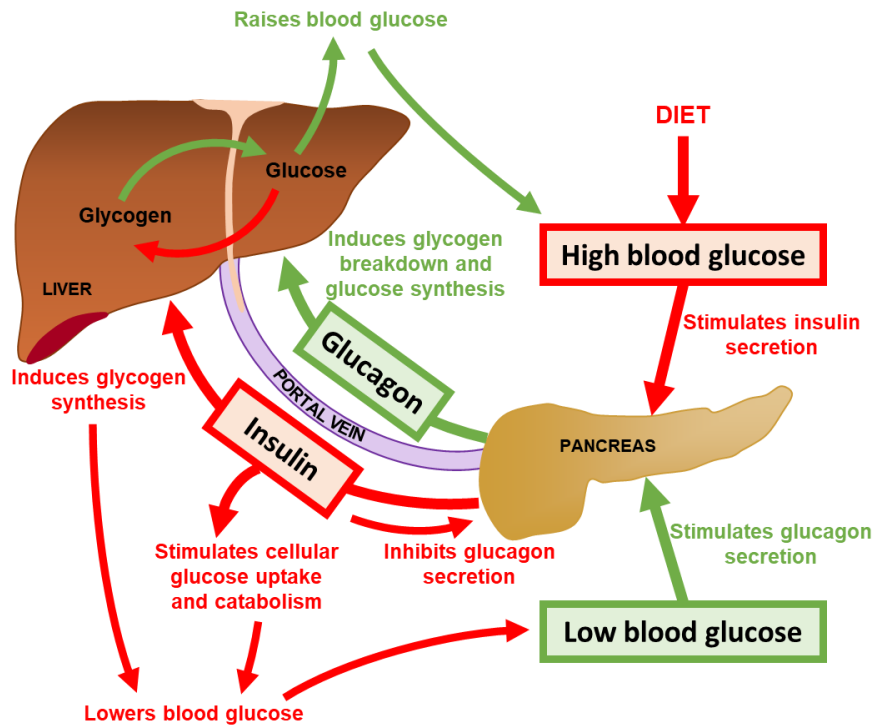
Figure 1. Glucose homeostasis in normal conditions regulated by insulin and glucagon. High blood glucose levels stimulate the secretion of insulin by β-cells of the endocrine pancreas. Insulin is delivered through circulation to its target organs, e.g., liver, muscle, adipose tissue and brain, stimulating several metabolic processes, including glucose uptake, glycolysis, and glycogen synthesis. This leads to a decrease in blood glucose levels. When blood glucose is low, pancreatic α-cells are responsible for the synthesis and secretion into the circulation of glucagon, an insulin counter-regulatory hormone, leading to stimulation of its target tissues with to the production of glucose from stored glycogen and later to the synthesis of glucose from gluconeogenesis, thus producing an increase in glycemia and restoring homeostasis.

However, in a DM scenario, these homeostatic regulatory processes are compromised, generating a disbalance in the body metabolism (**Fig. 2**). An essential condition in the etiopathogenesis and semiology of this disease is the existence of high blood glucose levels, i.e., hyperglycemia, due to the inability of insulin to secure the homeostasis of glucose metabolism with other eventual hormonal alterations such as hyperglucagonemia contributing to the clinical picture.

4
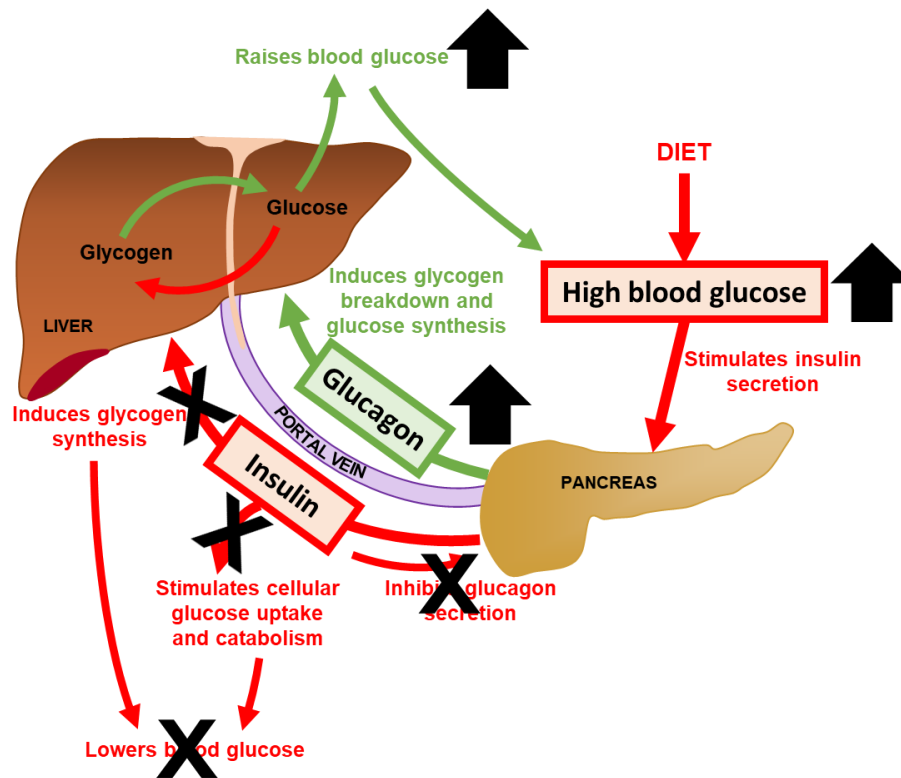
Figure 2. Glucose homeostasis disturbance in type 2 diabetes mellitus controlled by insulin and glucagon. There is a dysfunction in the sensitivity of the insulin's target tissues, which results in a failure to manage blood glucose levels and dysregulation of glucagon secretion, leading to hyperglucagonemia. High glucagon levels contribute to worsen the condition.

Among the most common conditions that can be categorized as DM, there are two that are the most frequent [1], Type 1 Diabetes Mellitus (T1DM) and Type 2 Diabetes Mellitus (T2DM). The second is by far the most prevalent [1]. The other forms of DM are minority [1], or specific of a temporary metabolic state as is the case of gestational diabetes [2,3].

In the case of T1DM there is a primary obliteration of the pancreatic β-cells, generally due to an autoimmune attack to these cells, and therefore the production of insulin decreases considerably until it disappears. In these cases, there is no control over high blood glucose since insulin is the only glucose-lowering hormone. Much research has been done to improve β-cell survival, increase their regeneration (or transdifferentiation) or their transplantation/implantation. However, in this kind of patients, hormone replacement is the only therapeutic alternative that continues to be effective since more than 100 years ago when researchers in Toronto discovered and

synthesized insulin. Although considerable progress has been made in the means of glycemia monitoring and insulin administration, there is still not a curative treatment.

On the other hand, T2DM occurs without a primary deficiency in insulin production. In this case, is a dysfunction in the sensitivity of the hormone's target tissues to be stimulated by it, which also results in a failure to manage blood glucose and metabolism in general. It has been shown that in this condition, sooner or later, dysregulation of glucagon secretion occurs, leading to hyperglucagonemia. High glucagon levels contribute to worsen the condition due to the hyperglycemic effects of this hormone.

I.1.2. Diabetes prevalence and associated health care costs.

In terms of global occurrence, DM is a very imperative concern for public health and its prevalence is increasing at an alarming rate with shocking new statistics every year (**Fig 3**). The costs derived from the treatment and prevention of diabetes are becoming one of the main budgetary matters to be assumed by the public health systems worldwide [1].

The increase in the prevalence of T2DM in the world population represents a major challenge from a scientific and health care perspective [1] (**Fig 4**).

1 in 10
Adults (20-79 years)
has diabetes
537 million people

1 in 18
Adults (20-79 years) has
impaired fasting glucose
319 million people

3 in 4
People with diabetes live in
low and middle-income countries

1 in 2
Adults is undiagnosed
240 million people

1 in 6
Live births (21 million) affected
by hyperglycaemia in pregnancy,
80% have mothers with GDM

11.5%
Of global health expenditure spent
on diabetes (USD 966 billion)

1 in 9
Adults (20-79 years) has
impaired glucose tolerance
541 million people

1.2 million
Children and adolescents below
20 years have type 1 diabetes

6.7 million
Deaths attributed to diabetes

1.67 million
More adults with impaired
glucose tolerance

US$206 billion
More USD spent on diabetes

700,000
More pregnancies affected
by hyperglycaemia

7.8 million
More adults with diabetes
undiagnosed

149,500
More children and adolescents
with type 1 diabetes

2.5 million
More deaths caused by diabetes

73.6 million
More adults with diabetes

Figure 3. Worldwide diabetes statistics in 2021 by IDF estimates. Taken from reference [1].
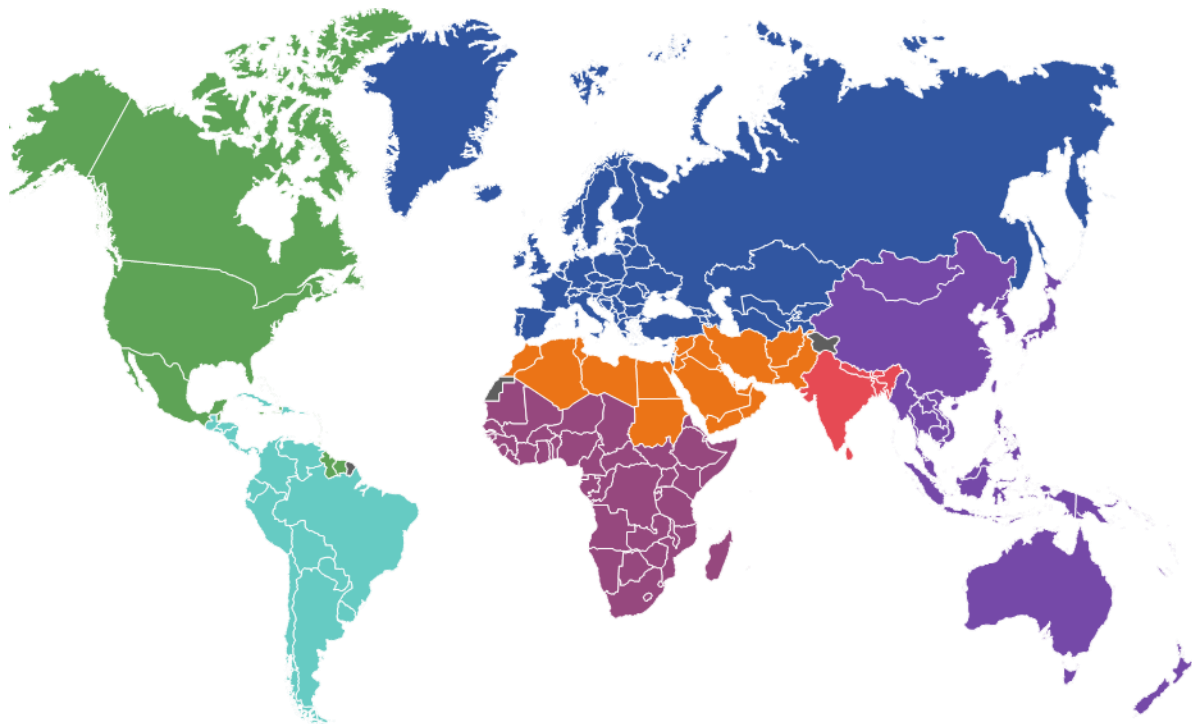
Figure 4. Diabetes prevalence in 2021 by International Diabetes Federation Regions and projections for 2030 and 2045. Taken from reference [1].

Therapeutics in T2DM are mainly aimed at increasing insulin production, decreasing glucose absorption, or improving tissue sensitivity to the hormone [4-6]. Nevertheless, a definitively curative treatment is yet to be discovered and due the persistent lack of knowledge in the pathophysiology of the disease, a great deal of research is still necessary.

I.2. Liver glucagon signaling and hyperglucagonemia in T2DM.

Glucagon signaling in liver is complex and time dependent, existing acute, chronic and dynamic effects of this hormone [7,8]. Glucagon receptor is a 7-helical transmembrane protein of ~60 kDa and a member of the class B of G proteins coupled receptors which are coupled to Gs protein, and to a lesser extent to Gq protein [7,8] (**Fig. 5A**).

When glucagon binds to its receptors on the plasma membrane of hepatocytes, this results in the release of the G proteins. Gq protein activates phosphoinositide-specific phospholipase C (PLC) which then hydrolyzes phosphatidylinositol 4,5-bisphosphate (PIP_2) to generate the secondary messengers inositol 1,4,5-triphosphate (IP3) and diacylglycerol (DAG) [8]. IP3-sensitive Ca^{2+} channels are then triggered leading, via calmodulin (CaM) activity, to the nuclear localization of the forkhead box O1 (FoxO1) transcription factor stimulating the transcription of glucose-6-phosphatase (G6PC) and phosphoenolpyruvate carboxylase (PCK1) encoding genes (**Fig. 5B**). These enzymes increase gluconeogenic activity [9,10]. On the other hand, with higher glucagon concentrations as in fasting conditions, Gs protein release leads to the activation of adenylate cyclase, enzyme which catalyze the formation of cyclic AMP (cAMP). The raise in intracellular concentration of cAMP promotes regulatory subunits of protein kinase A (PKA) to separate from catalytic subunit and therefore rending PKA activation. Then, PKA phosphorylates the transcription factor cAMP response element binding (CREB) protein among other substrates. Phospho-CREB is shuttled to the nucleus (effect potentiated also by above mentioned CaM activity) and directly and indirectly (through transcription of the PGC1A gene) stimulates the transcription of *G6PC* and *PCK1* genes (**Fig. 5B**), resulting in gluconeogenesis activation [9,10].
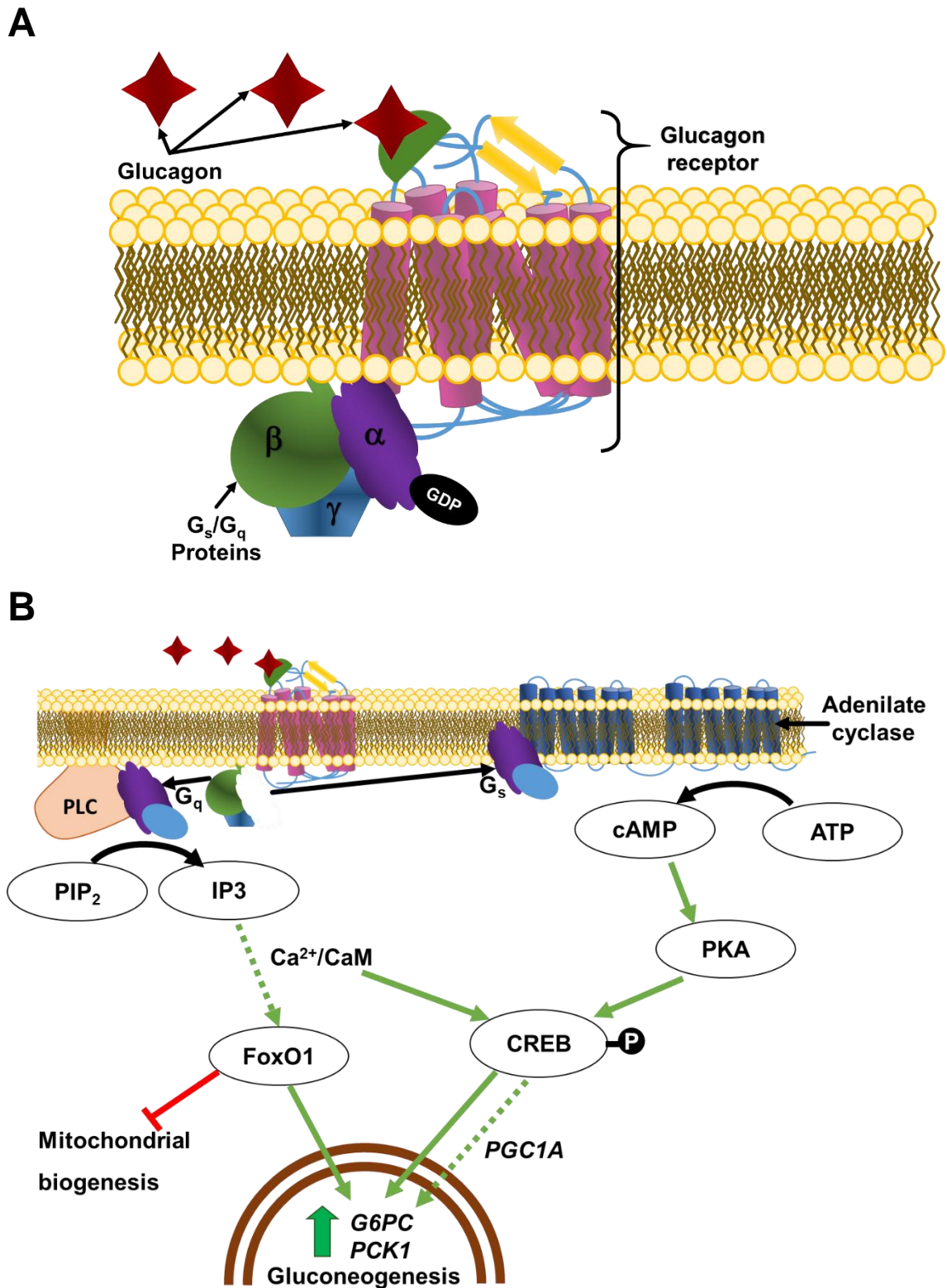
Figure 5. Glucagon signaling in the hepatocyte. A. Glucagon receptors are 7-helical transmembrane proteins bound to either Gs or Gq proteins. **B.** Glucagon receptors' activation leads to increased transcription of gluconeogenic genes by the synergic action IP3 and cAMP pathways.

10

One of the most relevant and least known aspects of T2DM is hyperglucagonemia. The loss of the ability to regulate glucagon secretion in α-pancreatic cells, and its deleterious effects on hepatic gluconeogenesis remain unclear [7,11-14]. This pathological state alters the functional capacity of the pancreas and liver, contributing to the pathogenicity of T2DM [7,9,10]. In this line of evidence our group has made a substantial contribution to explain the role of IDE in α-cells on hyperglucagonemia [15,16], however this topic is out of the scope of this thesis.

I.3. Insulin-degrading enzyme.

I.3.1. Overview.

Insulin-degrading enzyme (IDE), also known as insulysin or insulinase, is a Zn^{2+} metallo-endopeptidase that is ubiquitously expressed in insulin-responsive and non-responsive cells. IDE belongs to the M16 superfamily of zinc-metalloproteases, called "inverzincins" because of their zinc-binding consensus sequence (HxxEH) that is inverted in comparison with the sequence in most conventional metalloprotease (HExxH) [17,18].

IDE was first identified by its ability to degrade insulin *in vitro* into several fragments (**Fig. 6**). IDE has a high affinity for insulin (Km ~0.1 μM) and proinsulin is a poor substrate that is hydrolyzed at very slow rates, acting as a competitive inhibitor. Likewise, insulin-like growth factors I and II (IGF-I and IGF-II) are substrates of IDE, being IGF-II degraded more rapidly than IGF-I, but both acting as competitive inhibitors of IDE, on insulin degradation. However, IDE can degrade several other substrates with lower affinity than insulin, including glucagon, and others like somatostatin, amylin, Aβ, amyloid precursor protein intracellular domain, amyloid Bri and amyloid Dan, atrial natriuretic peptide, bradykinin and kallidin, calcitonin and β-endorphin, growth hormone-release factor, chemokine ligand 3 and 4 (CCL3 and CCL4) and HIV-p6 protein [17,18].
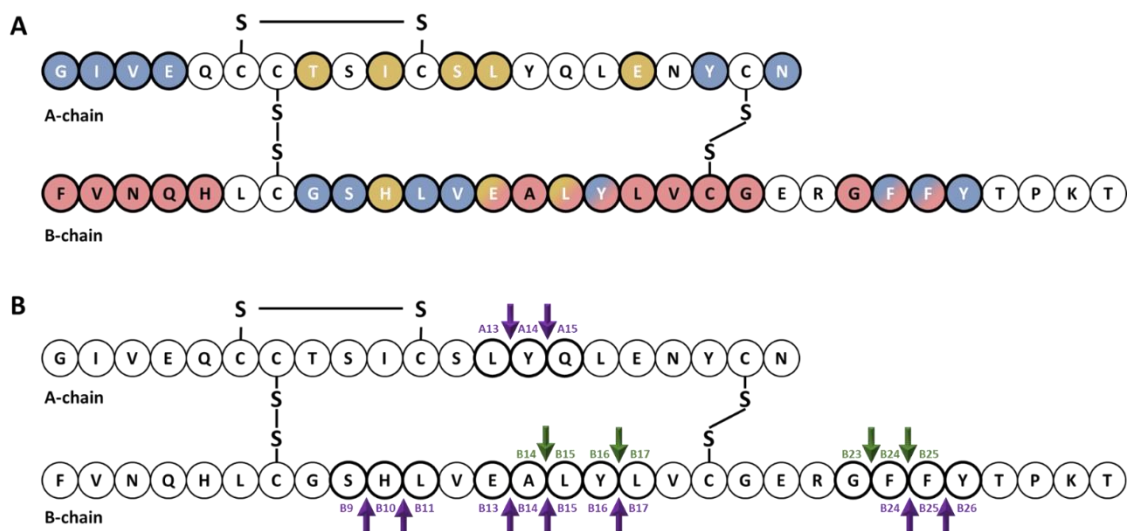
Figure 6. Primary structure and cleavage products of human insulin. A. Primary structure of insulin showing amino acids that interact with IDE (red color) [19-21] and with site 1 (blue color) and site 2 (gold color) of the insulin receptor [22-25]. **B**. Cleavage products generated by endosomal proteases. At an early time, following insulin endocytosis, endosomal proteases account for major degradation products containing an intact A-chain, and cleavages in the B-chain (green arrows). Purple arrows indicate IDE cleavage sites effected by IDE *in vitro*. Taken from reference [26].

In addition to its proteolytic function, other of non-proteolytic nature have been proposed due to its interaction with sorting nexin-5 (SNX5), sirtuin-4 (SIRT4), α-synuclein, retinoblastoma protein (RB), phosphatase and tensin homolog (PTEN) and others [17,18].

IDE is synthesized as a single polypeptide with a molecular weight of ~110 kDa. It assembles as a stable homodimer, although it can exist as an equilibrium of monomers, dimers, and tetramers. Each monomer comprised four homologous domains (named 1–4). The first two domains constitute the N-terminal portion (IDE-N), and the last two the C-terminal portion (IDE-C). IDE-N and IDE-C are joined by an extended loop of 28 amino acids. In the human IDE dimer, the interface between the two monomers is formed by 18 residues of domains 3 and 4 (IDE-C). The active site of IDE consists of a catalytic tetramer, $HxxEHx_{76}E$, located inside domain 1, in which two histidine residues (H108 and H112) and a glutamate (E189) coordinate the binding of the Zn^{2+} ion and a second glutamate (E111) plays an essential role in catalysis. Glutamate E111 activates a catalytic water molecule for the nucleophilic attack that mediates peptide hydrolysis. Although the catalytic site is entirely inside IDE-N domain, the IDE-C is necessary for correct substrate recognition [17,18]. Site-directed

12

mutagenesis revealed that mutating IDE H108 (i.e., H108L and H108Q) abolished catalytic activity of the enzyme, but not the ability to bind insulin. Similarly, mutation E111Q abolished proteolytic activity.

Substrates for IDE are almost exclusively intermediate-size (~20–40 amino acids) peptide substrates, with rare exceptions, such as oxidized hemoglobin [27]. This size preference is the result of the overall structure of IDE, which resembles a clamshell, with two bowl-shaped domains (IDE-C and IDE-N) facing one another, connected by a hinge, and together forming a ~13,000-$Å^3$ internal chamber. These domains can pivot on the hinge, thus adopting "open" and "closed" conformations (**Fig. 7**). Transition to the open conformation is required for entry of substrates and exit of proteolytic products, and there is strong evidence that transition to the closed conformation is a requirement for proteolytic processing [28]. Consistent with this, site-directed mutagenesis revealed that the complete active site of IDE is in fact bipartite, consisting of residues within both IDE-N and IDE-C, a conclusion that is confirmed by numerous crystal structures [17,18]. Due to the placement of the bipartite active site within the chamber of the closed protease, substrates must be small enough to fit completely within this chamber to be processed. To facilitate binding and subsequent cleavages at the catalytic site, larger substrates interact with an exosite within domain 2 located ~30 Å away from the active-site Zn^{2+}, which anchors the N-terminus of several substrates. Because of the unusual requirement that substrates fit within the internal chamber, the substrate selectivity of IDE is based more on the tertiary structure of substrates than their primary amino acid sequence. IDE shows some preference for cleavage at basic or bulk hydrophobic residues at P1´site of the target protein, but this subsite specificity is not strict, and IDE commonly cleaves at vicinal peptide bonds within substrates. Of note, substrates containing positively charged residues at their C-terminus are poor IDE substrates. Thus glucagon, which lack of positively charged amino acids at the C-terminal is a good IDE substrate, but not glucagon-like peptide [17,18].
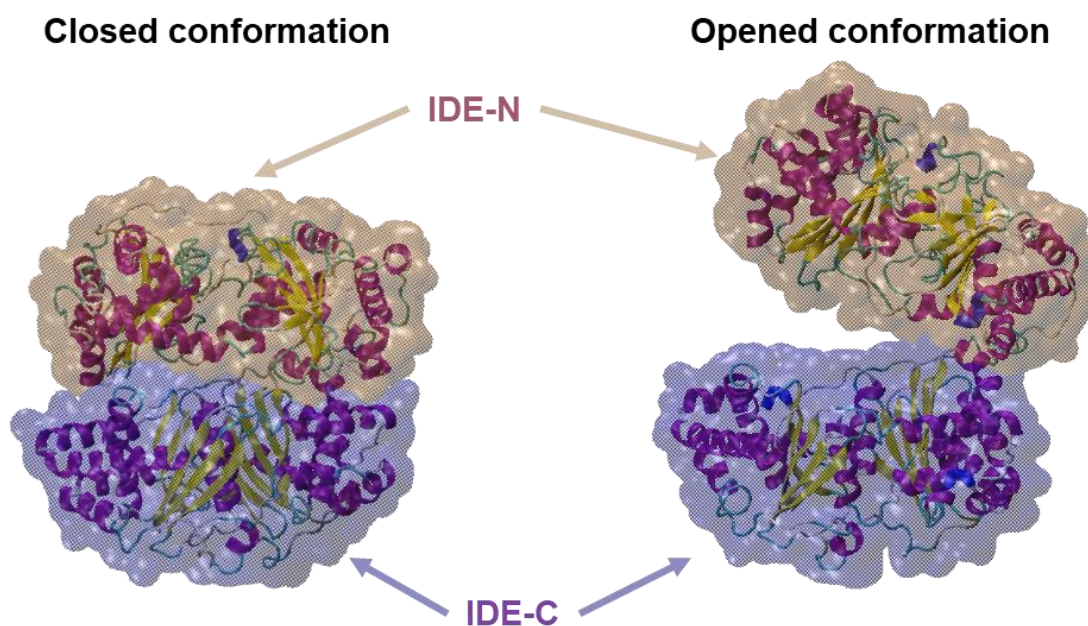
Figure 7. Different conformations of IDE. IDE is in an equilibrium between "opened" and "closed" conformational states. In the absence of substrates, IDE is preferentially in the closed conformation, and it adopts the opened conformation for substrates to enter the internal chamber, although it has to return to the closed conformation for proteolysis to occur. Release of the cleaved products requires coming back to the open conformation. This figure was constructed from PDB structure 6BF8 [28] using Visual Molecular Dynamics (VMD) software v1.9.4. [29]

The requirement for a transition between the "closed" and "opened" conformations has an additional implication for the activity of IDE. There is extensive hydrogen bonding between the two halves of IDE, creating a "latch" that tends to maintain the protease in the closed conformation. Consistent with this idea, most crystal structures of IDE, whether empty or occupied by substrate, show the protease in the closed conformation. Notably, mutation of some of the residues mediating this interaction has been shown to activate the protease by as much as 15-fold. It is estimated that in the absence of other factors, ~99% of IDE molecules are normally in the closed conformation, suggesting that a significant of latent IDE activity could be untapped, for example, by compounds that disrupt this "latch" [17,18].

I.3.2. Role of IDE on insulin resistance, glucose homeostasis and T2DM.

Genetic polymorphisms within the *IDE* locus are associated with increased risk of T2DM in humans and impaired insulin metabolism (i.e., decreased insulin secretion, insulin sensitivity and hepatic insulin degradation) [30-45]. Compiling

evidence has demonstrated an association between reduced IDE levels and lower insulin clearance in type 2 diabetics. Together, these studies show changes in IDE activity in patients with diabetes. *Ide* mutation in the Goto–Kakizaki rat model causes altered cellular insulin degradation and characteristics typical of T2DM. On the other hand, whole-body genetic ablation of *Ide* (IDE-KO) leads to insulin resistance, hyperinsulinemia and impaired glucose homeostasis in mice, supporting the notion of a physiologic role for IDE in insulin and glucose metabolism [17,18].

Some studies have shown an association between reduced IDE activity or expression levels and altered insulin metabolism. Thus, Fosam and colleagues showed that in African Americans, who are at a higher risk for developing T2DM compared with non-Hispanic whites, lower IDE activity in the liver was associated with reduced insulin clearance and higher plasma insulin levels [46]. Sofer and colleagues found higher serum IDE levels in subjects with metabolic syndrome compared to control subjects [47]. Additionally, this group showed a direct correlation between circulating IDE levels and triglycerides, insulin, and C-peptide; whereas HDL-cholesterol was inversely associated [47]. Pivovarova and colleagues, using gene expression profiling by microarrays, showed decreased hepatic *Ide* expression in subjects with T2DM [48]. In another intriguing finding, Fawcett and colleagues, using adipocytes isolated from fat deposits obtained from subjects undergoing elective abdominal surgery, showed that insulin degradation, potentially due to IDE, was lower in visceral fat from diabetic patients than from non-diabetic subjects [49]. Interestingly, short-term (3-day) feeding of a high carbohydrate/low fat diet, independent of total energy intake, markedly reduced insulin clearance in healthy non-obese subjects. In contrast, 3 days of a high fat/low carbohydrate diet resulted in an increase in insulin clearance [50].

I.3.2.1. Pancellular genetic deletion of Ide *on insulin and glucose tolerance* in vivo.

Farris and colleagues were the first team to investigate diabetes-related endpoints in mice with pancellular deletion of IDE (IDE-KO mice) [51]. They found that 6-month-old IDE-KO mice exhibited elevated fasting plasma glucose and insulin levels along with profound glucose intolerance [51]. Abdul–Hay and

15

colleagues subsequently conducted a longitudinal characterization of IDE-KO mice, performing glucose and insulin tolerance tests at 2, 4 and 6 months of age [52]. Whereas fasting plasma insulin levels were found to be elevated at all ages in IDE-KO mice, glucose and insulin tolerance transitioned from being modestly improved relative to wildtype (WT) controls at 2 months of age to profound glucose and insulin intolerance at 6 months of age [52]. The age-dependent emergence of the diabetic phenotype led Abdul–Hay and colleagues to propose that it arose as a consequence of chronic hyperinsulinemia, reporting that insulin receptor (IR) levels in muscle, adipose and liver tissue decreased as a function of age [52].

IDE-KO mice were also characterized by Steneberg and colleagues [53]. Consistent with previous reports, Abdul–Hay and colleagues found that IDE-KO mice fed a normal diet exhibit pronounced glucose intolerance that increased in severity in an age-dependent manner [53]. Unlike previous studies, however, Steneberg and colleagues conducted a detailed examination of glucose-stimulated insulin secretion, finding that plasma insulin levels were markedly reduced in IDE-KO mice after glucose challenge [53]. Collectively, these contradictory studies raise far more questions than they answer, suggesting that analysis of mice with global deletion of IDE might not be the most helpful approach to elucidating the precise role(s) of IDE in regulating insulin and glucose homeostasis.

I.3.2.2 Metabolic phenotype of the L-IDE-KO mouse.

The study of IDE-KO mice offered new possibilities for elucidating IDE's function in liver. However, as discussed above, the various studies of these animals have yielded conflicting results. Moreover, by virtue of the sheer complexity of the underlying endocrinology, and the many potential proteolytic and nonproteolytic functions of IDE, the study of animals with pancellular deletion of IDE is of limited value and may in fact yield confounding results. To investigate the role of IDE in liver in a more focused manner, our group generated a mouse line with selective ablation of *Ide* exclusively in hepatocytes, known as the L-IDE-KO model [54]. L-IDE-KO mice exhibit higher fasting and non-fasting glucose levels, glucose intolerance, and insulin resistance, despite normal plasma insulin

16

levels [54]. Contrary to historical predictions about IDE's function in liver, clearance of exogenously administered insulin was unaltered by hepatic ablation of Ide. Moreover, assessment of β-cell function (insulin and C-peptide plasma levels), and histomorphological analyses of pancreas (β-cell mass, β-cell area, number of islets, and mean islets size) revealed that β-cell function and mass in L-IDE-KO mice were similar to WT controls [54]. These findings indicate that hepatic *Ide* ablation causes insulin resistance independently of any effect on circulating insulin levels, suggesting that the hyperinsulinemia observed in IDE-KO mice emerged as a secondary compensatory response to systemic insulin resistance. Another highly intriguing observation made in L-IDE-KO mice involved carcinoembryonic antigen-related cell adhesion molecule 1 (CEACAM1), a substrate of the IR in liver, that upregulates receptor-mediated insulin endocytosis and degradation in a phosphorylation-dependent manner [55]. As expected, administration of insulin to WT mice resulted in robust phosphorylation of CEACAM1 [54]. In marked contrast, however, insulin administration to L-IDE-KO mice resulted in no detectable phosphorylation of CEACAM1, despite unchanged CEACAM1 protein levels [54].

To delve more deeply into IDE's role in the pathogenesis of hepatic insulin action, we fed L-IDE-KO mice a Western HFD (35% carbohydrates and 45% fat) [56]. As was true for animals fed a regular diet [54], L-IDE-KO fed a HFD mice exhibited insulin resistance and glucose intolerance [56]. Unlike the regular diet [54], however, feeding a HFD to L-IDE-KO mice triggered elevated fasting and non-fasting plasma insulin levels, but normal glucagon levels, relative to control mice fed a HFD [56]. The hyperinsulinemia in HFD-fed L-IDE-KO mice could theoretically be attributable to reduced hepatic insulin extraction and/or enhanced β-cell function and mass. Similar to the case with a regular diet [54], however, hepatic insulin clearance and β-cell mass remained unchanged in L-IDEKO mice fed a HFD [56]. On the other hand, β-cell function was improved, most likely as a compensatory response to insulin resistance triggered by loss of hepatic IDE function [56].

From a mechanistic point of view, the hepatic insulin resistance present in L-IDE-KO mice appears to be related to diminished insulin action in the liver under regular and HFD feeding [54,56]. Hepatic ablation of IDE causes a reduction in IR

protein levels and insulin-mediated phosphorylation of IR, leading to lower protein kinase B (PKB) activation and aberrant nuclear distribution of FoxO1, which in turn enhances expression of gluconeogenic genes (*G6pc* and *Pck1*). Interestingly, hepatic Ide ablation altered IR levels post-translationally, as IR mRNA levels were unaffected, and did not reduce protein or mRNA levels of the insulin-like growth factor-1 receptor, which exhibits 70% homology to IR and shares some insulin-responsive signaling pathways [54,56].

I.3.2.3. Metabolic phenotype of hepatic IDE gain of function in mice.

Merino and collaborators also examined the consequence of a gain-of-function manipulation to hepatic IDE *in vivo* [56]. To that end, an adenovirus IDE expression construct was administered to mice, resulting in ~4-fold increase in liver IDE levels. In mice fed a HFD, hepatic IDE overexpression improved glucose tolerance and insulin sensitivity independently of changes in body weight or food intake [56]. Moreover, plasma insulin and C-peptides levels, but not glucagon, were reduced by hepatic IDE overexpression [56].

Although the reduction in plasma insulin levels might theoretically be explained by increased hepatic insulin clearance by IDE, insulin clearance was found to be unaltered by hepatic IDE, suggesting instead that as a consequence of improved insulin sensitivity the pancreas reduced insulin production and secretion to meet the demand for the hormone in peripheral tissues. This study is the first proof-of-principle demonstration that augmenting hepatic IDE function in liver can partially revert insulin resistance and glucose intolerance in a preclinical mouse model of obesity and diabetes. The opposing effects of loss *versus* gain of IDE function on insulin levels and glucose tolerance are consistent with a role for IDE in promoting insulin sensitivity in liver of diet-induced obese mice.

In addition to regulation of IR levels, manipulation of hepatic IDE also alters glucose transporters levels. Thus, loss of IDE function in HFD fed mice resulted in a two-fold increase in GLUT2 protein levels, with a reciprocal 2-fold reduction of GLUT2 protein levels in mice overexpressing IDE. In addition, hepatic IDE gain-of-function resulted in a two-fold increase in GLUT1 protein levels, therefore altering the hepatic GLUT1/GLUT2 ratio [56]. Taken together, these findings lend support to the notion that IDE forms complexes with membrane proteins to

regulate the intracellular trafficking of the IR independently of its proteolytic function.

I.3.2.4. IDE as a therapeutic target for pharmacological treatment of metabolic diseases.

Because historically IDE has been proposed as the main enzyme involved in insulin degradation, efforts in the development of IDE inhibitors as therapeutics in diabetic patients has attracted attention during the last decades. The rationale behind this strategy was based on the idea that IDE was the main protease involved in hepatic insulin clearance. Because hepatic insulin degradation clears ~50-80% of secreted insulin by the pancreas, its pharmacological inhibition would significantly augment circulating levels of the hormone, helping glucose control in diabetic patients.
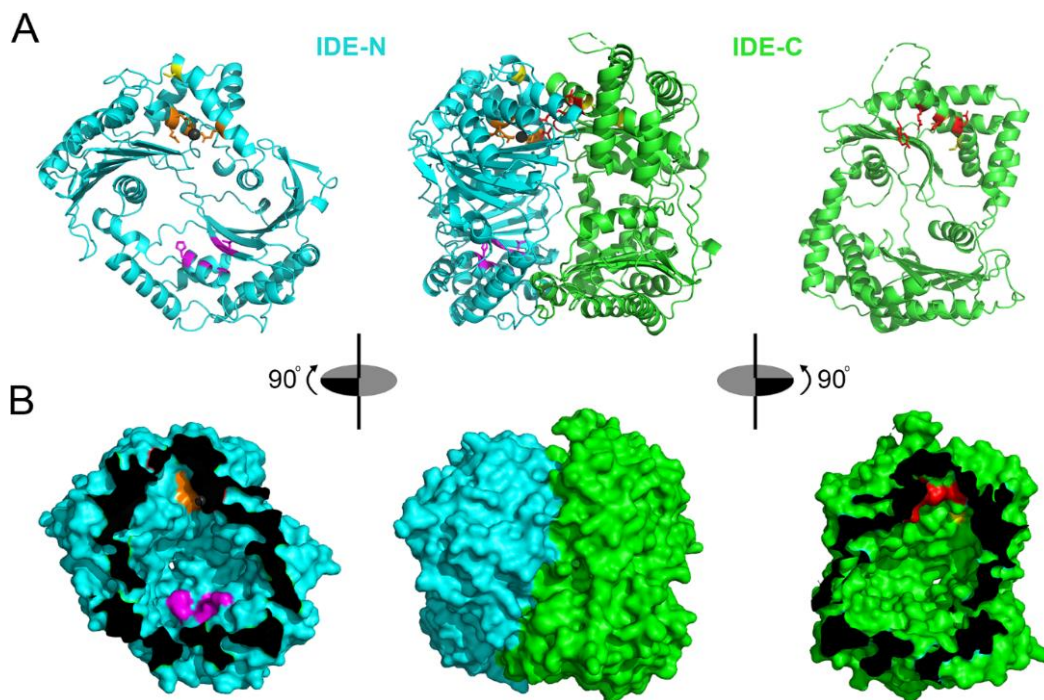
Figure 8. Structure of IDE and regions targeted by different inhibitors. A, B, Illustration of a single monomer of IDE (center) and IDE-N (left, cyan) and IDE-C (right, green) depicted in ribbon (A) and surface (B) representations. Zinc-binding and catalytic residues within the active site of IDE-N are depicted in orange, with the zinc atom shown as a gray sphere. Residues within IDE-C that make up the second portion of IDE's bipartite active site are shown in red. Cysteine residues targeted by thiol-modifying inhibitors are shown in yellow. The distal exosite is shown in magenta. In B, note that the portions of IDE-N and IDE-C that are adjacent when the protease is in the closed conformation are depicted in black. Taken from ref. [18].

Following this rationale, several IDE inhibitors have been developed and tested in preclinical mouse models of T2DM. However, none of them have demonstrated a valid therapeutic use (**Fig. 8**) [18].

On the other hand, preimplantation factor (PIF) is a fifteen-amino acid peptide (MVRIKPGSANKPSDD) expressed by both the mammalian embryo and its placenta, which is detected in the early stages and is present throughout the duration of viable pregnancy in the maternal circulation [57-61]. In the last decades, studies have revealed that PIF plays a significant role in early pregnancy by a supportive role in embryo development through multi-targeted effects including regulation of systemic immunity, adhesion, remodeling, apoptosis, and trophoblast invasion [58,62,63]. Interestingly, synthetic PIF (sPIF) replicates native PIF action *in vitro* and *in vivo* as reviewed in reference [62].

From the clinical point of view, sPIF administration in humans is safe and well-tolerated [64]. Because sPIF has immune-modulatory properties, its potential clinical application for treating human diseases can be envisioned. In this regard, it was shown that sPIF has a protective role for T1DM [65] and cardiovascular disease [66] in preclinical models.

Paidas and collaborators using a ProtoArray stringent analysis found that PIF primarily targets IDE [67]. Bioinformatic studies performed by Hayrabedyan and collaborators revealed that the core sequence R3-I4-K5-P6 of the PIF peptide (MV**RIKP**GSANKPSDD) modulates IDE function, and the specific P6 and I4 amino acids are essential for hydrophobic interactions with IDE. Interestingly, the PIF-IDE complex forms high affinity bond in the presence of insulin, suggesting that PIF sterically competes for the same place as insulin [68]. Although the details of this interaction are not fully elucidated, PIF may stabilize IDE in the open conformation, and makes its active pocket more accessible to substrates [68].

20

II. Hypotheses and Aims

II.1. General hypothesis.

Hepatic IDE expression and activity is regulated by metabolic status (diet type and nutritional state). In addition, IDE regulates hepatic glucagon signaling contributing to the etiology of hyperglucagonemia associated with type 2 diabetes mellitus.

II.1.1. Specific hypotheses.

- Hepatic IDE expression levels and proteolytic activity change in response to the nutritional state.

- IDE regulates intracellular glucagon signaling pathway in hepatocytes.

II.2. Aims.

To unveil the transcriptional and post-transcriptional regulation of hepatic IDE and its role in glucagon physiology in hepatocytes.

II.2.1. Specific aims.

- To determine the expression levels and activity of hepatic IDE in different nutritional states and upon consumption of a diet rich in fats and carbohydrates.

- To study effects of IDE on hepatic glucagon signaling pathways in hepatocytes.

- To generate *in silico* high quality models for IDE tridimensional structure.

III. Materials and methods

III.1. Experimental animals.

All mice were housed in ventilated cages under a 12:12 h light-dark cycle, with an *ad libitum* water supply, at the Service of Animal Research and Welfare (SIBA) of the University of Valladolid (UVa). All experiments were approved by the UVa Animal Welfare and Experimentation Ethics Committee (project no. 5003931).

III.1.1. Fasting and refeeding experiments.

For the study of the effect of diet and nutritional status on IDE regulation, 4-week-old male C57BL/6J mice were obtained from Charles River Laboratories (Les Oncins, France). Mice were fed either a standard rodent diet (SD; Ssniff Spezialdiäten GmbH # V1534-703, 19% protein, 3.3% fat) or a high-fat diet (HFD; Research Diets # D12451, 35 kcal% carbohydrate, 45 kcal% fat) for 8 weeks.

III.1.1.1. Animal weight control

Animal weight was weekly controlled using a digital weight scale (Adam Equipment, USA).

III.1.1.2. Intraperitoneal glucose tolerance test.

To evaluate alterations in glucose homeostasis *in vivo*, we performed intraperitoneal glucose tolerance test (ipGTT). Mice were fasted for 18 h and injected intraperitoneally with glucose at 2 g/kg body weight. Blood glucose levels were measured before glucose challenge (time 0) and at 15, 30, 60 and 120 min after glucose injection using a Contour Next digital glucometer (Ascensia, Barcelona, Spain). The area under the curve was calculated using an equation that quantifies the incremental area above the baseline, where only the area above the fasting level for each mouse is considered [69].

III.1.1.3. Endpoint procedure.

For the fasting and refeeding experiments, the mice were kept fasted for 18 h. Then, the SD-fed groups of mice were refed the same diet for 30 min or 3 h *ad libitum*. Likewise, the HFD-fed groups were refed for 30 min or 3 h with a HFD *ad libitum*. (**Fig. 9**)
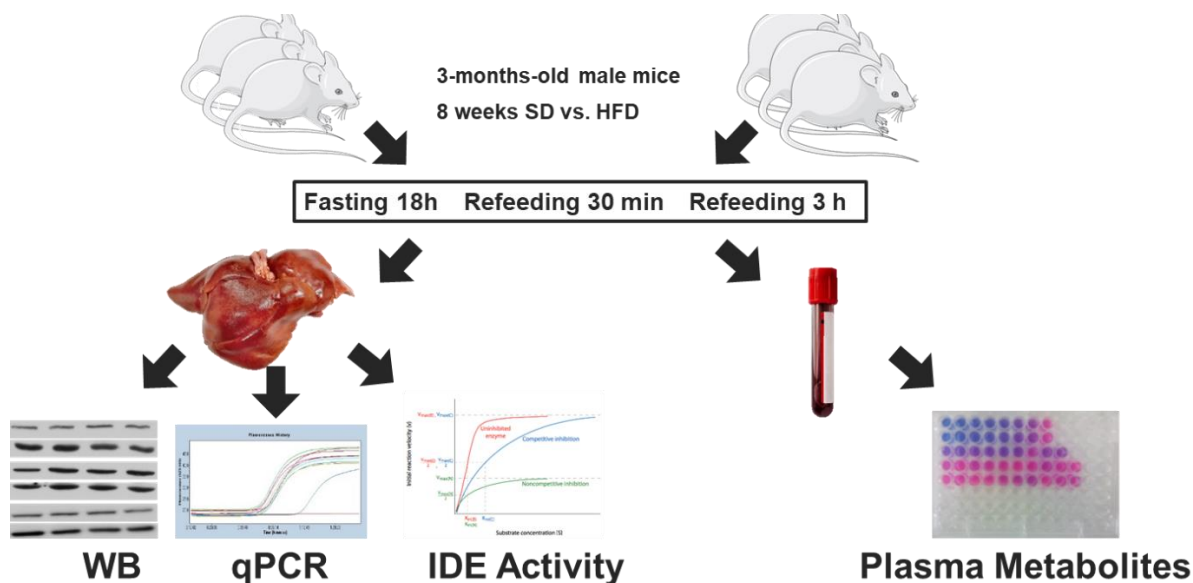
Figure 9. Fasting and refeeding experiment design.

At the nutritional states of fasting, 30 min refeeding and 3 h refeeding, respectively, mice were sacrificed and exsanguinated. Liver was extracted and flash frozen in liquid nitrogen and plasma was separated by centrifugation and frozen on dry ice. Tissue and plasma samples were kept at -80°C until specific determinations were performed.

III.1.2. L-IDE-KO mice.

For the study of the effects of liver-specific IDE ablation in glucagon signalling, L-IDE-KO mice [70] with a genetic background of C57BL/6J were used (**Fig. 10**); to obtain liver lysates, only males animals were used to avoid estral cyclic interference *in vivo* and for collection of primary hepatocytes, animals from both sexes were used indistinctly, taking into consideration that isolated hepatocytes in culture are no longer in contact with *in vivo* secreted sexual hormones. In every case, WT littermates were used as controls (**Fig. 10**). All animals were three months old and generated as previously described by our group (**Fig. 10**) [70]. Mice were fed a SD or a HFD as described above. These animals were sacrificed in a fasting state and exsanguinated. For tissue lysate analysis, liver was removed and flash frozen in liquid nitrogen. Samples were kept at -80°C until further processing.

25
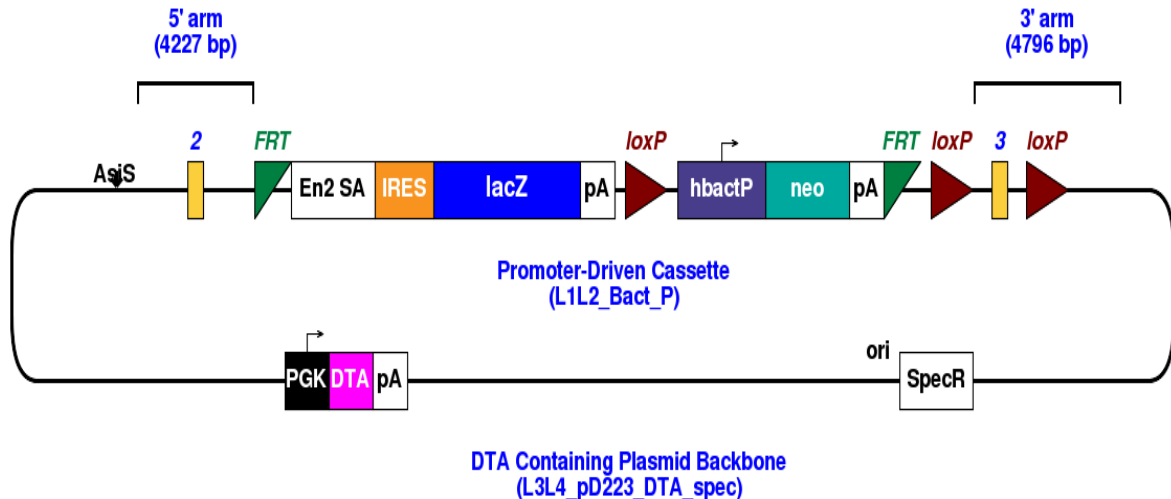
Figure 10. Details of *Ide* gene deletion in L-IDE-KO mice. Ide[flox/flox] mice were generated from the Ide[tm1a(EUCOMM)Wtsi] mouse line (European Mouse Mutant Archive), which contained a "knockout first" allele with a lacZ and neomycin resistance cassette flanked by FRT sites. The latter cassette was removed by crossing with the B6.Cg-Tg(Pgk1-flpo)10Sykr/J mouse line (The Jackson Laboratory), which express Flp-recombinase in all tissues. After deletion of the Frt-flanked cassette, the Flp-recombinase transgene was removed by crossing the offspring to the wild-type background strain (C57BL/6J), and the mice were bred to homozygosity to yield Ide[flox/flox] mice. Alb-*Cre* (*Ide*^{+/+};Alb-*Cre*/+) mice were crossed to *Ide*[flox/flox] (*Ide*[flox/flox];+/+) to generate L-IDE-KO (*Ide*[flox/flox]; Alb-*Cre*/+) and their WT littermates (*Ide*[flox/flox];+/+).

III.2. Plasma biochemistry.

III.2.1. Blood glucose assessment.

Blood glucose levels were measured at fasting and after feeding in mice taking the sample from the tail vein as previously reported [70,71] and using a Contour Next™ digital glucometer.

III.2.2. Plasma insulin and glucagon assessment.

Insulin and glucagon levels from mouse plasma were determined by direct sandwich ELISAs, Mercodia Mouse Ultrasentive Insulin ELISA and Mercodia Glucagon ELISA, respectively (Mercodia, Sweden).

In these assays, wells are pre-coated with a first antigen specific antibody. The samples are deposited inside these wells together with a second antigen directed antibody, this time peroxidase-conjugated, and incubated 2 or 22 h respectively for

each kit. Thus, each molecule of antigen will be bound to an antibody in the base that retains it and a second antibody that label it (**Fig. 11**).

After that, wells were manually washed 6 times to remove unbound sample and enzyme labelled antibody. Then, the bound conjugate is detected by reaction with 3,3'-5,5'-tetramethylbenzidine (TMB) incubation between 15 and 30 min depending on the kit. The reaction is finally stopped by the addition of an acid stop solution, giving a colorimetric endpoint that is read spectrophotometrically at 450 nm (HEALES microplate reader, China).
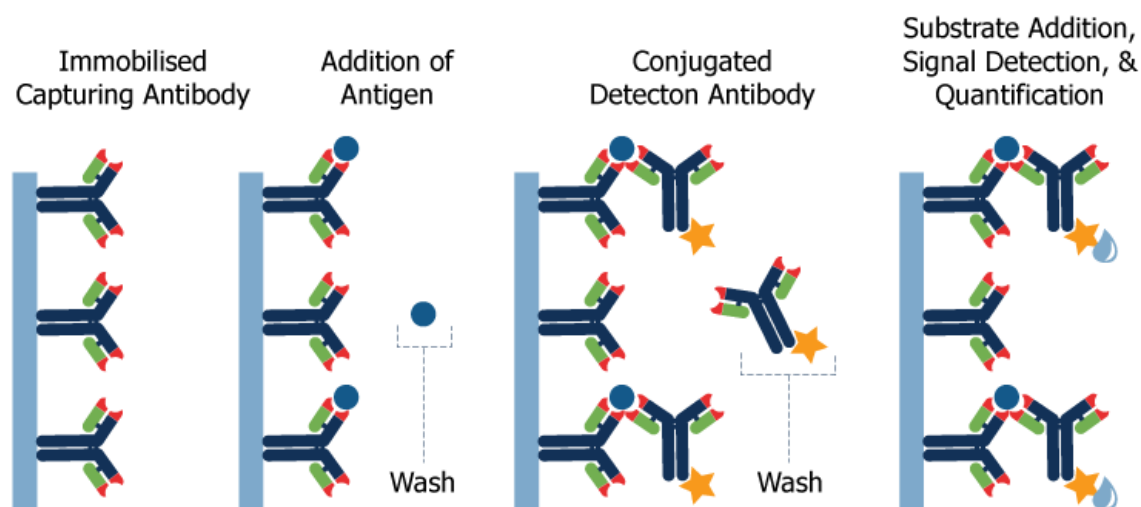
Figure 11. Direct Sandwich ELISAs steps and working principle. Retrieved from: https://www.rockland.com/resources/elisa-technique/

III.2.3. Plasma triglycerides assessment.

Triglycerides levels were assessed employing the triglycerides colorimetric kit (Biosystems, Spain), using 5µL of mouse plasma. Triglycerides in the samples originates, by means of the coupled reactions, a coloured complex that can be measured by spectrophotometry at a wave length of 500 nm using a microplate reader (Heales, China). The intensity of this coloured product is directly proportional to the concentration of triglycerides present in the sample.

A standard curve of known concentration can be established accordingly. The unknown concentration in samples can be determined by extrapolation to this standard curve.

III.2.4. Plasma cholesterol assessment.

Cholesterol levels were assessed employing the cholesterol colorimetric kit (Biosystems, Spain), using 3µL of mouse plasma.

Free and esterified cholesterol in the samples originates, by means of the coupled reactions, a coloured complex that can be measured by spectrophotometry at a wavelength of 500 nm using a microplate reader (Heales, China). The intensity of this coloured product is directly proportional to the concentration of free and esterified cholesterol present in the original specimen.

III.2.5. Plasma glycerol assessment.

Plasma levels of glycerol were determined using the glycerol colorimetric assay kits (Cayman Chemical, MI, USA). The glycerol assay employs a coupled enzymatic reaction system that yields a brilliant purple product with a maximum absorbance at 540 nm.

III.2.6. Plasma L-lactate assessment.

L-lactate levels of deproteinated mouse plasma were assessed with Cayman's Chemicals L-lactate Assay. This kit provides a fluorescence-based method for detecting L-lactate in biological samples such as plasma. In the assay, lactate dehydrogenase catalyzes the oxidation of lactate to pyruvate, along with the concomitant reduction of NAD+ to NADH. NADH reacts with the fluorescent substrate to yield a highly fluorescent product. The fluorescent product was analyzed with an excitation wavelength of 535 nm and an emission wavelength of 590 nm on a GENios Pro TECAN multi-plate reader (TECAN, Switzerland). The samples L-lactate concentrations were calculated using a logarithmic regression for the standard curve.

III.2.7. HOMA index calculation

The homeostatic model assessment (HOMA) index was calculated using fasting glucose and insulin concentrations according as it was first described under the name HOMA by Matthews et al in 1985 [72]. The HOMA index is a method used to quantify insulin resistance. This index is overnight fasting blood glucose levels

multiplied for the fasting plasma insulin levels and divided for 22.5. The normal HOMA value of healthy humans ranges from 1.5-2.0; however, values above 2.0 indicates significant insulin resistance. In mice, there is not a HOMA cut off value, in fact, insulin resistance is determined comparing HOMA values obtained from experimental mice to their control littermates.

III.3. Cell cultures.

III.3.1. Mouse primary hepatocytes isolation and culture.

For the extraction, purification and culture of primary hepatocytes, the protocol described by Valdecantos *et al* [73] was adapted. Primary mouse hepatocytes were isolated from the liver of non-fasting 12-week-old WT and L-IDE-KO mice.

Briefly, in order to later perfuse with a pulsating pump, working solutions to the liver, isoflurane-anesthetized mice were cut open and inferior cava vein was cannulated from the right atrium in direction to liver and tied before and after liver vein derivation (**Fig 12**).
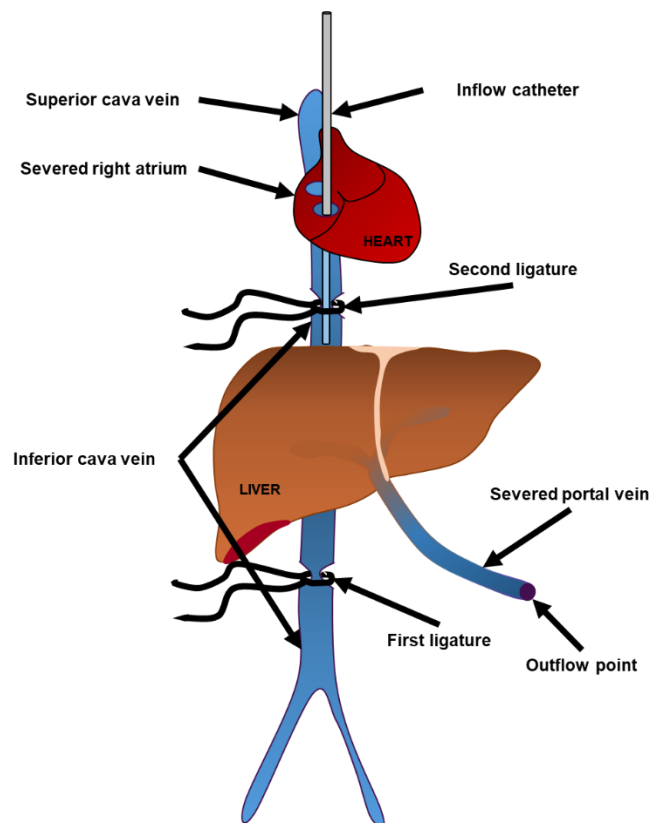
Figure 12. Points of mouse inferior cava vein to be tied through mouse hepatocytes extraction.

Subsequently, mice livers were perfused with 25 ml of warm perfusion solution [calcium-free Hank´s balanced salt solution (HBSS), 10 mM HEPES pH 7.4, 0.2 mM EGTA] at 200 µl/s, followed by perfusion at 150 µl/s and digestion with collagenase solution (Sigma-Aldrich Aldrich, St. Louis, MO, USA). Following digestion, hepatocytes were released by mechanical dissociation of the tissue and underwent to filtration with attaching medium (DMEM:F12 base medium, supplemented with 10% fetal bovine serum (FBS), 100 U/mL penicillin, 100g/mL streptomycin) and centrifugation at 50 x g for 5 min. Pellets containing cells were resuspended in attached medium and loaded onto isotonic Percoll solution at 40 % (v/v) and centrifuged at 200 x g for 10 min at room temperature. Supernatants were discharged and cells were washed with attached medium. Afterwards, cells were seeded at 200,000 cells/mL on 6-well collagen-coated plates (Nunclon™ Delta Surface, Thermo Scientific, USA) and cultured in DMEM:F12 medium supplemented with 10% FBS, 100 U/mL penicillin, 100g/mL streptomycin for 24 h before glucagon stimulation experiments.

III.3.2. Cell line culture conditions.

Hepatocytes cell line, alpha mouse liver 12 (AML12), was obtained from the American Type Culture Collection (ATCC, USA) and checked for mycoplasma contamination. Cells were cultured at 37°C in a 5% CO_2 incubator in DMEM:F12 medium containing 16 mM glucose, 10% (v/v) heat-inactivated FBS, 2.5 mM L-glutamine, 0.5 mM sodium pyruvate, 1.2 g/L sodium bicarbonate, 15 mM HEPES, 10 µg/ml insulin, 5.5 µg/ml transferrin, 5 ng/ml selenium, 40 ng/ml dexamethasone, 10 IU/ml penicillin and 10 µg/ml streptomycin.

III.3.3. shRNA-mediated stable Ide knockdown in AML12 cells.

To study the effect of stable IDE silencing on hepatocyte phenotype, AML12 cells were transduced with a lentiviral vector of an IDE-specific short hairpin silencing RNA (shRNA) in parallel with an empty vector, therefore generating the AML12-shRNA-IDE and AML12-CONTROL lines. The vector used was the MISSION® pLKO.1-puro Lentiviral Transduction Particles (Sigma-Aldrich, St. Louis, MO, USA) with ID number TRCN0000009487 for the shRNA-IDE, containing the sequence 5'-GCTTGCTATTAGAGAGAGACAAA-3' of the 3'UTR region, and reference SHC001 for the empty vector control (**Fig. 13**).
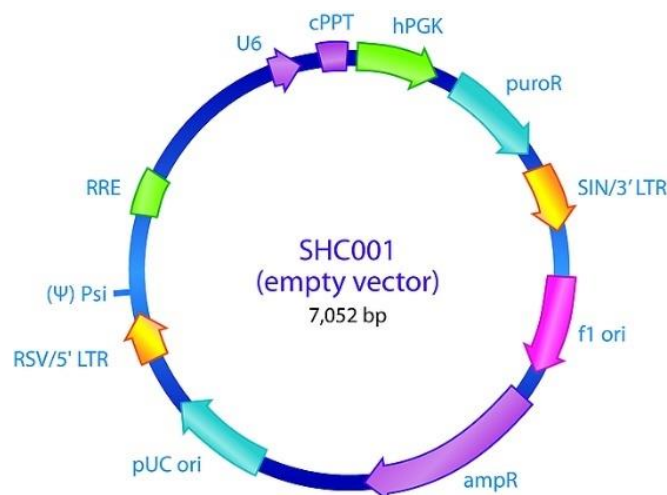
Figure 13. The pLKO.1-puro™ vector is a retrovirus-based expression lentivector. It contains the puromycin resistance gene, which allows the pharmacological selection of target cells stably expressing the shRNA and a GFP gene, which functions as a fluorescent marker.

AML12 cells were seeded into 6-well plate at 2×10^5 cells per well. After 24 h, the lentiviral particles were added to the cells with a multiplicity of infection (MOI) of 100 and hexadimethrine bromide (polybrene; 8 µg/mL) (Sigma-Aldrich, St. Louis, MO, USA). After 96 h, the transduction efficiency was observed through a fluorescence microscope. Then, the medium was discarded, and cells were incubated with DMEM:F12 medium containing 2 µg/mL puromycin. Cells were further cultured under selection conditions, and IDE knockdown was tested through RT-PCR and western blot analyses.

III.3.4. Insulin stimulation of culture cells.

AML12-shRNA-IDE and AML12-CONTROL cells were seeded at a confluence of 500,000 cells per well in 6-well plates. 24 h later, cells were incubated in serum-free medium for 18 h before the experiment. Next day, they were treated with serum free medium containing 100 nM human insulin (Sigma-Aldrich, I9278, USA) at 0, 5, 15 and 30 min respectively. Protein was collected for further process as described below.

III.3.5. Glucagon simulation of culture cells.

Either AML12-shRNA-IDE and AML12-CONTROL cells or L-IDE-KO and WT primary hepatocytes were seeded at a confluence of 500,000 cells per well in 6-well

plates (collagen coated for primary cells). 24 h later, cells were incubated in serum-free medium for 18 h before the experiment. Next day, they were treated with serum free medium containing 50 ng/ml glucagon (Sigma-Aldrich, G2044, USA) at 0, 1, 4 and 8 h respectively. RNA and protein were collected for further process as described below.

III.4. Gene expression assays by real-time quantitative PCR.

III.4.1. RNA purification.

Total RNA was purified from ~20 mg tissue samples of mouse liver or $1 - 2 \times 10^6$ AML12 cells in culture using TRIzol™ reagent (Invitrogen™, USA) According to the manufacturer's instructions (**Fig. 14**).
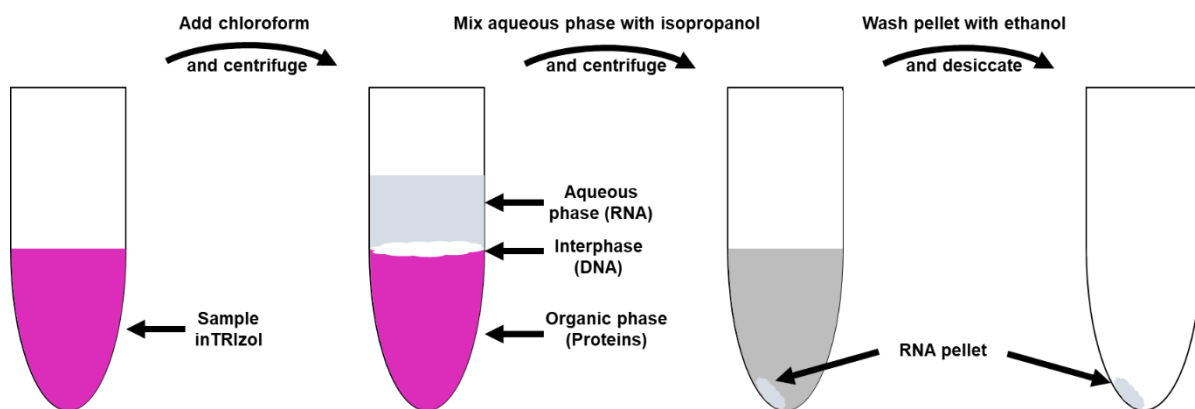
Figure 14. Principle of RNA isolation with TRIZol Reagent.

Quantification of total RNA was performed by measuring ultraviolet absorbance on a NanoDrop® ND-1000 full spectrum spectrophotometer. Removal of any possible genomic DNA contamination was achieved by treating the samples with the RapidOut DNA removal kit (Thermo Scientific™, USA).

III.4.2. cDNA Synthesis.

First strand of complementary DNA (cDNA) (**Fig. 15**) was synthesized using the iScript™ cDNA synthesis kit (Bio-Rad™, USA), according to the manufacturer's instructions.
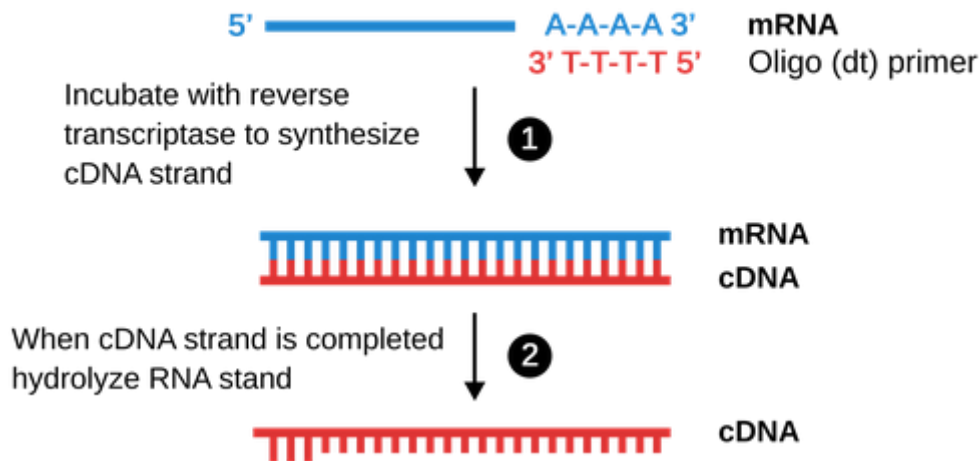
Figure 15. **cDNA single strand synthesis by retrotranscription.** Retrieved from https://theory.labster.com/reverse-transcriptase-pcr/

III.4.3. RT-PCR.

Target gene mRNA and housekeeping mRNA levels were determined by real-time quantitative PCR (qPCR) with TaqMan™ or SYBR™ Green assays on a LightCycler® 480 system. The qPCRs were performed on equal amounts of cDNA in triplicate for each sample using Maxima Probe qPCR Master Mix (Thermo Scientific™, USA) for TaqMan™ assays and Maxima SYBR Green qPCR Master Mix (Thermo Scientific™, USA) for SYBR™ Green assays.

Data were analyzed using the 2 fit point absolute quantification protocol and setting the fluorescence threshold at 1.00. Target mRNA expression levels were normalized using the $2^{-\Delta\Delta Ct}$ relative quantification method [74] to the mRNA levels of the housekeeping gene for ribosomal protein L18 (*Rpl18*) as reported by our laboratory in previous studies [70,71,75].

Homemade primers and probe of TaqMan® gene expression assay for mouse *Rpl18* were:

- Forward: 5′-AAGACTGCCGTGGTTGTGTGG-3';

- Reverse: 5'-AGCCTTGAGGAGGATGCGACTC-3';

- Probe: 5′-FAM-TTCCCAAGCTGAAGGTGTGTGTGTGCA-BHQ1-3′.

The references of TaqMan® gene expression assays (from Applied Biosystems, USA) are indicated in **Table 1**.

mRNA	Description	Reference
Ide	Insulin-degrading enzyme	Mm00473077_m1
Pck1	Phosphoenolpyruvate carboxykinase	Mm00839363_m1
G6pc	Glucose-6-phosphatase	Mm00839363_m1
Gcgr	Glucagon receptor	Mm00433546_m1
Foxo1	Forkhead-box-O1	Mm00490671_m1
Creb1	cAMP response element-binding 1	Mm00501607_m1

Table 1. Commercial TaqMan® Assays used in this study.

In order to discriminate between *Ide* isoforms expression. The following SYBR™ Green assays were designed, using mouse specific sequence, with a common forward primer expanding from exon 14 and two different reverse primers for each variant of exon 15 (**Table 2**).

mRNA	Description	Primers
Ide-15a	Canonical (exon 15a) *Ide* spliceoform	F: 5'-CAGCCATGAGTAAGCTGTGG-3' R: 5'-TCCCATAGATAGATGGTATTTTGG-3'
Ide-15b	Alternative (exon 15b) *Ide* spliceoform	F: 5'-CAGCCATGAGTAAGCTGTGG-3' R: 5'-TCAATAACCTGATAAACAGG-3'

Table 2. SYBR™ Green Assays used in this study.

III.5. Quantification of proteins expression and signalling activation.

III.5.1. Protein extraction and quantification.

For protein extraction, ~20 mg of liver samples from or AML12 cells (1-2 x106 cells) were homogenized in 200 μL and 100 μL respectively of cold assay buffer

[125 mmol/L Tris-HCl pH 6.8, 2% (m/v) dodecyl sulphate (SDS) and 1 mmol/L dithiothreitol (DTT)] supplemented with protease and phosphatase inhibitor cocktails (Sigma, USA) and 1 mmol/L phenylmethylsulfonyl fluoride (PMSF; Merck Life Science, Spain). The lysates were then sonicated for 3 min on ice and centrifuged at 18,500 X g for 10 min at 4 °C to separate and discard insoluble materials. Supernatants were retained and an aliquot was used to quantify protein content using the Pierce BCA protein assay kit (Thermo-Fisher, USA) for tissue and Micro BCA (Thermo-Fisher, USA) for cell lysates.

III.5.2. Protein electrophoresis and western blot.

Solubilized proteins (40 µg for liver and 20 µg for cells) were resolved by 10% SDS-PAGE and electroblotted onto polyvinylidene difluoride membranes (PVDF, Immobilon-P, Millipore) for immunoblotting by conventional means. The membranes were blocked with 5% m/v non-fat dry milk in PBS-Tween 20 solution. After probing with protein specific primary antibodies (**Table 3**), the membranes were washed for 10 min three times with 0.2 % (v/v) PBS-Tween 20 and incubated with specific secondary antibodies conjugated with horseradish peroxidase (HRP).

Target Protein	Host species	Reference	Working dilution	Trade Mark
IDE	Rabbit	AB9210	1:40000	Millipore™
GCGR	Rabbit	AB75240	1:10000	Abcam™
CREB	Rabbit	9197S	1:2000	Cell Signaling™
pCREB	Rabbit	9198S	1:2000	Cell Signaling™
FoxO1	Rabbit	2880S	1:2000	Cell Signaling™
pPKA-subts	Rabbit	9624S	1:2000	Cell Signaling™
IRβ	Rabbit	3025S	1:2000	Cell Signaling™
pIRβ	Rabbit	3024S	1:2000	Cell Signaling™
PKB	Rabbit	9272S	1:2000	Cell Signaling™
pPKB	Rabbit	9271S	1:2000	Cell Signaling™
PKB2	Rabbit	2964S	1:2000	Cell Signaling™
pPKB2	Rabbit	8599S	1:2000	Cell Signaling™
GSK3α	Rabbit	5676S	1:2000	Cell Signaling™
pGSK3α	Rabbit	8566S	1:2000	Cell Signaling™
GS	Rabbit	3886S	1:2000	Cell Signaling™
pGS	Rabbit	3891S	1:2000	Cell Signaling™
GLUT2	Rabbit	07-1402-I	1:5000	Millipore™
GAPDH	Mouse	MAB374	1:40000	Millipore™
Actin	Mouse	612656	1:40000	BD Biosciences™
Rabbit IgG (H+L)	Donkey	711-035-152	1:20000	Jackson Immunoresearch™
Mouse IgG	Sheep	NA9310	1:5000	Amersham™

Table 3. Primary and secondary antibodies used for immunoblotting assays in this study.

36

Membranes were rewashed for 10 min three times with 0.2 % v/v PBS-Tween 20. Signals were detected by chemiluminescence (Clarity Western ECL Substrate, Bio-Rad™, USA) and exposure to X-ray film to produce bands within the linear range. Developed films were scanned at 600 pixels per inch with HP Scanjet G4010 (Hewlett-Packard, Spain) using HP Photosmart Premier 6.5 software (Hewlett-Packard, Spain). The obtained images (negative) were converted to 32-bit format and inverted to generate an image with detectable bands. Band intensity was quantified with ImageJ software (NIH, USA). Each band was individually selected with a rectangular ROI selection, followed by quantification of the peak area of the histograms obtained. Data were plotted in arbitrary units.

III.6. IDE activity assay.

IDE activity was assessed with the SensoLyte® 520 fluorometric IDE activity assay kit (AnaSpec, Inc., CA, USA) according to the manufacturer's instructions. The assay utilizes a fluorescence resonance energy transfer (FRET) substrate derived from an amyloid precursor protein (APP) sequence designed to reduce cross-reactivity with other peptidases such as neprilysin, disintegrin and metalloproteinase domain-containing protein 10 (ADAM10), tumor necrosis factor α-converting enzyme (TACE), beta-site amyloid precursor protein cleaving enzymes 1 and 2 (BACE-1 and BACE-2). In the presence of FRET substrate, the active IDE cleaves the substrate resulting in increased 5-FAM fluorescence, which was monitored at excitation/emission = 490 nm/520 nm.

To prepare homogenate of biological samples, liver fragments (~20 mg tissue) or AML12 cells (1-2 x10^6 cells) were homogenized in 200 µL and 100 µL respectively of cold assay buffer (AnaSpec, Inc., USA) In the presence of protease inhibitors (Protease Inhibitor Cocktail, Merck Life Science, USA) plus 1 mmol/L PMSF (Merck Life Science). Homogenates were incubated on ice for 15 min, followed by centrifugation at 10,000 X g for 10 min at 4 °C to separate and discard insoluble materials. Supernatants (lysates) were kept and an aliquot was used to quantify protein content using the Pierce BCA protein assay kit (Thermo-Fisher, USA). 50 µL of tissue or cell lysates were added to each reaction well in a 96-well plate. The enzymatic reaction was initiated by adding 50 µL of IDE FRET substrate solution to each well. The plate was gently shaken for 30 sec and the fluorescence of the

sample (5-FAM) was monitored on the GENios Pro TECAN multi-plate reader (TECAN, Switzerland) every 5 min for 100 min at 37 °C. Reactions were performed in duplicate per sample. As a positive control, purified human IDE enzyme (provided by the kit) was added to the reaction mixture. As a negative control, lysates of liver, muscle or kidney tissue from IDE-KO mice were added to the reaction mixture. Wells containing the reaction mixture without tissue lysates were used as blank, which was used as background fluorescence and subtracted from the readings of the other wells containing tissue lysates. For kinetic analyses, all fluorescence readings are expressed in relative fluorescence units (RFU). The RFU data were plotted as a function of time for each sample. Subsequently, we calculated the initial reaction rate in RFU/min by determining the slope of the linear portion of the data plot. The specific activity of IDE is expressed as RFU/µg total protein/min. The assay can detect as little as 0.8 ng/mL of active IDE.

III.7. Cyclic AMP Competitive ELISA.

To quantify cAMP levels in cell lysates, the Cyclic AMP Competitive ELISA Kit (Invitrogen™, EMSCAMPL, USA) was used. This assay exclusively recognizes both natural and recombinant cAMP.

This cyclic AMP solid-phase competitive sandwich ELISA is designed to measure the amount of the target bound between a matched antibody pair. A target-specific antibody was pre-coated in the wells of the microplate.

Samples, standards and controls were then added into these wells and bind to the immobilized (capture) antibody. The sandwich is formed by the addition of the second (detector) antibody, binding to the target on a different epitope from the capture antibody. A conjugated enzyme is incorporated into the assay. After incubation and washing steps to rid the microplate of unbound substances, a substrate solution was added that reacted with the enzyme-antibody-target complex to produce measurable signal. The intensity of this signal is inversely proportional to the concentration of target present in the original specimen.

III.8. *In silico* study of IDE.

III.8.1. Sequences analysis.

The InterPro [76,77] site for analysis and classification of protein sequences was used to identify the human and murine canonical isoforms of IDE. Amino acid sequences of canonical and alternative exon 15 splicing derived IDE isoforms were obtained from the UniProt database [78].

Multiple sequence alignments of the proteins selected for the study were performed from UniProt. The local alignment search tools BLAST [79] was used to identify templates in the Protein Data Bank (PDB) [80,81] with high identity percentage from the IDE isoforms. Subsequently, multiple alignments between systems exhibiting high sequence identity were visualized and refined using the ClustalW tool [82,83], which specializes in multiple sequence alignment.

The structures of IDE reported in the PDB were selected regarding conformational state and substrate/ligand free resolution. Only 2JG4 structure [84] was found to be in both closed conformation and substrate/ligand free. However, due to 2JG4 gaps and mutations, several structures were selected to improve modelling quality, prioritizing those structures obtained with the best resolution and coverage. The 3D structure of human IDE, not yet reported experimentally in the conformational state of interest, was calculated by homology modeling, using reference structures from the PDB with high sequence identity identified with BLAST.

III.8.2. Designation of 3D models.

Homology-generated 3D models of canonicals IDEs of *Homo sapiens* and *Mus musculus* were calculated as well as for the exon 15b spliceoforms for both species, due to the non-existence, to our knowledge, of structures for these alternative splice isoforms reported experimentally.

The following systems were addressed:

 - hIDE15a: Monomeric structure of canonical human (*Homo sapiens*) IDE with the sequence downloaded from UniProt and generated by homology from the multiple template alignment.

- mIDE15a: : Monomeric structure of canonical murine (*Mus musculus*) IDE with the sequence downloaded from UniProt and generated by homology from the multiple template alignment.

- hIDE15b: : Monomeric structure of alternative exon 15b isoform of human (*Homo sapiens*) IDE with the sequence downloaded from UniProt and generated by homology from the multiple template alignment.

- mIDE15b: Monomeric structure of alternative exon 15b isoform of murine (*Mus musculus*) IDE with the sequence manually corrected from the canonical downloaded from UniProt and generated by homology from the multiple template alignment.

III.8.3. Homology modeling.

The molecular models used in the present study were obtained by homology modeling, a valid method to generate three-dimensional models comparable to experimentally solved structures [85]. For this purpose, the spatial constraint satisfaction technique was used with the Modeller program [86,87], v. 10.2.

This tool uses optimization techniques to satisfy the spatial constraints resulting from the sequence alignment between the problem protein and those designated as templates. Here, the spatial constraints are obtained from two sources: (I) homology derivatives coming from the templates sequence related to distances and dihedral angles of the problem sequence and (II) stereochemical constraints such as bond distance and bond angle that are obtained from the CHARMM 22 [88-90] force field of Molecular Mechanics (MM) for proteins. The statistically most probable values of dihedral angles and non-bonding atomic distances are incorporated from a sample of all known proteins.

A set of 10 models was generated with all atoms included. Each model was optimized by Variable Target Function Method (VTFM) with the Conjugate Gradient (CG) algorithm and refined by Molecular Dynamics (MD) with simulated annealing [87] to minimize violations of the established spatial constraints. The model in each set with the lowest Discrete Optimized Protein Energy (DOPE) value was selected by employing the DOPE-HR method using the standard Modeller energy function [86,87].

40

Each of the selected models was inspected ensuring fidelity to the template structure in key structural aspects such as zinc binding and classical domains formation. Special attention was also paid to the internal location of water molecules responsible for the nucleophilic attack involved in the proteolytic activity.

III.8.4. Internal cavity hydration.

The locations of water molecules in the internal cavities of the IDE isoforms under study were calculated using the DOWSER tool [91].

The above allowed evaluation of protein internal cavities in terms of interaction energy to locate interacting water molecules with surrounding atoms within the 3D structure of the catalytic site [92]. Specifically, only cavities with interaction energies less than -12 kcal/mol were hydrated within the protein matrix. On the other hand, the DOWSER program allowed a considerable reduction in computational times by facilitating faster convergences of the systems to a given hydration state compared with simulations that do not use that tool [92,93].

III.8.5. Calculation of pKa values and estimation of protonation states of amino acid residues with dissociable groups.

The pKa values of the dissociable of the IDE isoforms to be studied were calculated using the PropKa tool [94] in its version 2.0 [95]; all atoms were included in the calculation and the presence of the zinc ion was considered. Also, PropKa was used to calculate protein stability as a function of pH [96].

Finally, the protonation states of all dissociable residues were assigned by visual inspection and pKa values computed, considering experimentally reported pH values for hepatocytes cytoplasm [97-100].

III.8.6. Structural validation.

Several tools were used to check the quality of the 3D structures studied. The compatibility between sequences and three-dimensional structures was evaluated with Verify-3D [101], the conformation of the peptide axis of the proteins was inspected with the Ramachandran map (Psi/Phi) [102], obtained from the analysis with Procheck [102-104], the packing quality of the three-dimensional structures, was

analyzed by Z-score value calculations via the WHAT_CHECK tool [105], the quality of the non-bonding atomic interaction patterns was evaluated with ERRAT2 [106], and the three-dimensional quality was assessed with ProSA [107,108] using knowledge-based average strength potentials.

Verify-3D, Procheck, WHAT_CHECK, and ERRAT2 were run online from the SAVES [109] (Structure Analysis and Verification Server) site at the University of California, Los Angeles (UCLA). ProSA was run from the ProSA-web online service [107,110]. Also, VMD (Visual Molecular Dynamics) [111-113] v.1.9.4 was used to calculate the root mean square deviation (RMSD) between the homology-derived models and the corresponding templates. In addition, VMD was used to analyze other structural properties of the systems and perform the graphical representations.

III.8.7. Quantification of hydrogen bonds.

Hydrogen bonds constitute one of the most important non-bonding interactions in the stabilization of the three-dimensional structure of proteins, in addition to the fact that networks formed by them participate in the functional dynamics of these macromolecules [114,115]. Therefore, any variation in the number of such interactions constitutes an indicator to be considered when evaluating both stability and complexity of the systems studied.

After optimization of the generated systems with MM, the hydrogen bonds in each structure were identified using VMD v.1.9.4. A distance of 3.5 Å [116] and an angle of 25 degrees were used as cut-off points.

III.9. Seahorse analysis.

In order to evaluate the effect of IDE loss of function over cell respiration and energetic phenotype, we performed Seahorse XF Cell Mito Stress Tests (Agilent Technologies, USA) in AML12-shRNA-IDE and controls cells. The experiments were performed using a Seahorse XFe24 Analyzer (Agilent Technologies, USA) which measure the oxygen consumption rate (OCR) and extracellular acidification rate (ECAR) of live cells in a 24-well plate format.

OCR and ECAR rates are key indicators of mitochondrial respiration and glycolysis as well as adenosine triphosphate (ATP) production rate, and together these measurements provide a systems-level view of cellular metabolic function in cultured cells.

The Seahorse XF Cell Mito Stress Test Kit uses modulators of cellular respiration that specifically target components of the electron transport chain (ETC) to reveal key parameters of metabolic function. The compounds, oligomycin, carbonyl cyanide-p-trifluoromethoxyphenylhydrazone (FCCP), and a mix of rotenone and antimycin A, are serially injected to measure ATP-linked respiration, maximal respiration, and non-mitochondrial respiration, respectively. Proton leak and spare respiratory capacity are then calculated using basal respiration and these parameters.

After basal measures, oligomycin is injected in order to inhibit ATP synthase. This will significantly reduce electron flow through the electron transport chain and therefore reducing OCR. Some electron flow is expected to remain occurring due to proton leak, a natural mitochondrial uncoupling. After measuring in this state, FCCP is injected, which acts as a potent uncoupling agent disrupting ATP synthesis by dissipating proton gradient through the mitochondrial membrane before it can be used to provide the energy for oxidative phosphorylation. This augments at to its maximum the OCR due to the overregulation of the ETC. Rotenone and antimycin A are then injected. They are inhibitors of complex I and III of the ETC, respectively, and, combined, virtually abolish all ETC function. This allows to measure the OCR of non-mitochondrial origin.

III.10. Statistical analysis.

Statistical analysis was performed using Prism v. 9.0.0 (GraphPad Software, San Diego., USA). The normality of the data was checked with the Kolmogorov-Smirnov test. Data are presented as means ± SEM. Comparisons between two groups were performed using Student's t-test for unpaired data. Comparisons between more than two groups were performed using one-way or two-way ANOVA followed by Bonferroni post-hoc test for parametric data and Kruskal-Wallis test for nonparametric data. Bivariate analyses were performed using the Pearson's

correlation coefficient for parametric variables and Spearman's rank correlation coefficient for correlations with at least one nonparametric variable. Differences were considered significant at $p<0.05$.

III.11. Available means.

This research project was carried out in the Laboratory of the Group for the Study of the Physiopathology of Metabolic Diseases of the Institute of Biology and Molecular Genetics (IBGM), University of Valladolid-CSIC. This laboratory has equipment for routine molecular and cellular biology tasks (heating plates, thermostatized baths, pipettes, microcentrifuges, etc) and desktop computers for basic *in silico* analyses.

In terms of equipment and infrastructure, the IBGM has a distilled and bi-distilled water system, ice machine, autoclave, cold chamber, liquid nitrogen tanks, -80ºC and -20ºC freezers, cell culture room (incubators, cabinets, bathrooms, microscope, etc), microscopy room (microscopes and confocal), genomics room (thermal cyclers, DNA sequencers, LightCycler® 480 system), proteomics room (image analysis system, HPLC, protein purification equipment, and automated plate readers), centrifugation and ultracentrifugation room, Seahorse equipment, etc.

IV. Results

IV.1. Transcriptional and posttranscriptional regulation of insulin-degrading enzyme by fasting and feeding and HFD.

IV.1.1. Metabolic responses to the transition fasting-refeeding in mice fed SD or HFD.

Mice fed HFD exhibited a ~18% increased body weight compared to those fed SD (**Fig. 16 A**) in parallel with glucose intolerance and insulin resistance (**Fig. 16 B-D**).
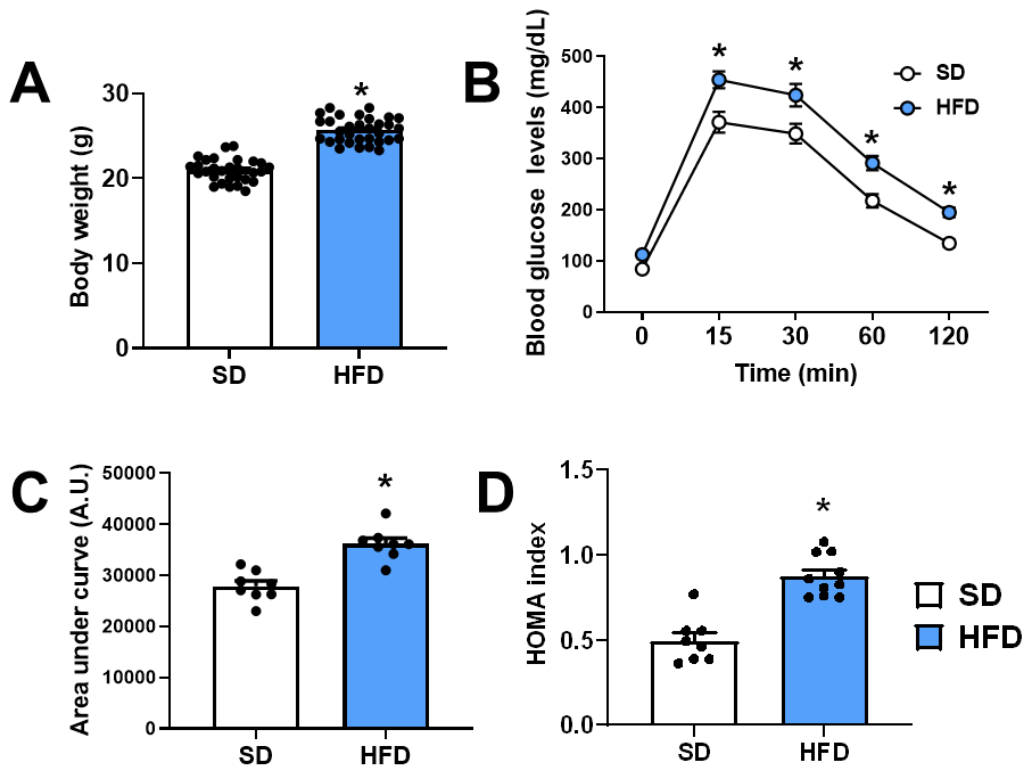
Figure 16. Mice fed HFD exhibit overweight, impaired glucose homeostasis and insulin resistance. **A.** Body weight of mice fed SD or HFD for 8 weeks. Data are mean ± SEM. N=29/32 mice per condition. *p<0.05 vs. SD. **B.** Intraperitoneal glucose tolerance (ipGTT) in mice fed SD or HFD for 8 weeks. **C.** Area under the curve (AUC) of the ipGTT. **D.** HOMA index. Data are mean ± SEM. N=8 mice per condition. *p<0.05 vs. SD.

Mice fed SD and HFD were randomly assigned to fasting and refeeding groups maintaining the body weight difference in each nutritional state (**Fig. 17 A**). During refeeding there were no difference in caloric intake rates between the groups fed SD or HFD, noting that in the 30 min refeeding state caloric intake rate was higher than after 3h for both dietary conditions (**Fig. 17 B**). Refeeding in mice fed both SD and HFD, augmented blood glucose and plasma insulin levels, measured 30 min and 3 h after refeeding. In addition, plasma insulin levels were still increasing

3 h after refeeding in the HFD group (**Fig 17 C-D**). Mice fed the HFD had relative hypoglucagonemia in fasting state compared with the SD mice. (**Fig. 17 E**).

Plasma cholesterol levels were increased (~30%) by the HFD consumption but they were not modified by fasting-feeding transition in either diet group (**Fig. 17 F**). Plasma triglycerides levels were decreased (~10%) by refeeding in both fed states in the SD group, however in mice fed HFD those levels remained similar to the fasting state (**Fig. 17 G**). In response to 3 h refeeding, non-esterified fatty acids (NEFA), glycerol, and lactate levels were significantly increased in mice fed SD (**Fig. 17 H-J**).
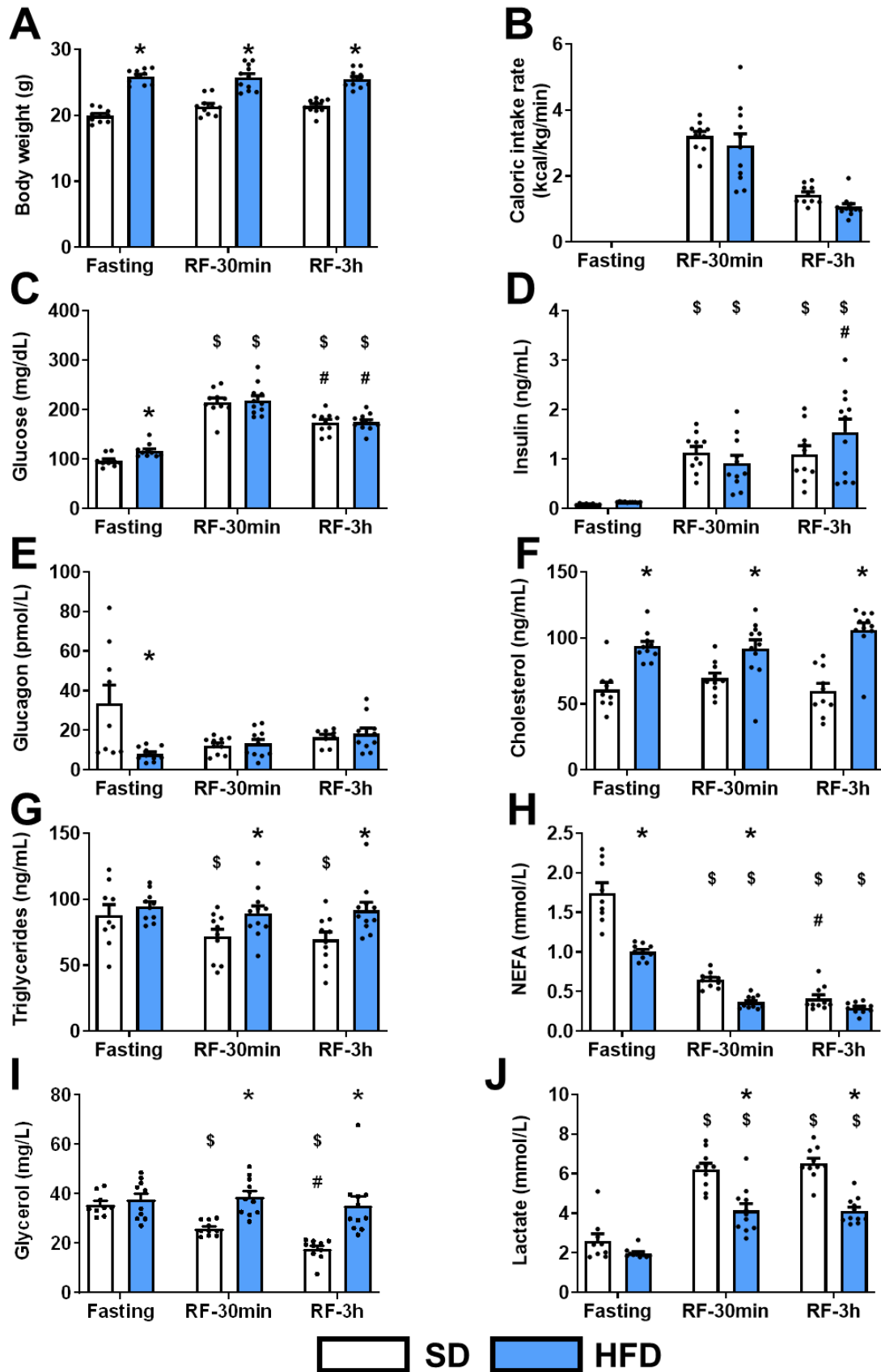
Figure 17. Metabolic responses to fasting or refeeding in mice fed SD or HFD. Data are mean ± SEM. * $p<0.05$ *vs.* SD; $ $p<0.05$ *vs.* Fasting; and # $p<0.05$ *vs.* Refeeding by two-way ANOVA.

IV.1.2. Liver IDE protein levels and activity.

To investigate the impact of the fasting-feeding transition on hepatic IDE regulation, C57BL/6J mice were fed a SD or HFD for 8 weeks. When comparing nutritional states within each of the dietary conditions, IDE protein levels showed no significant variations by fasting or refeeding (**Fig 18 A-C**).
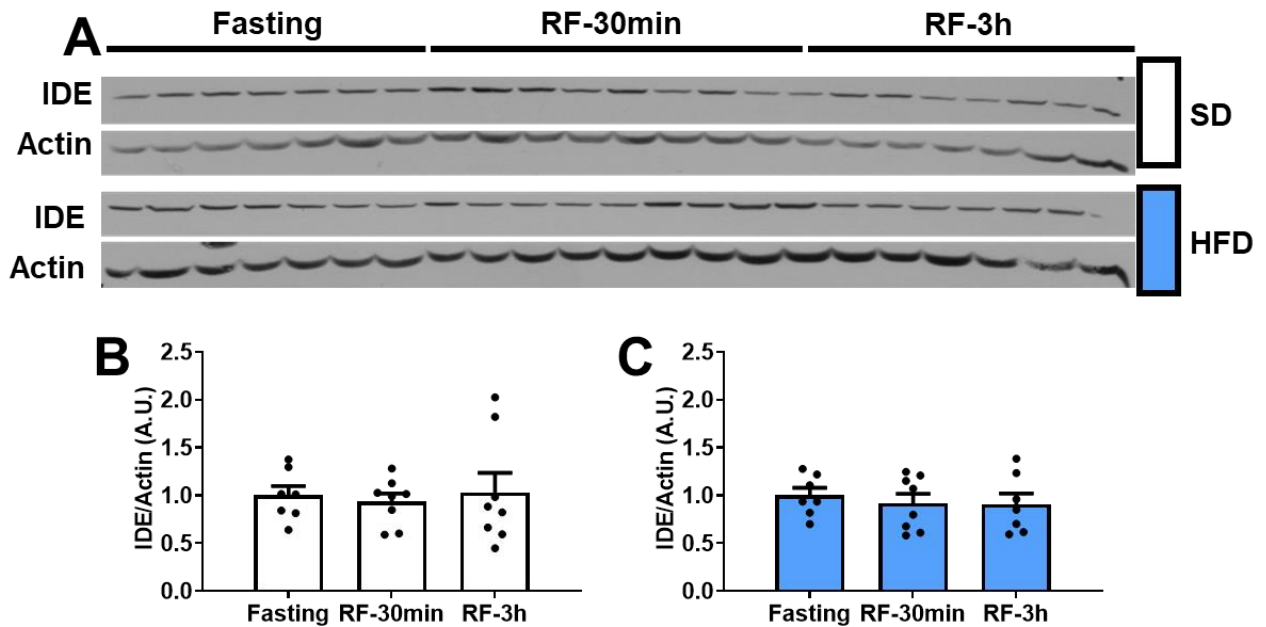
Figure 18. **Regulation of hepatic levels of IDE protein by fasting-feeding transition. A.** IDE and actin blots. **B.** Protein levels of SD-fed mice livers. **C.** Protein levels of HFD-fed mice livers. Densitometric analyses of IDE were performed using blots depicted in A, and data were plotted for each diet and nutritional state. Data are mean ± SEM. N = 7 - 8 mice per condition.

Then, we compared both dietary condition in each nutritional state. Interestingly, in fasting, protein levels of IDE were downregulated by ~30% but in refeeding of 30 min, IDE protein levels were upregulated by ~30%, both in mice fed HFD as compared to SD (**Fig. 19 A-B**). To further investigate posttranscriptional regulation of IDE levels, we performed bivariate analyses between IDE levels and metabolic parameters. As shown in **Fig. 19 C-D**, under fasting conditions body weight and plasma glucagon levels correlated inversely and directly, respectively, with hepatic IDE levels. On the other hand, under refeeding of 30 min conditions, body weight and plasma glycerol concentration directly correlated with IDE levels, whereas NEFA inversely correlated. These results indicate that changes in body weight, glucagon and metabolites (glycerol and NEFA) levels are able to predict hepatic IDE levels.

50
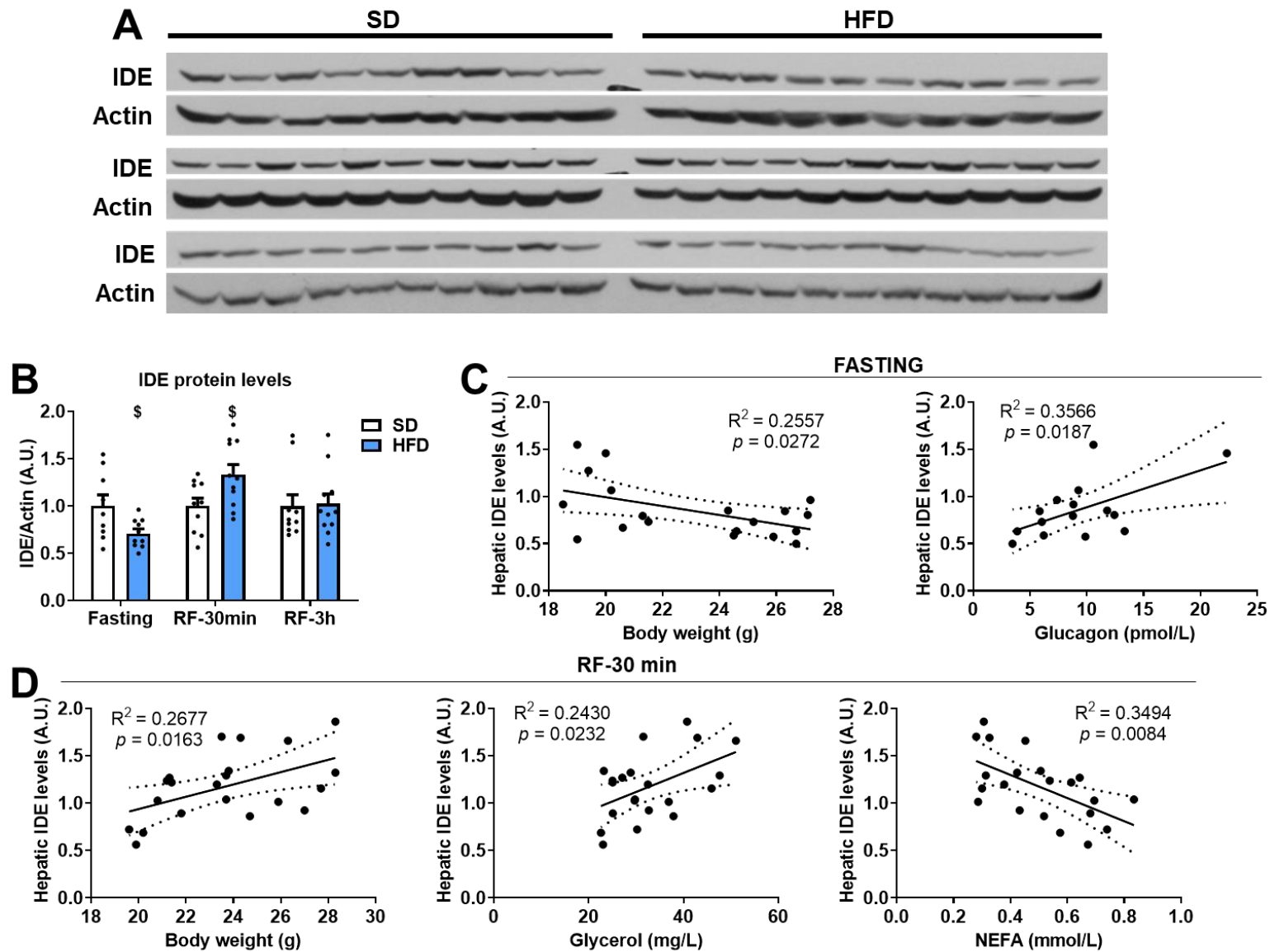
Figure 19. Regulation of hepatic levels of IDE protein by diet. A. IDE and actin blots. **B**. Protein levels. Densitometric analyses of IDE were performed using blots depicted in A, and data were plotted for each nutritional state and diet. Data are mean ± SEM. N = 9 - 11 mice per condition. $^{\$}$p<0.05 *vs*. SD by ANOVA. **C-D.** Regression analyses indicating the correlation coefficient (R^2) between hepatic IDE levels and fasting body weight and plasma glucagon (**C**) and refeeding 30 min body weight, plasma glycerol and plasma non-esterified free fatty acids (NEFA) (**D**).

In addition, we assessed hepatic IDE activity in response to metabolic adaptations to nutritional changes. Refeeding increased IDE activity in mice fed SD and HFD (**Fig. 20 A**). Bivariate analyses between IDE levels and metabolic parameters showed that IDE activity was inversely correlated with NEFA, but directly correlated with lactate, glucose and insulin levels (**Fig. 20 B-E**). Surprisingly, plasma lactate levels showed stronger correlation than circulating insulin (R^2= 0.388 *vs.* 0.209).
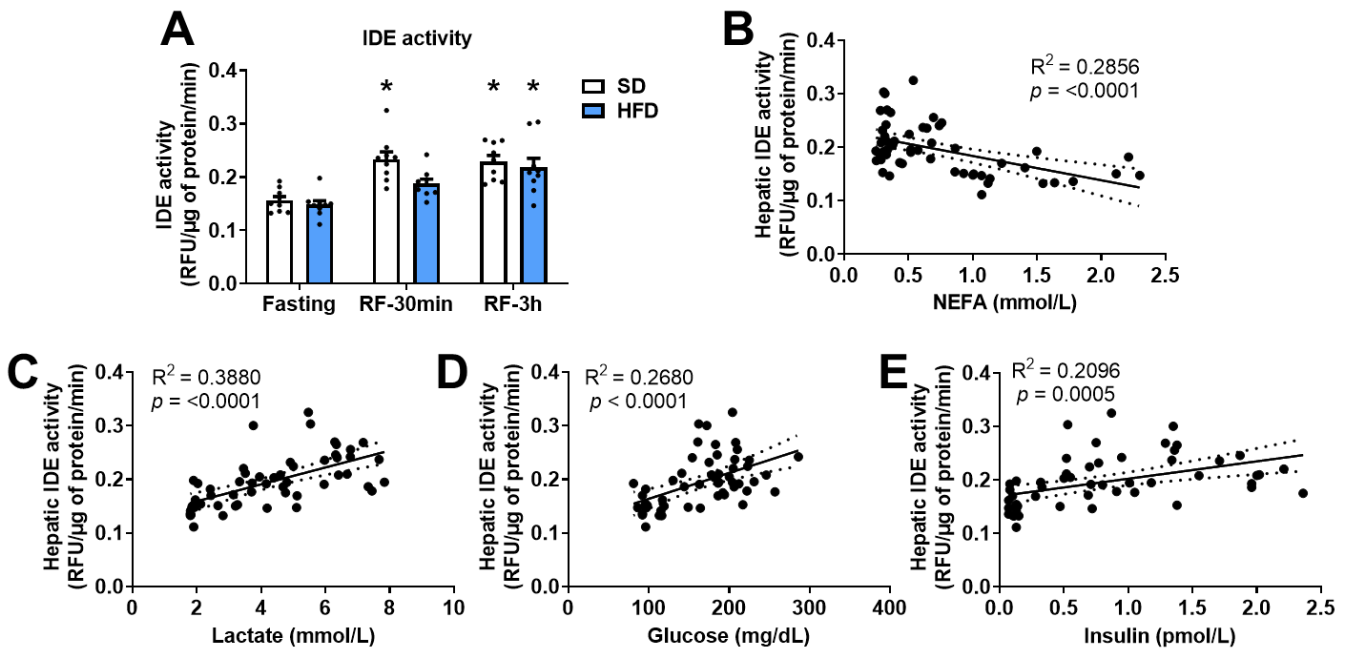
Figure 20. Effects of the nutritional status on hepatic IDE activity. A. Liver extracts from mice fed SD or HFD under fasting and non-fasting conditions were assessed for IDE activity. Data are mean ± SEM. N = 9 mice per condition. * $p<0.05$ *vs.* Fasting by ANOVA. Regression analyses indicating the correlation coefficient (R^2) between hepatic IDE activity and plasma NEFA (**B**), lactate (**C**), glucose (**D**), and insulin (**E**).

Taken together these results suggest that metabolites (NEFA, lactate, and glucose) and insulin levels are main regulators of hepatic IDE activity in response to nutritional adaptations to refeeding.

IV.1.3. Reduced hepatic IDE levels but not activity associates with insulin resistance.

We showed that HFD feeding led to insulin resistance and glucose intolerance in mice (**Fig. 16**). To further analyze the relationship between IDE and insulin

resistance, we performed bivariate analyses between hepatic IDE levels in fasting conditions and the HOMA index. As shown (**Fig. 21**), there is an inverse correlation between IDE protein levels and insulin resistance. Interestingly, no significant correlations between IDE activity and HOMA index were found. Taken together, these data indicate that fasting reduced hepatic IDE levels by ~30%, which associates with whole-body insulin resistance.
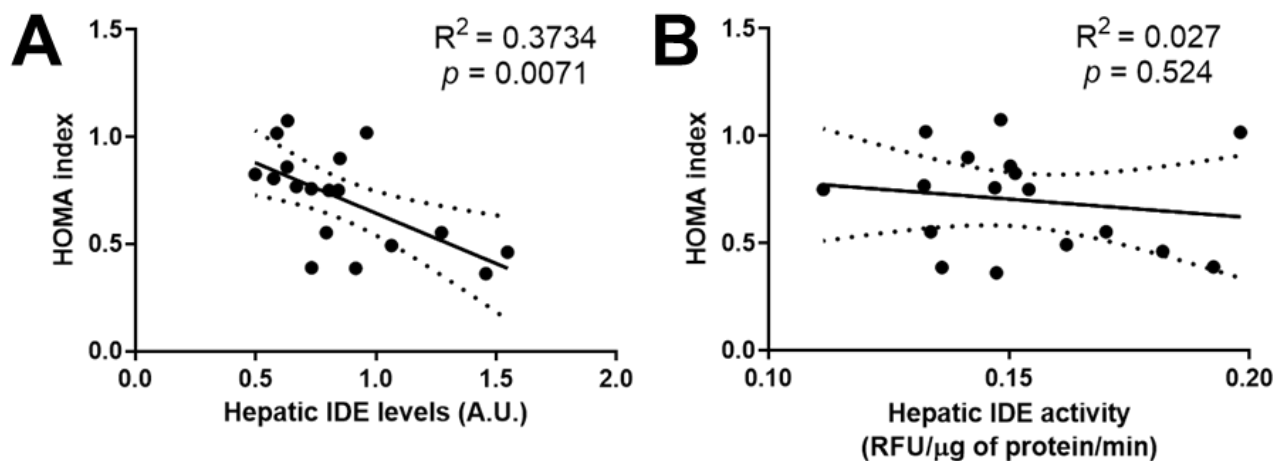
Figure 21. Hepatic IDE protein levels correlate with insulin resistance. Protein and activity levels in fasting conditions were assessed in mice fed SD or HFD as described in Materials and Methods. Regression analyses indicating the correlation coefficient (R^2) between hepatic IDE protein levels (**A**), or hepatic IDE activity (**B**) and HOMA index.

IV.1.4. Regulation of Ide at transcriptional level.

Neither fasting nor refeeding affected hepatic *Ide* gene mRNA expression in mice fed SD. In contrast, *Ide* gene expression was upregulated (~2-fold) by 3 h refeeding in mice fed HFD (**Fig. 22 A**). This transcriptional upregulation of *Ide* was not paralleled with changes in protein levels (**Fig. 19 A-B**) or activity (**Fig. 20 A**). Farris and colleagues reported two human IDE splice isoforms in which exon 15a is replaced by exon 15b, with significantly lower catalytic efficiency [117]. To further investigate changes in IDE activity in response to refeeding conditions, we determined the abundance of exons 15a and 15b by quantitative PCR in liver of mice fed SD or HFD. For the first time, we identified both exons in mice *Ide* gene sequence and generated specie-specific primers discriminating mouse mRNAs containing either exon 15a or exon 15b (**Fig 22 B**). Therefore, we found the basal expression of the 15a splice isoform was ~1000-fold higher that the isoform 15b (**Fig. 22 C-D**). However, the increased hepatic IDE activity during refeeding was

53

neither associated with reduced expression of the 15b isoform, nor to augmented *Ide-15a*/*Ide-15b* ratio (**Fig. 22 D-E**). If anything, *Ide-15b* expression was ~2-fold augmented by 3 h of refeeding in SD. We also reported the 1D-3D structure of exons 15a and 15b amino acids translation into IDE isoforms. (**Fig 22 F-G**).
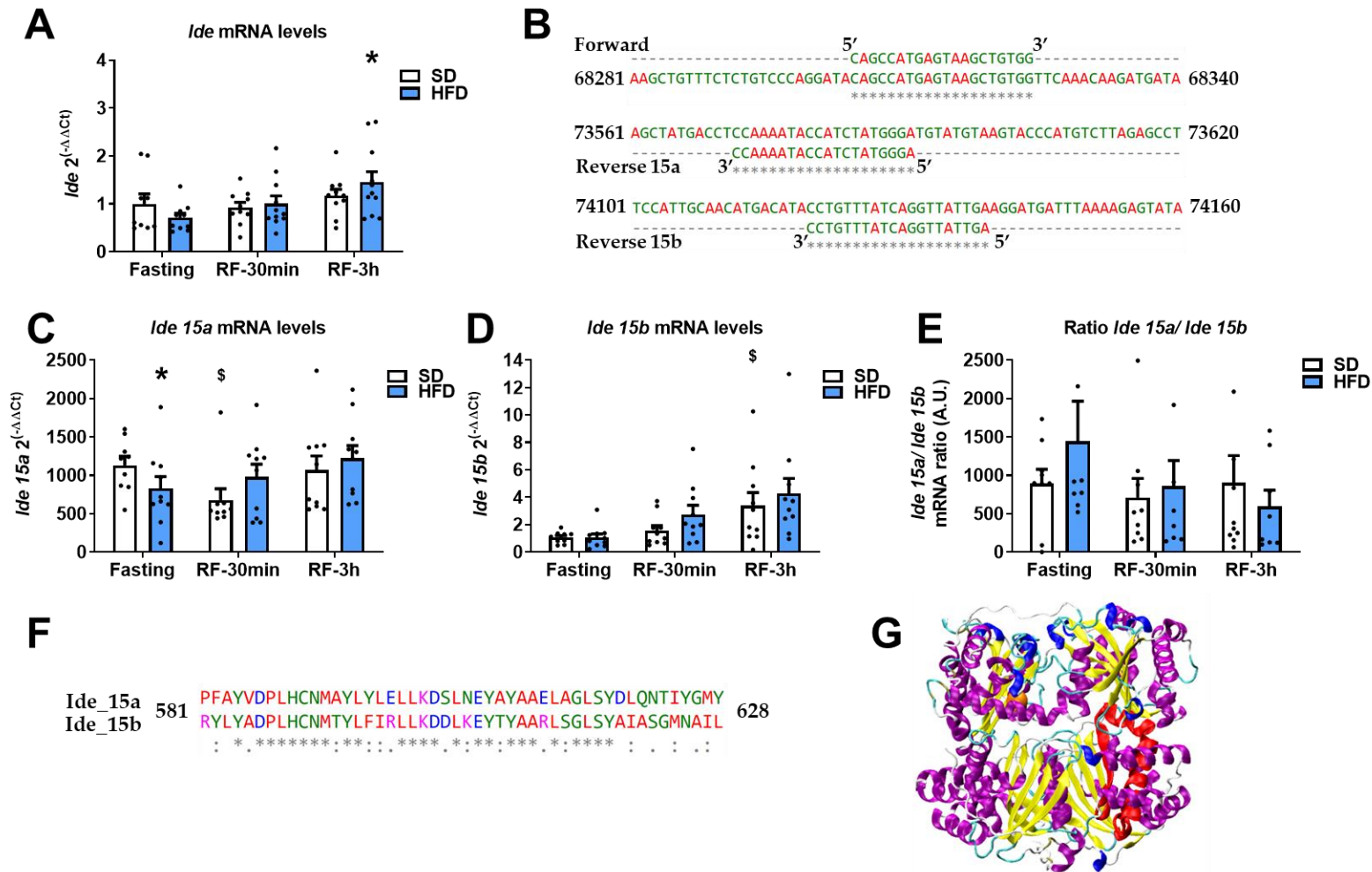
Figure 22. Measure of transcriptional regulation of IDE expression. A. Livers from mice fed SD or HFD under fasting and non-fasting conditions were analyzed for mRNA levels of *Ide*. Data are mean ± SEM. N= 9-11 mice per condition. * $p<0.05$ *vs.* Fasting by ANOVA. **B.** Alignment of forward and reverse primers to mouse *Ide* gene sequence (NC_000085.7:c37341664-37246140). **C.** Levels of *Ide 15a* mRNA in the liver. * $p<0.05$ *vs.* SD and $ $p<0.05$ *vs.* Fasting by ANOVA. **D.** Levels of *Ide 15b* mRNA in the liver $ $p<0.05$ vs. Fasting by ANOVA. **E.** Ratio *Ide 15a/ Ide 15b*. **C, D, E.** Data are mean ± SEM. N= 9 mice per condition. **F.** Alignment of the amino acid's translations of exons 15a and 15b for mouse IDE isoforms. **G.** 3D structure of a mouse IDE model portraying in **red** the exon 15-related residues position.

IV.1.5. Lactate and IDE activity.

As described above, we found a direct correlation between circulating lactate levels and hepatic IDE activity. To further investigate whether this association was due to a causal relationship, we incubated lysates obtained from fasted livers (of the group of mice fed SD), or purified human recombinant IDE, with lactate levels that mimic those in circulation (**Fig. 17 J**). In a concentration-dependent manner, lactate increased IDE activity (~ 20-30 %) in liver lysates (**Fig. 23 A**), but had no significant effects on activity of purified IDE (**Fig. 23 B**). Of note, IDE activity levels observed *in vitro* (**Fig. 23 A**) are similar to those observed *in vivo* (**Fig. 20 A**). Taken together, these results demonstrate that lactate indirectly regulates hepatic IDE activity, lending support to the notion that the observed correlation between circulating levels of lactate and hepatic IDE activity was due to a cause-effect relationship.
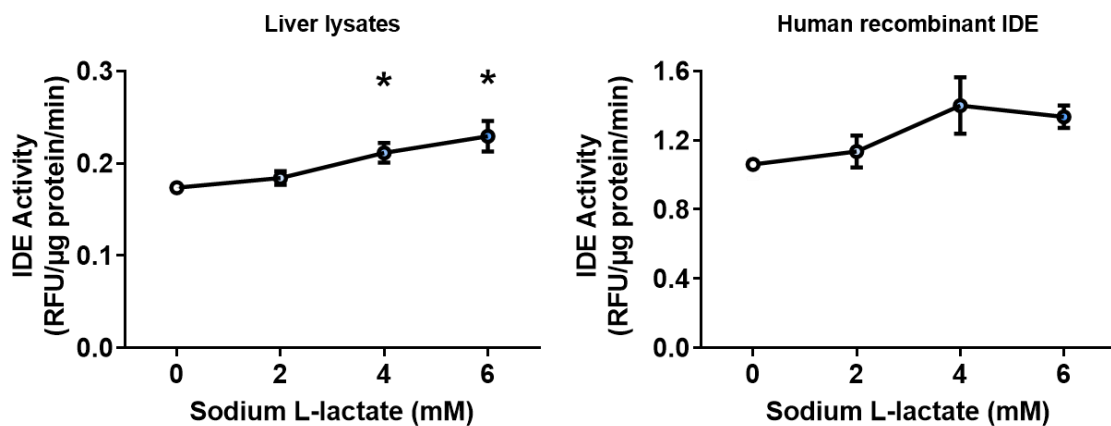
Figure 23. Effects of lactate on IDE activity. A. IDE activity in the absence or presence of different concentrations of lactate in lysates from fasted livers of the group of mice fed SD for 8 weeks. Data are mean ± SEM. N= 3 livers of mice per condition in duplicate. *$p < 0.05$ vs. no lactate by ANOVA. **B.** Activity of purified human recombinant IDE in the absence or presence of different concentrations of lactate. Data are mean ± SEM. N= 3.

IV.1.6. Section summary.

In summary, below we present the main findings of this section:

- NEFA, lactate, glucose, and insulin levels are main regulators of hepatic IDE activity in response to nutritional adaptations to refeeding.

- There is an inverse correlation between IDE protein levels and insulin resistance, but no significant correlations between IDE activity and HOMA index were found.

- For the first time, we identified both exons in mice *Ide* gene sequence and generated specie-specific primers discriminating mouse mRNAs containing either exon 15a or exon 15b, but the increased hepatic IDE activity during refeeding was neither associated with reduced expression of the 15b isoform, nor to augmented *Ide-15a*/*Ide-15b* ratio.

- In a concentration-dependent manner, lactate increased IDE activity (~ 20-30 %) in liver lysates but had no significant effects on activity of purified IDE.

IV.2. Role of IDE activity on the recovery of hepatic insulin resistance.

Given IDE's potential role in T2DM, there has been considerable interest in the development of IDE inhibitors as therapeutics in diabetic patients, with controversial results regarding their application as modulators of insulin clearance and glucose tolerance (reviewed in [18]). Yet, the approach treating diabetes by pharmacological activation of IDE has received much less attention.

In marked contrast to previous thinking, we found that overexpression of IDE in liver resulted in improved insulin sensitivity and glucose homeostasis in diet-induced mice [71], suggesting that the development of IDE activators, rather than IDE inhibitors, may be a viable pharmacological approach for the treatment of diabetic patients. In this thesis, we have investigated the potential pharmacological use of sPIF for improving hepatic insulin sensitivity in primary mouse hepatocytes from a mouse model of T2DM.

IV.2.1. Concentration-dependent effects of sPIF on IDE activity in hepatocytes

In order to investigate the effect of sPIF on IDE activity, hepatocytes from a human cell line (HepG2) were pre-incubated in the absence or presence of sPIF at different concentrations for 4 h, followed by IDE activity assessment. In a concentration-dependent manner, sPIF increased IDE activity by ~20-35% (**Fig. 24**).

IDE activity in HepG2 cells
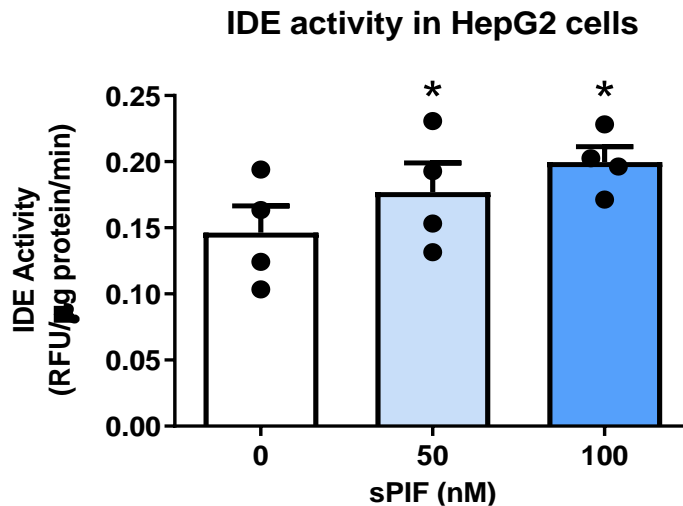
Figure 24. Effects of sPIF on IDE activity in HepG2 cells. Cells were pre-incubated in the presence or absence of sPIF at the indicated concentrations for 4 h and IDE activity was determined. Data are mean ± SEM. n = 4 for condition. *$p < 0.05$ vs. untreated cells by one-way ANOVA.

To further demonstrate the effects of sPIF on IDE, we knock-downed *Ide* expression in a murine hepatocyte cell line (AML12) using an shRNA specific for *Ide* mRNA.

IV.2.1.1. Generation of AML12-shRNA-IDE cells.

Using a lentiviral vector, we transduced AML12 cells with a gene encoding for an shRNA specific for *Ide* mRNA in parallel with the transduction using an empty vector as control. We used puromycin and GFP expression as selective condition and transduced cells verification, respectively (**Fig. 25**).
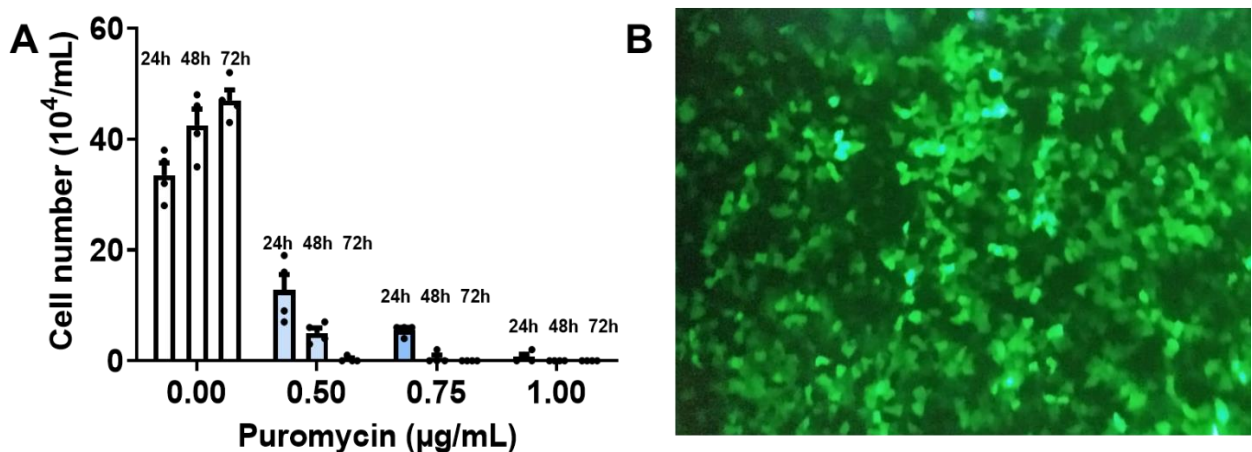
Figure 25 Selection of AML12 cells transduced with control and IDE specific shRNA. A. Lethality of puromycin concentrations for AML12 untransduced cells. **B.** GFP expression of effectively transduced cells.

As shown, (**Fig. 26**), *Ide* gene and IDE protein expression were reduced by ~50%, in parallel with a similar decreased in its specific activity.
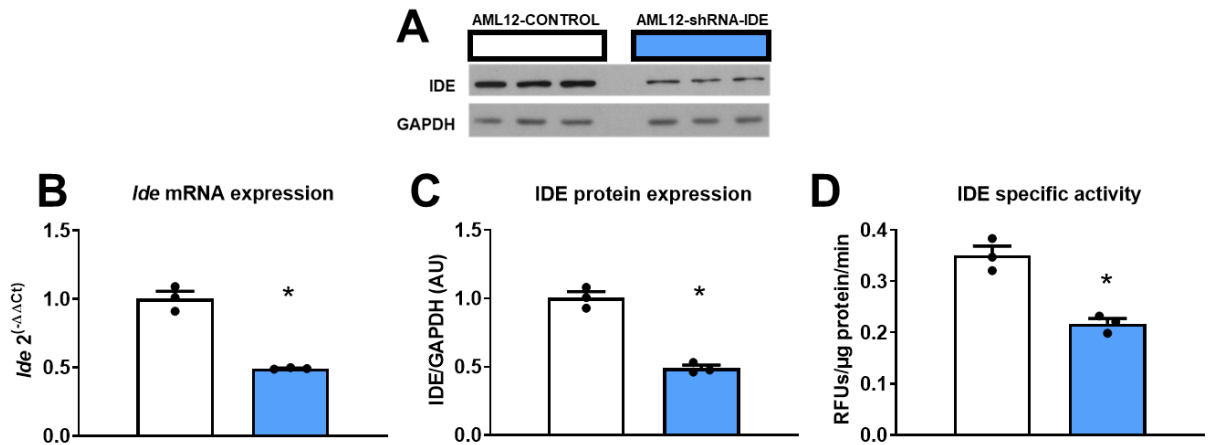
Figure 26. Knockdown of IDE in mouse hepatocytes cell line. AML12 cells were transduced with a lentivirus containing *Ide* specific and control shRNA. **A.** IDE protein levels in control and AML12-shRNA-IDE. **B.** *Ide* mRNA expression **C.** IDE protein levels quantified by densiometric analyses of blots depicted in A. **D.** IDE activity assessed in AML12-shRNA-IDE and AML12-CONTROL cell lysates. Data are mean ± SEM. N=3 for condition. *$p < 0.05$ vs. control cells by Student's t-test.

In AML12-CONTROL cells, sPIF augmented IDE activity by ~50%, confirming the effects seen in HepG2 cells. Surprisingly, sPIF was able to restore IDE activity under conditions of IDE knockdown to similar levels seen in sPIF-treated control cells (**Fig. 27**). These results demonstrate that sPIF was able to increase IDE activity in hepatocytes, even in the scenario of reduced IDE protein levels.
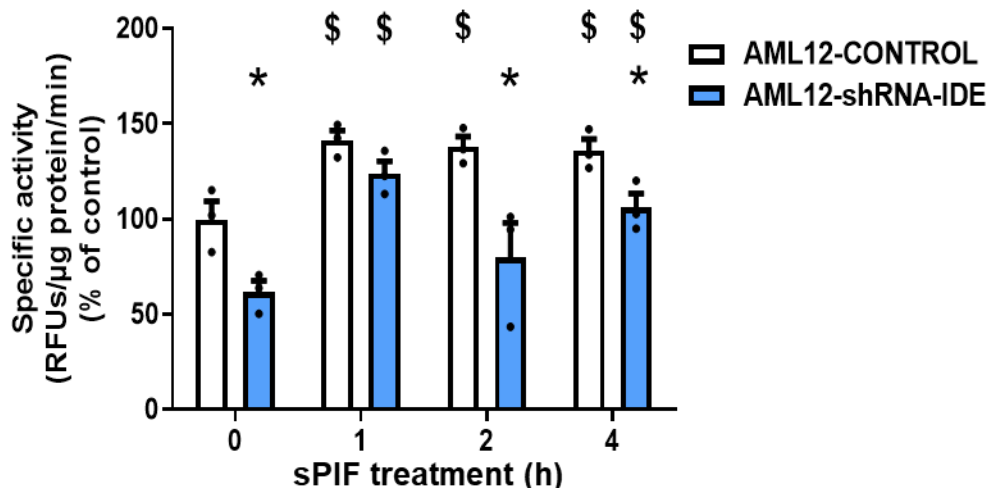
Figure 27. Effects of sPIF on IDE activity in IDE-deficient AML12 cells. AML12-CONTROL and AML12-shRNA-IDE cells were pre-incubated in the absence (control) or in the presence (100 nM) of sPIF for 1, 2 and 4 h. Data are mean ± SEM. n=3 for condition. *$p < 0.05$, vs. AML12-CONTROL by two-way ANOVA. $^{\$}p < 0.05$, vs. control by two-way ANOVA.

IV.2.1.2. Generation and characterization of a diet-induced obese mouse model.

To decipher the contribution of sPIF-mediated activation of IDE to hepatic insulin resistance and β-cells insulin secretion in the setting of obesity, C57BL/6J mice were fed a HFD for 22 weeks. As shown, (**Fig. 28**), mice exhibited a significant increase in body weight, fasting and non-fasting blood glucose levels, glucose intolerance, and higher non-fasting circulating insulin levels as compared to mice fed SD. Taken together, these results indicate that mice fed a HFD were glucose intolerant and insulin resistant.
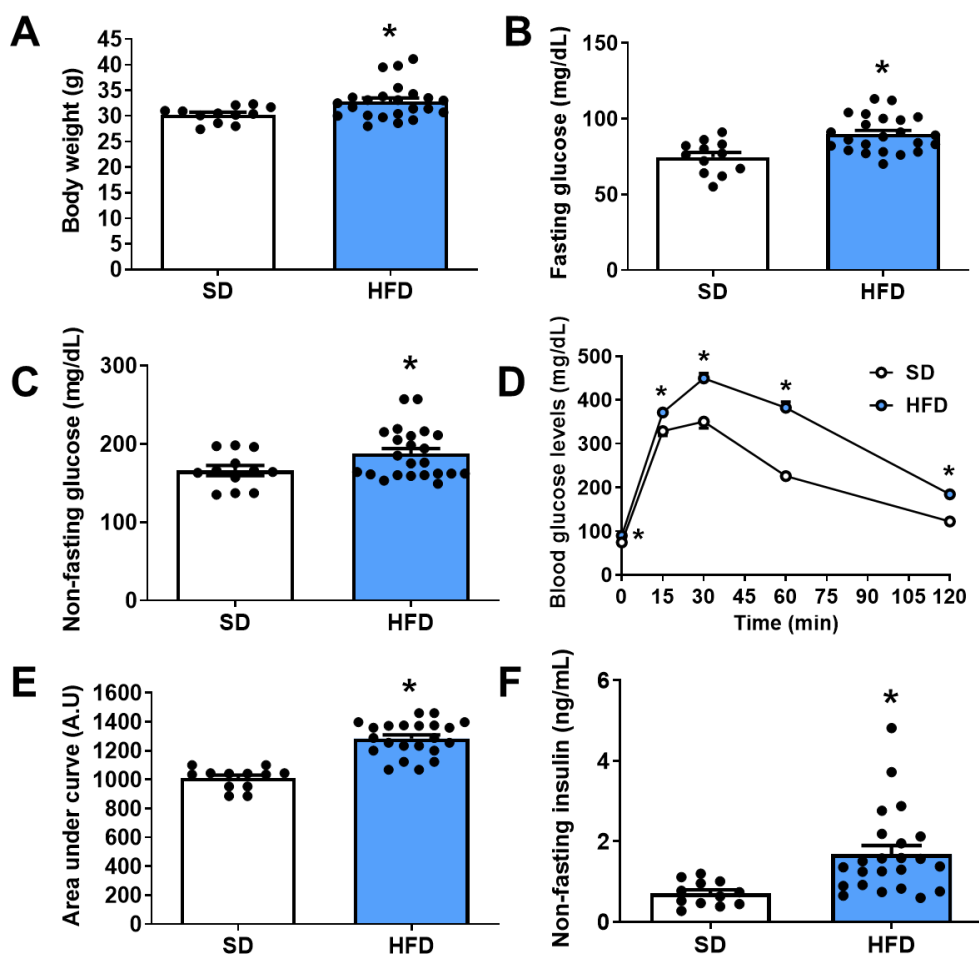
Figure 28. Metabolic features of C57BL/6J mice fed a HFD for 22 weeks. A. Body weight. **B.** Fasting blood glucose levels. **C.** Non-fasting blood glucose levels. **D.** Intraperitoneal glucose tolerance test (ipGTT). **E.** Area under the curve of the ipGTT. **F.** Non-fasting plasma glucose levels. Data are mean ± SEM. N=12 for SD feeding; N=22 for HFD feeding. * $p < 0.05$ *vs.* SD by Student's t-test.

IV.2.1.3. Effects of sPIF-mediated activation of IDE in primary hepatocytes isolated from livers of diet-induced obese mice.

Initial experiments demonstrated that sPIF increased IDE activity in human (HepG2) and murine (AML12) hepatocytes (**Figs. 24 and 27**). Hence, we further investigate if sPIF could increase IDE activity in primary mouse hepatocytes isolated from livers of diet-induced obese mice (**Fig. 28**). Thus, primary hepatocytes were cultured with or without sPIF (200 nM) for 18 h, followed by incubation in the absence (0 min) or in the presence (5, 15, 30 min) of insulin (100 nM).

sPIF treatment did not modify IDE activity in hepatocytes from mice fed SD (SD-sPIF) as compared to control hepatocytes (SD-Control) (**Fig. 29**). Likewise, insulin stimulation did not change IDE activity in SD-Control or in SD-sPIF treated hepatocytes (**Fig. 29**).
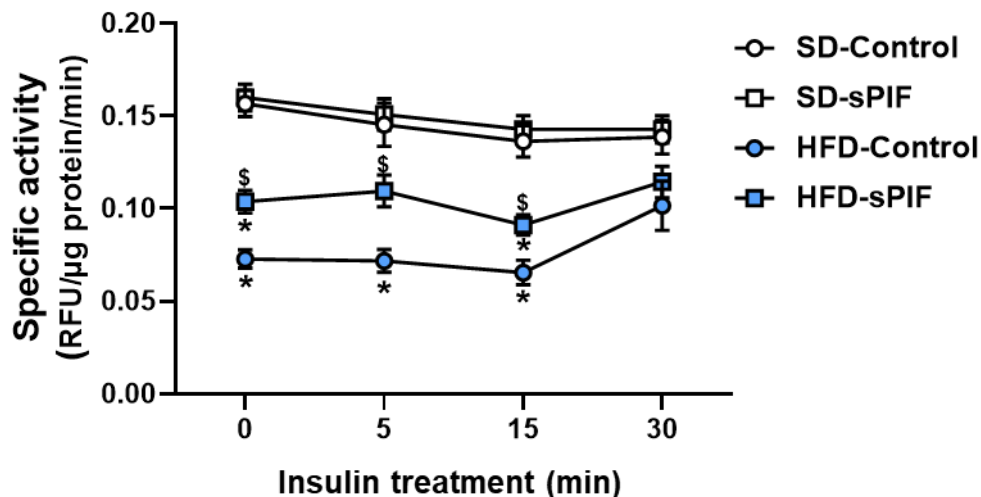
Figure 29. sPIF partially restores IDE activity in primary mouse hepatocytes from diet-induced obese mice. Hepatocytes from mice fed SD or HFD were preincubated in the absence (SD-Control and HFD-Control) or in the presence of 200 nM sPIF (SD-sPIF and HFD-sPIF) for 18 h. Then, hepatocytes were stimulated with 100 nM insulin for 5, 15, and 30 min followed by IDE activity assessment. Data are mean ± SEM. n=3 per condition. * $p < 0.05$, *vs.* SD-Control; $^\$ p < 0.05$, *vs.* HFD-Control by two-way ANOVA.

However, IDE activity was significantly reduced (~55%) in hepatocytes from mice fed a HFD (HFD-Control) as compared to hepatocytes from SD-Control (**Fig. 29**). Importantly, sPIF treatment increased by ~45% IDE activity in HFD-sPIF treated hepatocytes as compared to HFD-Control hepatocytes, although this recovery did not restore those levels seen in SD-Control hepatocytes (**Fig.**

29). Interestingly, after 30 min of stimulation with insulin, IDE activity increased by ~40% in HFD-Control hepatocytes, but this insulin-mediated effect on IDE activity was not observed in HFD-sPIF treated hepatocytes (**Fig. 29**). Taken together, these results demonstrate that sPIF partially restores IDE activity in primary mouse hepatocytes from diet-induced obese mice.

Next, we sought to determine if this partial recovery of IDE activity was sufficient to counteract insulin resistance in hepatocytes isolated from diet-induced obese mice. To this end, we analyzed IDE protein levels, as well as total and phosphorylated levels of protein kinase B (PKB; a critical node in the intracellular signaling pathway of insulin) in primary mouse hepatocytes.

As shown, (**Fig. 30**), IDE levels remained unchanged in sPIF-treated hepatocytes as compared to control hepatocytes from mice fed SD. Likewise, insulin stimulation did not alter IDE levels in SD-Control or in SD-sPIF treated hepatocytes (**Fig. 30 A-B**). In contrast, IDE levels were significantly reduced (~55%) in hepatocytes from HFD-Control as compared to hepatocytes from SD-Control. Neither sPIF nor insulin treatment affected IDE levels in hepatocytes from mice fed a HFD (**Fig. 30 A-B**). Taken together, these results demonstrate that sPIF did not restore IDE levels in primary mouse hepatocytes from diet-induced obese mice.

On the other hand, insulin stimulated phosphorylation of PKB in hepatocytes from SD-Control mice (**Fig. 30 A, C**), although treatment with sPIF did not alter the phosphorylation levels of PKB in SD-Control hepatocytes (**Fig. 30 A, C**). In contrast, a marked reduction (~50%) in phosphorylation levels of PKB was observed in hepatocytes from HFD-Control mice. Additionally, the lower insulin-mediated activation of PKB seen in HFD-Control hepatocytes was not recovered by sPIF treatment (**Fig. 30 A, C**). Taken together, these results demonstrate that sPIF treatment did not overcome insulin resistance in hepatocytes from diet-induced obese mice.
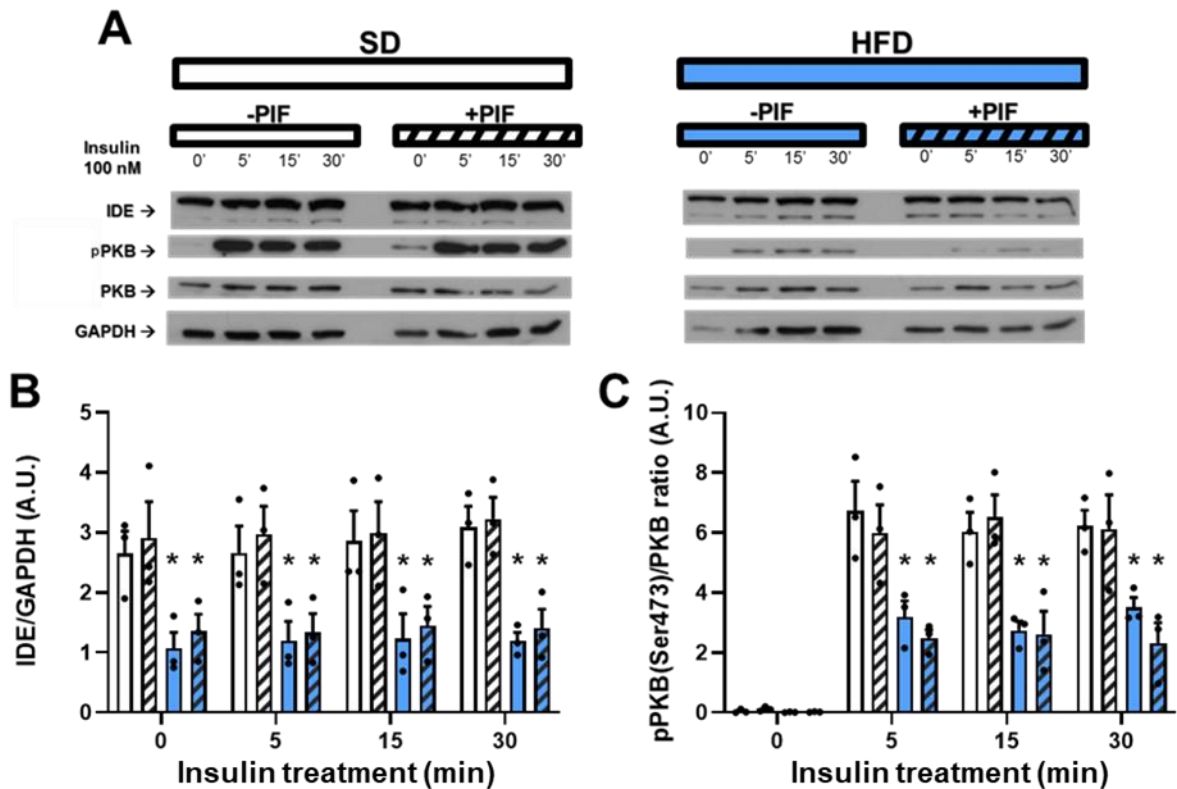
Figure 30. sPIF-mediated activation of IDE is not sufficient for insulin resistance recovery in primary mouse hepatocytes from diet-induced obese mice. Hepatocytes from mice fed SD or HFD were preincubated in the absence (SD-Control and HFD-Control) or in the presence of 200 nM sPIF (SD-sPIF and HFD-sPIF) for 18 h. Then, hepatocytes were stimulated with 100 nM insulin for 5, 15, and 30 min followed by determination of IDE, pPKB and PKB levels. **A.** A representative picture of the western blots is shown. **B.** Quantification of IDE levels. **C.** Quantification of the ratio pPKB/PKB. Data are mean ± SEM. n=3 per condition. *$p < 0.05$ vs. SD by two-way ANOVA.

IV.2.2. Section summary.

In summary, below we present the main findings of this section:

- sPIF was able to increase IDE activity in hepatocytes, even in the scenario of reduced IDE protein levels

- sPIF did not restore IDE levels in primary mouse hepatocytes isolated from livers of diet-induced obese mice.

- sPIF treatment did not overcome insulin resistance in primary hepatocytes isolated from livers of diet-induced obese mice

IV.3. Role of IDE in glucagon signaling in hepatocytes.

IV.3.1. Glucagon signaling in liver specific IDE knockout mice.

As described [70], at 3-month-old, the liver-specific IDE knockout (L-IDE-KO) mouse presented a phenotype including hyperglucagonemia and increased expression of genes coding for PCK1 and G6PC enzymes, and increased subcellular localization of FoxO1 in the nucleus of liver cells [70]. These findings suggest that IDE may play a role on glucagon signaling in the hepatocyte. Thus, we evaluated the glucagon intracellular signaling pathway in mouse hepatocytes under conditions of IDE loss of expression.

IV.3.1.1. Glucagon signaling pathway in L-IDE-KO mouse liver lysates under physiological and high-fat diet feeding conditions.

With liver lysates of 3-month-old male mice under 18-h fasting conditions, in which a predominance of glucagon action is presumed, we were able to verify that there was a decrease (~60%) in glucagon receptor (GCGR) expression in the liver of L-IDE-KO mice as compared to their controls. In addition, there was a decrease in the expression (~40%) of CREB protein as well as its phosphorylation (~50%) with a net decrease in the phosphorylated form of the protein by ~70% in livers of L-IDE-KO mice (**Fig. 31**).
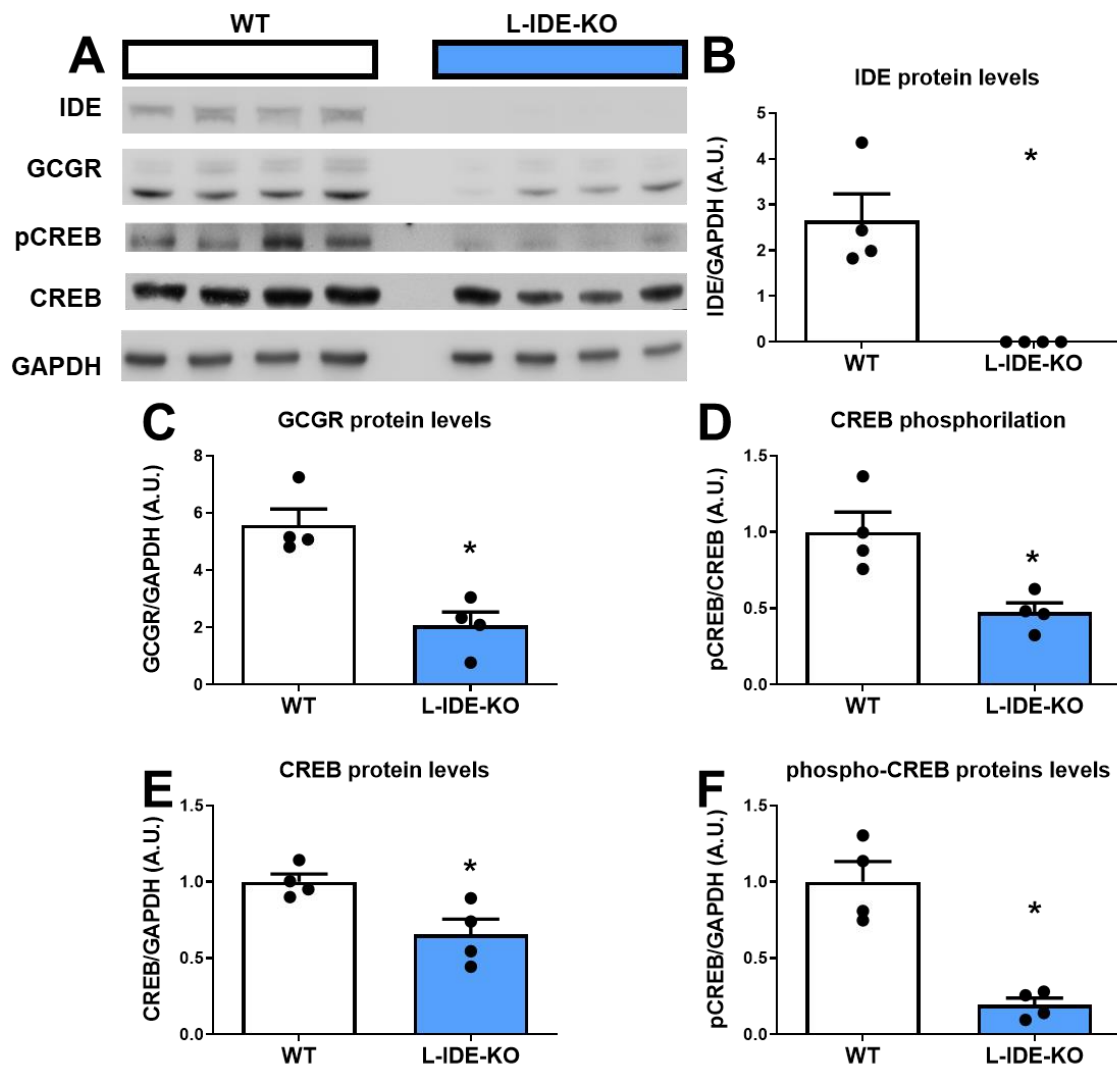
Figure 31. Glucagon signaling in livers of L-IDE-KO mice fed SD. A. Blot panel of proteins assessed. **B**. IDE protein levels. **C**. GCR protein levels. **D**. Ratio phospho-CREB/total CREB levels. **E**. CREB protein levels. **F.** phospho-CREB protein levels. Densitometric analyses of IDE were performed using blots depicted in A, and data were plotted for genotype. Data are mean ± SEM. N = 4 mice per genotype. *p<0.05 *vs.* WT by Student's t-test.

Taking into consideration that the phenotype of insulin resistance in L-IDE-KO mice is exacerbated under conditions of a high-fat diet [71], we evaluated the expression of proteins involved in glucagon signaling in livers of mice fed with HFD for 12 weeks. In this case, decreased glucagon receptor expression (~50%) was corroborated in L-IDE-KO mice fed with HFD relative to their WT littermates fed with HFD (**Fig. 32 A-C**), but there were no differences in CREB protein expression or phosphorylation levels. (**Fig. 32 D-F**)
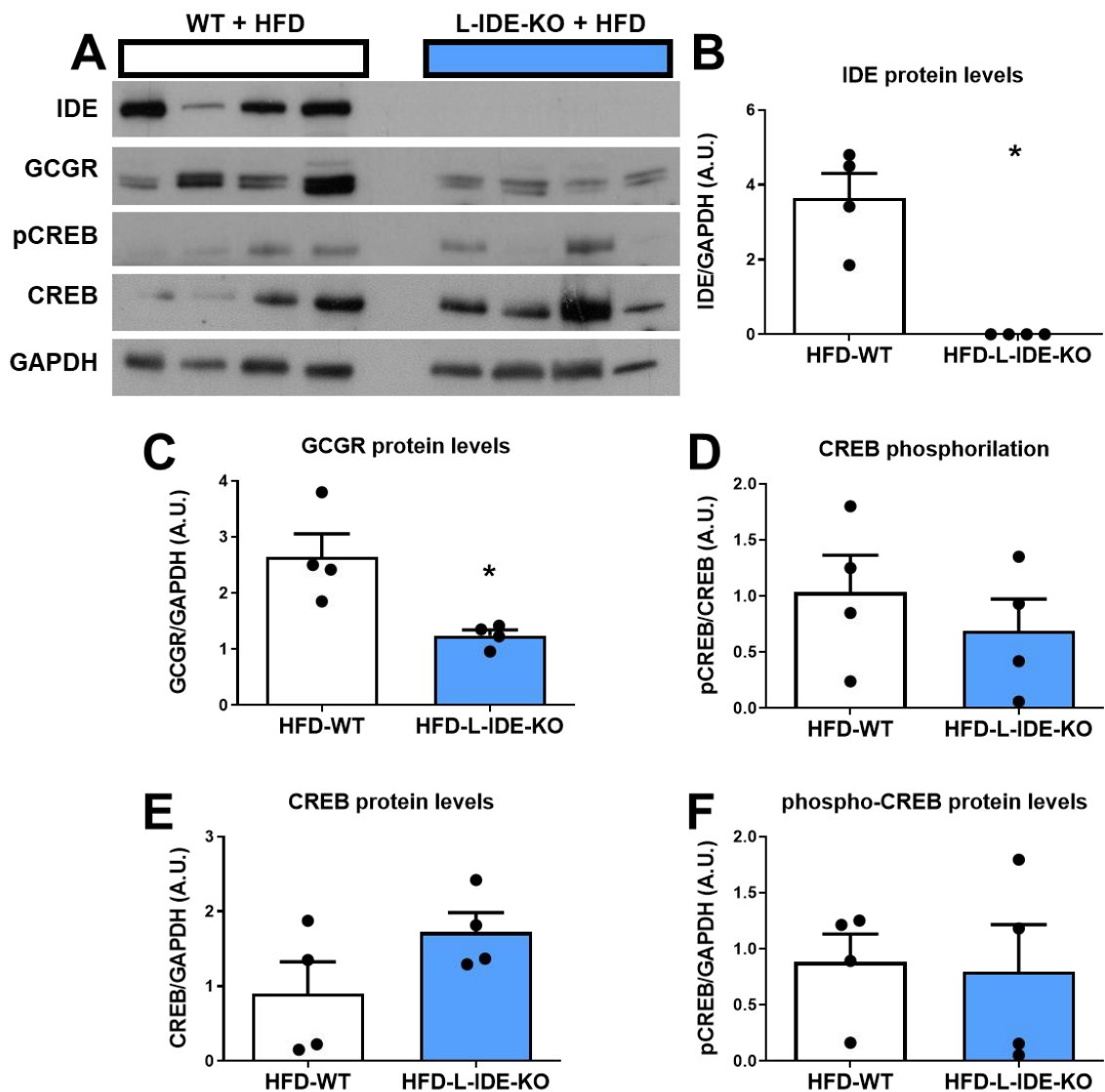
Figure 32. Glucagon signaling in livers of L-IDE-KO mice fed a HFD. A. Blot panel of proteins assessed. **B**. IDE protein levels. **C**. GCR protein levels. **D**. Ratio phospho-CREB/total-CREB levels. **E**. CREB protein levels. **F.** phospho-CREB protein levels. Densitometric analyses of IDE were performed using blots depicted in A, and data were plotted for each genotype. Data are mean ± SEM. N = 4 mice per genotype. *p<0.05 *vs.* WT by Student's t-test

IV.3.1.2. Glucagon signaling pathway in primary hepatocytes isolated from L-IDE-KO and control mice.

In order to evaluate the effect of IDE ablation on glucagon signaling, we isolated and cultured primary hepatocytes from 3-month-old male and female L-IDE-KO mice and their WT littermates and stimulate them with glucagon 50 ng/ml for 0, 1, 4 and 8 h (**Fig. 33 A-B**).

Glucagon receptor was found diminished (~50%) in hepatocytes isolated from L-IDE-KO mice (**Fig. 33 C**). Surprisingly, glucagon stimulation after 4 and 8 h decreased glucagon receptor levels in control hepatocytes (**Fig. 33 C**). However, in hepatocytes isolated from L-IDE-KO the effects of glucagon on CGCR levels at 4 and 8 h were not statistically significant (**Fig. 33 C**). There is a non-statistically significant augment of the ratio pCREB/CREB in hepatocytes from L-IDE-KO compared to control hepatocytes at 1 h (**Fig. 33 D**). On the other hand, CREB protein levels were decreased by ~30% in hepatocytes from livers of L-IDE-KO as compared to control hepatocytes (**Fig. 33 E**). Glucagon increased phospho-CREB levels at 1 h in and hepatocytes from WT and L-IDE-KO mice (**Fig. 33 F**).
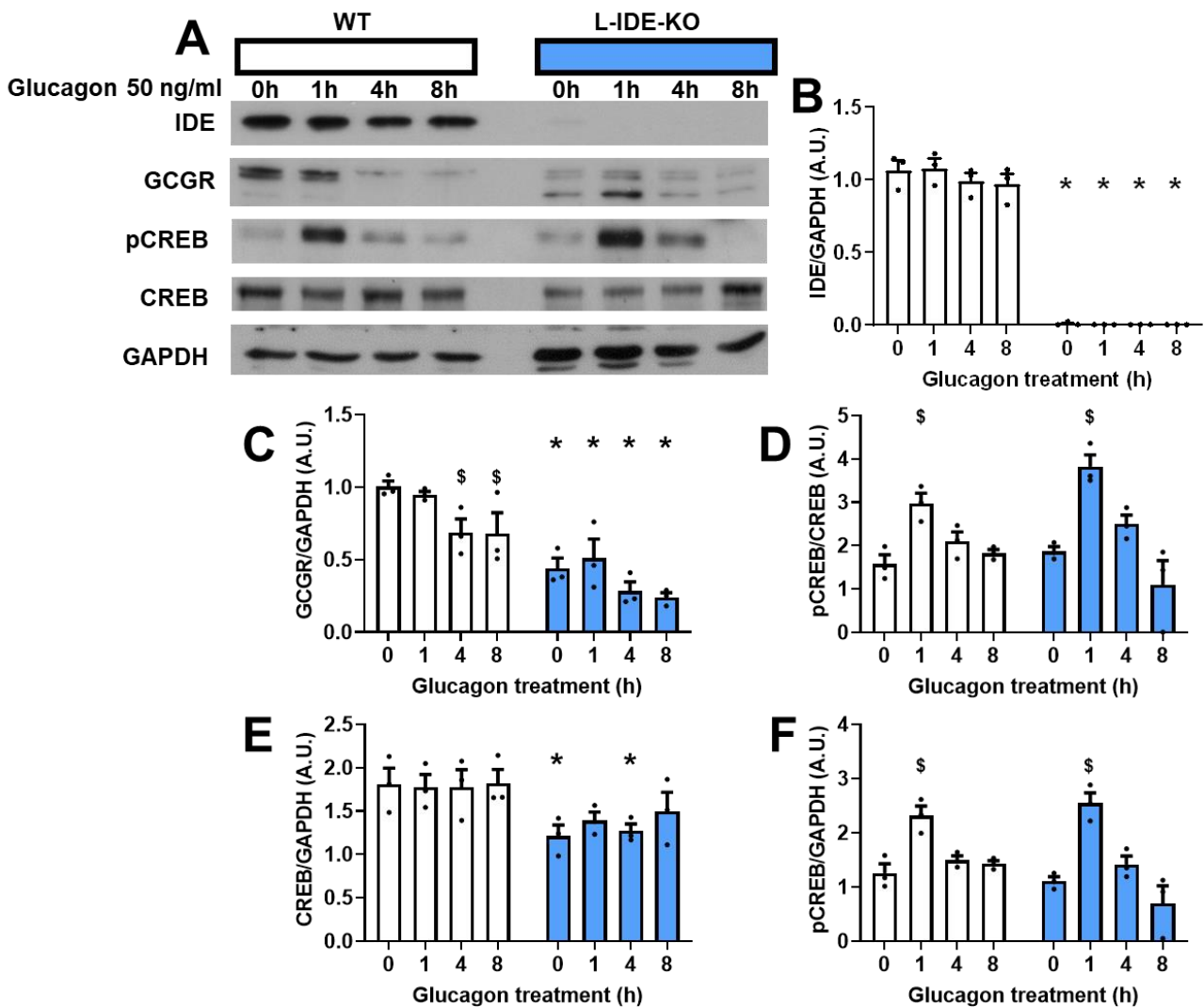
Figure 33. Glucagon signaling in primary hepatocytes isolated from L-IDE-KO mice. A. Blot panel of proteins assessed. **B**. IDE protein levels. **C**. GCR protein levels. **D**. Ratio phospho-CREB/total-CREB levels. **E**. CREB protein levels. **F.** phospho-CREB protein levels. Densitometric analyses were performed using blots depicted in A, and data were plotted for each genotype and time point of glucagon treatment. Data are mean ± SEM. N = 3 mice liver per condition. *p < 0.05 *vs.* WT by ANOVA.

IV.3.2. Signaling in IDE-deficient AML12 cells.

In order to go further exploring the effects of the lack of IDE on hepatic glucagon signaling, we used the previously described mouse hepatocyte cell line AML12-shRNA-IDE, which has knocked-down *Ide* expression (**Figs. 24-25**).

IV.3.2.1. Insulin signaling in AML12-shRNA-IDE cells.

We previously showed that loss of IDE expression in vivo (L-IDE-KO mice) led to hepatic insulin resistance [70,71]. Hence, we decided to further investigate the impact of IDE loss of expression on insulin signaling in AML12-shRNA-IDE cells compared to AML12-CONTROL cells.

Surprisingly, insulin stimulation (100 nM) for 0, 5, 15, and 30 min augmented insulin sensitivity in AML12-shRNA-IDE cells as compared to control cells in line with the decreased IDE protein levels (**Fig. 34 A-B**). Thus, insulin stimulation increased IR phosphorylation by ~2-fold (**Fig. 34 C**), in parallel with PKB and PKB2 activation (**Fig. 34 D-E**). Nevertheless, in the case glycogen synthase kinase 3 (GSK3α), classic PKB substrate, the ratio pGSK3α/GSK3α remained unchanged (**Fig. 34 F**). In parallel, total glycogen synthase (GS) and phosphorylated GS were significantly augmented in AML12-shRNA-IDE cells as compared to control cells, whereas the ratio pGS/GS remained unchanged (**Fig. 34 G**).

68

Figure 34. Insulin signaling in AML12-shRNA-IDE cells. A. Blot panel of proteins assessed. **B**. IDE protein levels. **C**. IR phosphorylation levels. **D**. Ratio phospho-PKB1/total-PKB1 levels. **E**. Ratio phospho-PKB2/total-PKB2 levels. **F.** Ratio phospho-GSK3α/total-GSK3α. **G.** Ratio phospho-GS/total-GS. **H.** GS protein levels. **I.** phospho-GS protein levels. **J.** GLUT2 protein levels. Densitometric analyses were performed using blots depicted in A, and data were plotted for each group and time point of glucagon treatment. Data are mean ± SEM. N = 3 per condition. *p<0.05 *vs.* AML12-CONTROL cells by ANOVA. $^{\$}$p<0.05 *vs.* untreated cells by ANOVA.

IV.3.2.2. Glucagon signaling in AML12-shRNA-IDE cells.

To further investigate the impact of IDE loss of expression on glucagon signaling, AML12-shRNA-IDE and control cells were stimulated with glucagon (50 ng/ml) for 0, 1, 4 and 8 h (**Fig 35**). In this case, we obtained similar results to those observed *in vivo* (L-IDE-KO mice) and *ex vivo* (primary hepatocytes isolated from livers of L-IDE-KO mice).

Even though IDE protein levels were only decreased by half (**Fig. 35 A-B**), we observed a loss of GCGR expression by ~50% (**Fig. 35 C**). As expected, cAMP levels were reduced by ~30% at 30 min of glucagon stimulation in AML12-shRNA-IDE as compared to control cells (**Fig. 35 D**). In addition, CREB and FoxO1 protein levels were significantly reduced by ~ 90% and ~ 80% respectively, in AML12-shRNA-IDE as compared to control cells (**Fig. 35 F, I**). Importantly, diminished GCGR, CREB and FoxO1 protein levels were not associated with a decreased expression of *Gcgr*, *Creb1* and *Foxo1* mRNAs, suggesting a post-translational effect (**Fig. 35 J-L**). Interestingly, although CREB levels were reduced in AML12-shRNA-IDE cells, glucagon stimulation increased phosphorylation levels of CREB at 1h in AML12-shRNA-IDE cells compared to control cells (**Fig. 35 E, G**) in concordance with the phosphorylation levels of other PKA substrates (**Fig. 35 H**).

In view that IDE loss of expression resulted in reduced GCGR, CREB and FoxO1 protein levels, we unexpectedly found an increased expression of gluconeogenic genes *G6pc* and *Pck1* (**Fig. 35 M-N**)*.* Thus, in unstimulated AML12-shRNA-IDE cells, expression levels of *G6pc* were elevated by ~ 5-fold as compared to control cells (**Fig. 35 M**). The effect is even more pronounced (~15-fold) after 4-8 h of glucagon stimulation (**Fig. 35 M**). On the other and, *Pck1* expression levels were upregulated after 1h of glucagon stimulation in AML12-shRNA-IDE cells by ~ 5-fold compared to control cells (**Fig. 35 N**). As described for *G6pc*, the effect was more pronounced (~15-fold) after 4-8 h of glucagon stimulation (**Fig. 35 N**).
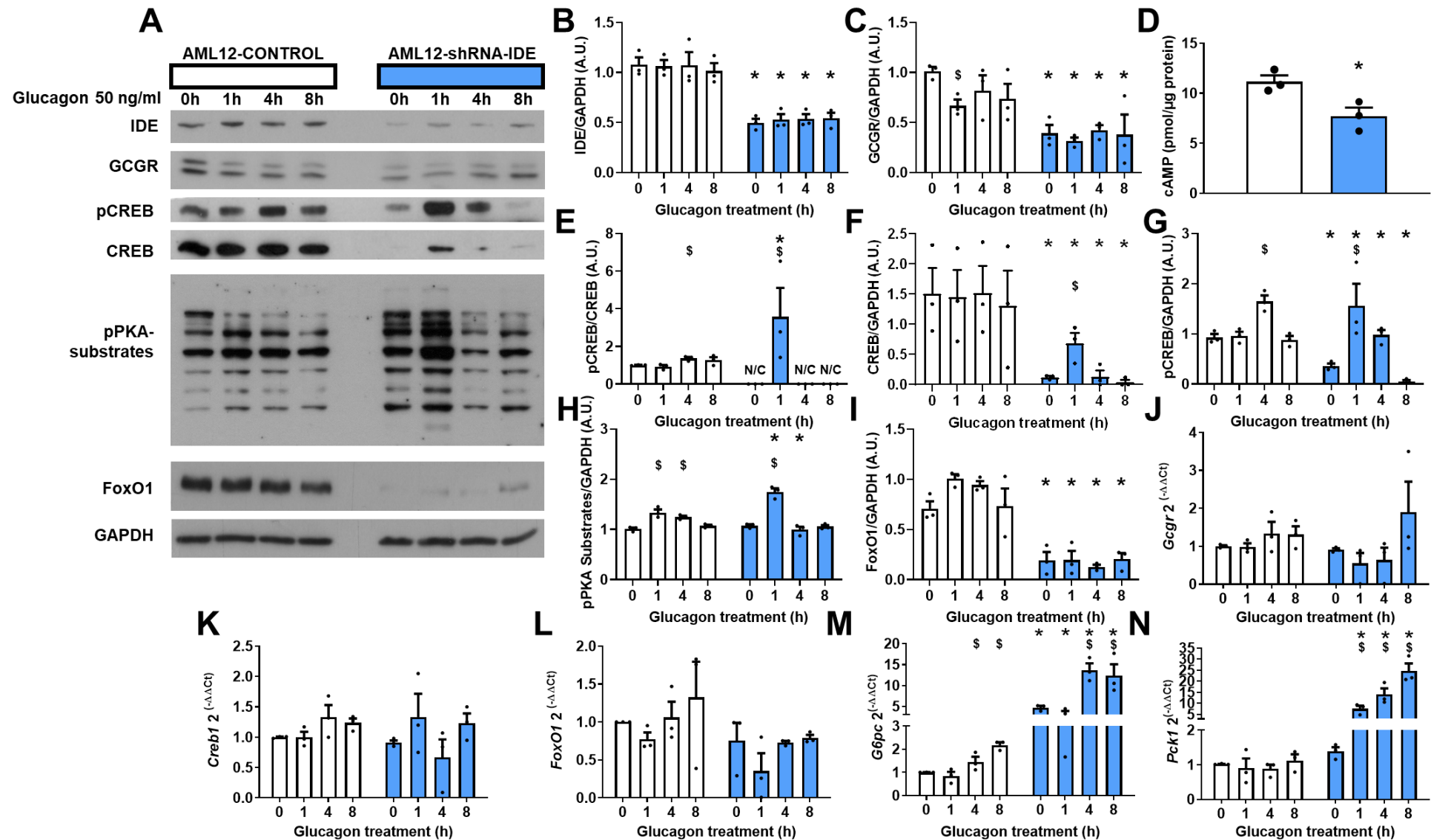
Figure 35. Glucagon singling in AML12-shRNA-IDE cells. A. Blot panel of proteins assessed. **B.** IDE protein levels. **C**. GCR protein levels. **D**. cAMP levels after 30 min of glucagon stimulation. **E.** CREB phosphorylation levels. **F.** CREB protein levels. **G.** phospho-CREB protein levels. **H.** phospho-PKA substrates protein levels. **I.** FoxO1 protein levels. Densitometric analyses were performed using blots depicted in A, and data were plotted for each group and time point of glucagon treatment. Data are mean ± SEM. N = 3 cell passes per condition. *p<0.05 *vs.* control cells by ANOVA. **J.** *Gcgr* mRNA levels **K.** *Creb1* mRNA levels **L.** *FoxO1* mRNA levels **M.** *G6pc* mRNA levels **N.** *Pck1* mRNA levels Data are mean ± SEM. N = 3 per condition. *p<0.05 *vs.* control cells by ANOVA. $p<0.05 *vs.* untreated cells by ANOVA.

IV.3.2.3. Mitochondrial function in AML12-shRNA-IDE cells.

We did not anticipate the effects of IDE loss of expression on FoxO1 when we formulated hypotheses and designed the studies of my thesis. In addition, during the development of my thesis, Yang and collaborators reported that glucagon, in a FoxO1-dependent manner, inhibited hepatic mitochondrial function. Furthermore, the suppression of mitochondrial function by glucagon was largely rescued by deleting the FoxO1 gene in hepatocytes [118].

In view of the results showed above (i.e., IDE loss of expression in hepatocytes was associated with severe reduction in FoxO1 levels), we hypothesized that IDE in a FoxO1-dependent manner regulates mitochondrial function.

In order to study the potential impact of IDE on cellular respiration, we performed analyses using the Seahorse XF Cell Mito Stress Test Kit in AML12-shRNA-IDE and controls cells. Seahorse analyses showed that both oxygen consumption rate (OCR) (**Fig 36. A-B**) and extracellular acidification rate (ECAR) (**Fig. 36 C-D**) increased by ~2-fold in AML12-shRNA-IDE compared to AML12-CONTROL cells. Those differences indicate a more energetic phenotype in the cells lacking IDE (**Fig. 36 E**) with an even more noticeable shift during the stress assay (**Fig. 36 F**). Furthermore, we determined that there was a ~2-fold increment of both mitochondrial and glycolytic ATP production rates in AML12-shRNA-IDE as compared with control cells, with a clear predominance of mitochondrial ATP production in both AML12 cell lines (**Fig. 36 G-H**).
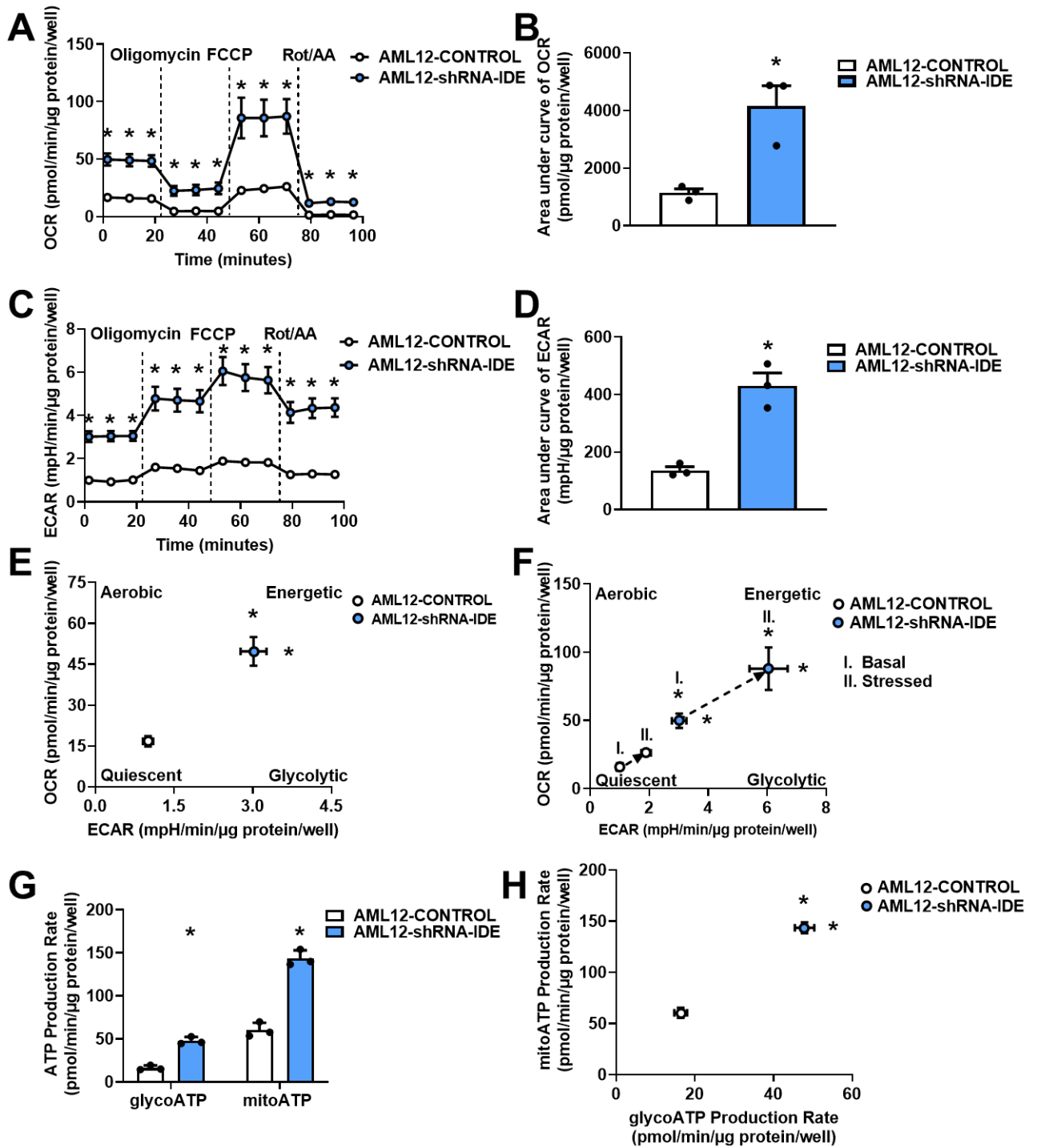
Figure 36. Seahorse analytics in AML12-shRNA-IDE cells. A. OCR assessed with Mito Stress Kit. **B.** Area Under Curve of OCR. **C.** ECAR assessed with Mito Stress Kit. **B.** Area Under Curve of ECAR. **E.** Energy Phenotype in basal conditions. **F.** Energetic shift from basal conditions to stress. **G.** Estimated ATP Production Rate both glycolytic and mitochondrial. **H.** Energy Map facing ATP Production rates from glycolytic and Mitochondrial origins. Data are mean ± SEM. N = 3 per condition. *p<0.05 vs. control cells by ANOVA.

IV.3.2.5 Section summary.

In summary, below we present the main findings of this section:

- Loss of IDE expression in livers from L-IDE-KO mice, primary mouse hepatocytes isolated from L-IDE-KO mice, and AML12-shRNA-IDE cells leads to reduced levels of GCGR, CREB and p-CREB levels in parallel with increased expression of gluconeogenic genes.

- We have developed a mouse hepatocyte cell line (AML12-shRNA-IDE) in which IDE expression was reduced by ~50%.

- We found that AML12-shRNA-IDE cell line does not recapitulate the impairment of insulin signaling seen in livers of L-IDE-KO mice. A expression-dependency effect may account for these differences between *in vivo* and *in vitro*.

- Loss of IDE expression in AML12-shRNA-IDE resulted in increased expression of gluconeogenic genes despite reduced glucagon signal transduction through CREB and FoxO1.

- Loss of IDE expression in AML12-shRNA-IDE resulted in increased respiration and ATP production.

IV.4. *In silico* study of IDE isoforms.

IV.4.1. Sequences alignments.

First, multiple alignments of the sequences of the IDE template structures and the isoforms used as queries were performed (**Fig. 36**). Consequently, it was confirmed that these selected templates are adequate for homology modeling, given the high identity percentage and sequence covering.
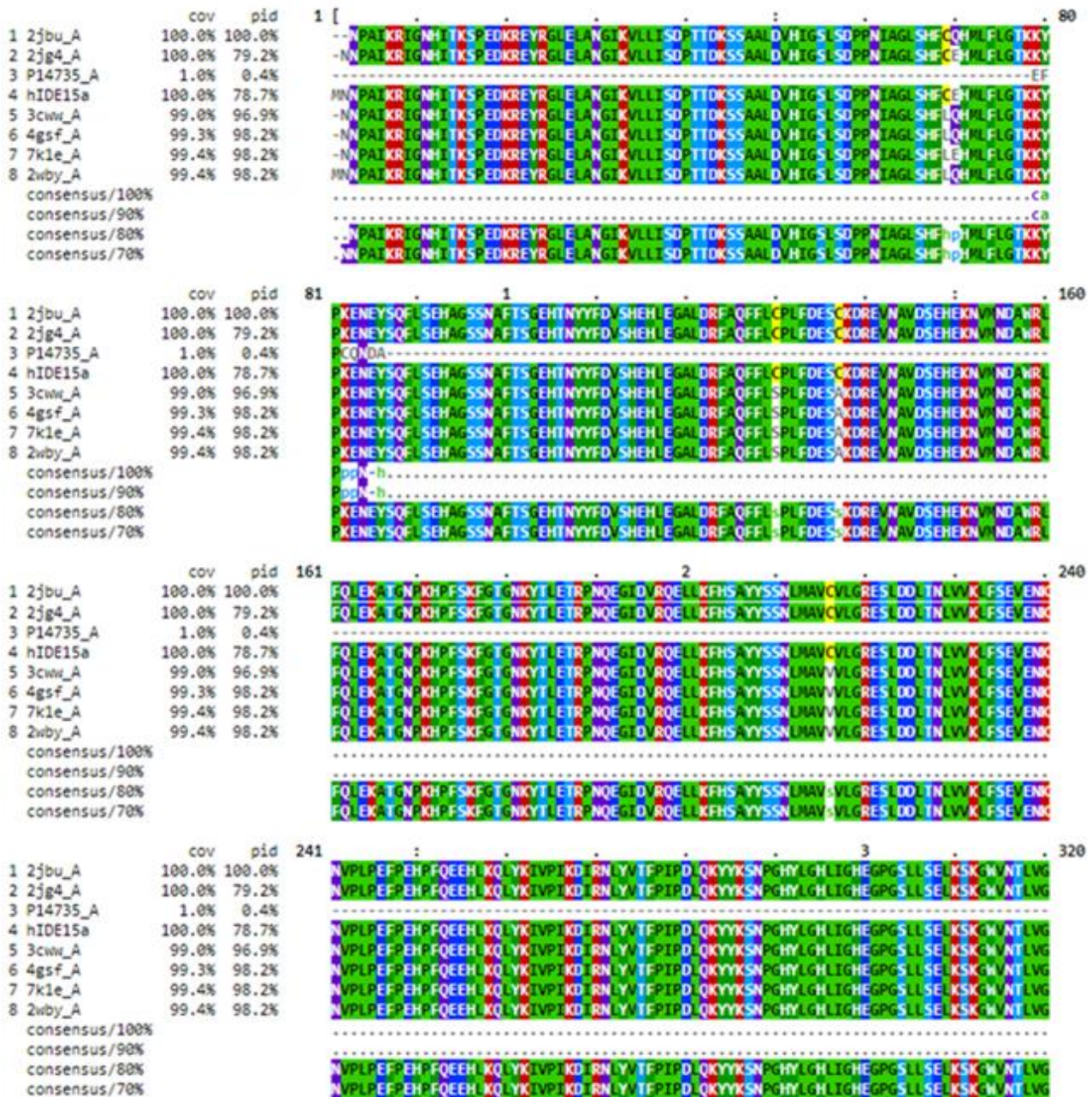
Figure 36. First segment of multiple alignment of IDE templates and query sequences. In a representative manner, the query sequence depicted is from human IDE-15a.

IV.4.2. Homology modeling.

From the 10 models generated for each IDE isoform by Modeller, the one that exhibited the lowest DOPE-HR score was selected (**Fig. 37**). All of them having a value lower than -15,000 kJ/mol. This selection procedure is in accordance with methodology of elsewhere described studies which exhibited satisfactory results [119,120].
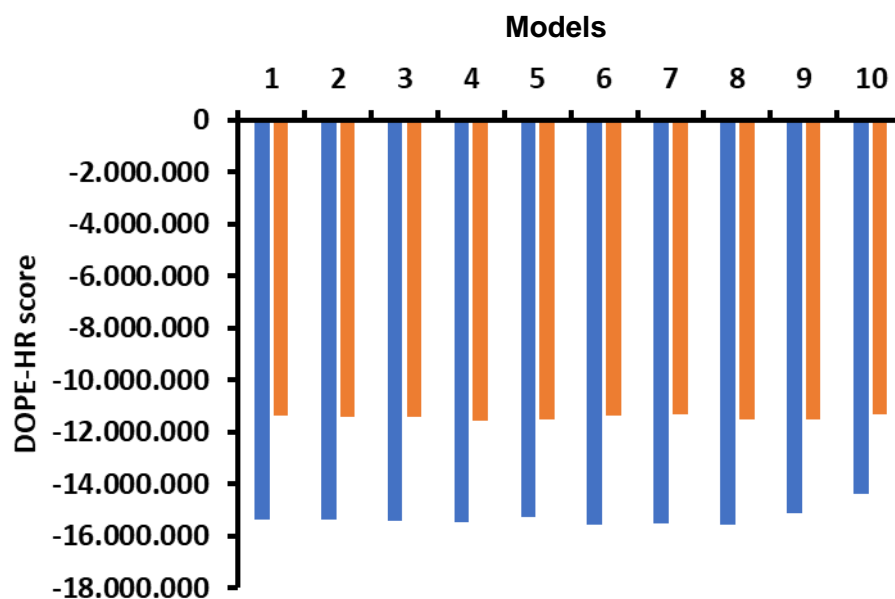
Figure 37. DOPE-HR score obtained with Modeller. Using both a single (best) template and a multiple template alignment, 10 models were generated for each IDE isoform. In all cases multiple template alignments (blue bars) had lower DOPE-HR score indicating a more stable structure than those using single template (orange bars). Finally, the lowest DOPE-HR score model was selected for each IDE isoform to be used in subsequence steps which was in all cases from multiple templates arrangements. In a representative manner, the models DOPE-HR depicted are from human IDE-15a models.

The use of DOWSER++ tool to compute the presence of water molecules in internal cavities of the polypeptide moieties of human and murine IDE isoforms wasn't possible due to hardware limitations. Instead, crystallographic water molecules were included in the closed conformation template and parametrized to query sequences. However, due to the structural and functional relevance of these water molecules, the use of DOWSER for future studies is advised.

IV.4.3. pKa values and protonation states of amino acid residues with dissociable groups.

Analysis of the protonation states (**Fig. 38**) from the pKa values, allowed to assign adequate protonation states to residues with dissociable groups. Protonation states of amino acids residues are important for stabilizing IDE conformations.
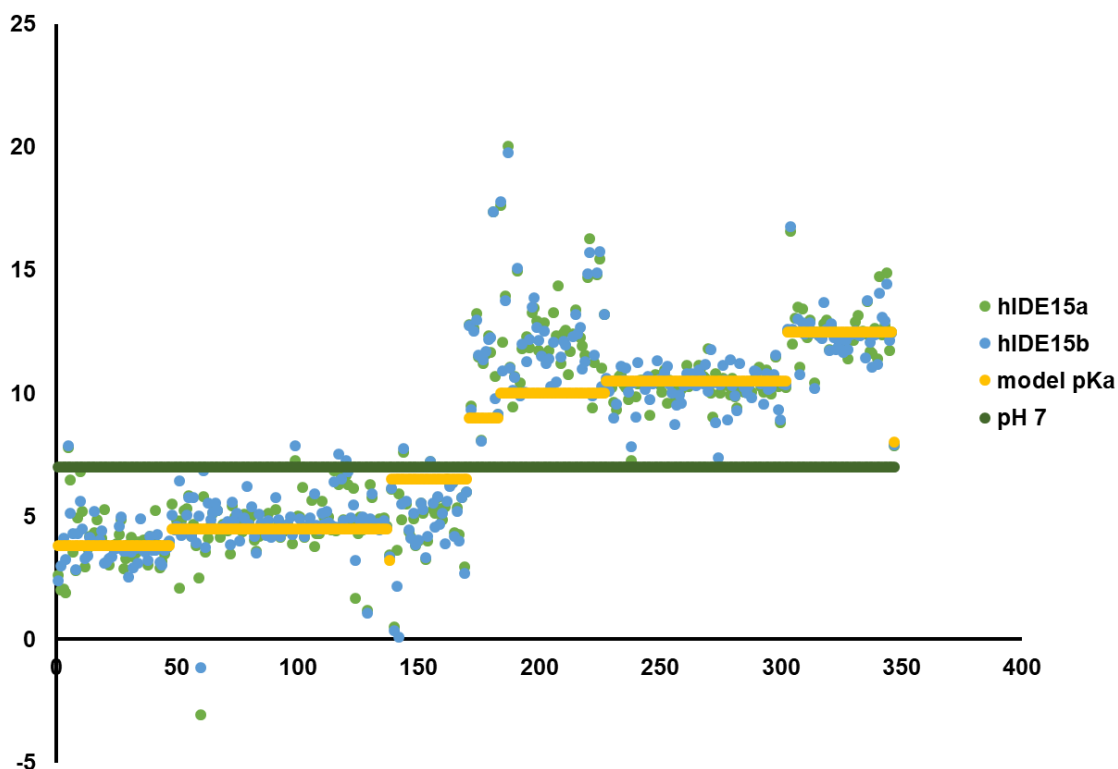
Figure 38. Differences between the pH of the medium, the calculated pKa and the model pKa in residues with dissociable groups for each structure. The dissociable groups were ordered from left to right, from lowest to highest model pKa (from most acidic to most basic) and within the same type were ordered by position in the primary sequence. The dark green line represents the pH of the hepatocyte cytosol, the yellow line represents the model pKa values for each residue, the dots illustrates the calculated pKa values. Residues whose calculated pKa difference location in relation with the pH are in the same direction as that of their ideal pKa have a protonation state identical to that of the model amino acid. In those values that do not fulfill this condition these residues have a protonation state different from that of the model amino acid. In a representative manner, the calculated pKa depicted are from humans IDE-15a and IDE-15b models.

IV.4.4. Structural validation.

The 3D structures generated were adequate according to the parameter values obtained for each of the tools used.

IV.4.4.1. ERRAT2.

The ERRAT2 tool score showed that the quality of the non-bonding atomic interaction patterns of the generated structures was in accordance with expectations of a protein of this size [121], with all the systems presenting a quality factor higher than 80 (**Table 4**).

ERRAT2 score			
hIDE15a	hIDE15b	mIDE15a	mIDE15b
80.6818	82.8866	83.1959	81.0114

Table 4. Total quality factor according to ERRAT2 [121] for the studied structures.

IV.4.4.2. Procheck.

All the structures generated showed values above 90% for the amino acid residues located in the most favored regions in the Ramachandran plot (**Table 5**). The IDE isoforms modeled in this study exhibited an overall G-factor value greater than ₋0.5 (**Table 6**). Thus, all the analyzed structures were found to be suitable.

Percentage of residues in each regions of Ramachandran plot.			
hIDE15a	hIDE15b	mIDE15a	mIDE15b
94.1%	94.1%	94.1%	92.8%

Table 5. Percentage of residues located regions of Ramachandran plot. According to Procheck for each of the generated systems.

Total G-factor according to Procheck			
hIDE15a	hIDE15b	mIDE15a	mIDE15b
-0.25	-0.29	-0.27	-0.25

Table 6. Total G-factor of the systems under study according to Procheck

IV.4.4.3. WHAT_CHECK.

The Z-score value resulted higher than ₋0.50 for all the IDE isoforms studied (**Table 7**), with therefore an adequate packing quality in the protein structures [122].

WHAT_CHECK: 1st generation Z-score			
hIDE15a	hIDE15b	mIDE15a	mIDE15b
-0.406	-0.479	-0.484	-0.465

Table 7: 1st generation packing quality of the structures in study. Values are shown for each studied structure according to WHAT_CHECK [122] tool.

IV.4.4.4. Verify-3D.

In all the IDE isoforms studied, the compatibility between primary structure and 3D structure was of high quality according to the 3D-1D index [123,124] since all of them presented more than 90 % of their residues with indices ≥ 0.2 (**Table 8**).

Verify-3D: percentage of residues with indices ≥ 0.2			
hIDE15a	**hIDE15b**	**mIDE15a**	**mIDE15b**
92.94%	**92.13%**	**94.27%**	**90.08%**

Table 8: Percentage of residues with optimal 3D-1D indices (≥ 0.2). Values are shown for each studied structure from the analysis with the Verify-3D [123,124] tool.

IV.4.4.5. ProSA.

The Z-score calculated from the ProSA tool evidenced that the 3D structure quality of the studied structures agreed with those of structures of equal number of residues and obtained by NMR or X-ray diffraction. Similar values were obtained for the four modelized IDE structures (**Fig. 39**).
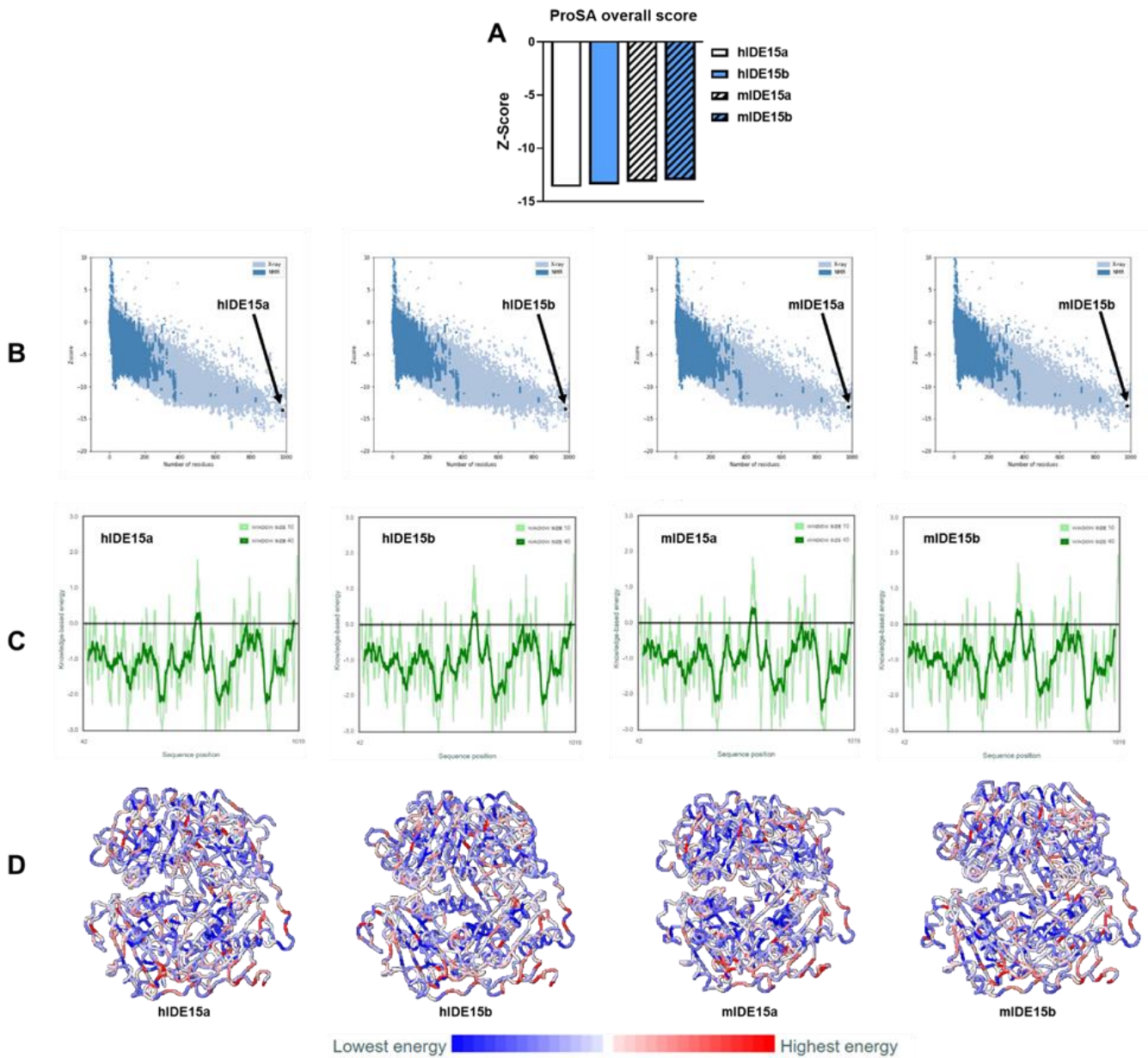
Figure 39. ProSA quality chech results. A. Z-score indicating overall model quality **B.** Z-score values in a plot that contains the z-scores of all protein chains in current PDB. In this plot, groups of structures from different sources (X-ray, NMR) are distinguished by colors allowing to check that the z-score of IDE isoforms modeled structures are within the range of scores found for proteins of similar size. **C.** Plot of residue scores showing local model quality by energies as a function of amino acid sequence position. Positive values correspond to problematic parts of the structure. The plot is smoothed by calculating the average energy over each 40-residue fragments, which is then assigned to the 'central' residue of the fragment at position (thick line). A second line with a smaller window size of 10 residues is shown in the background of the plot (thin line). **D.** 3D structure of the input proteins. Residues are colored from blue to red in the order of increasing residue energy.

IV.4.5. Hydrogen bonds.

The number of hydrogen bonds in the generated IDE isoform models was calculated using the VMD tool taking into consideration all atoms present in the structure including those from water molecules, and these were found in greater number in the canonical sequence's models (**Fig. 9**).

Number of hydrogen bonds			
hIDE15a	**hIDE15b**	**mIDE15a**	**mIDE15b**
166	**130**	**156**	**143**

Table 9. Number of hydrogen bonds estimated by VMD for each generated structure. Structures containing 15a exons translations are more abundant in hydrogen bonds that their 15b counterpart in each specie.

IV.4.6. Stability of the generated models and free energy calculation

The energy required to cause protein denaturation was calculated, a parameter offered by the PropKa v.2.0 program. No significant differences were observed in the stability of evaluated models (**Fig. 40**).
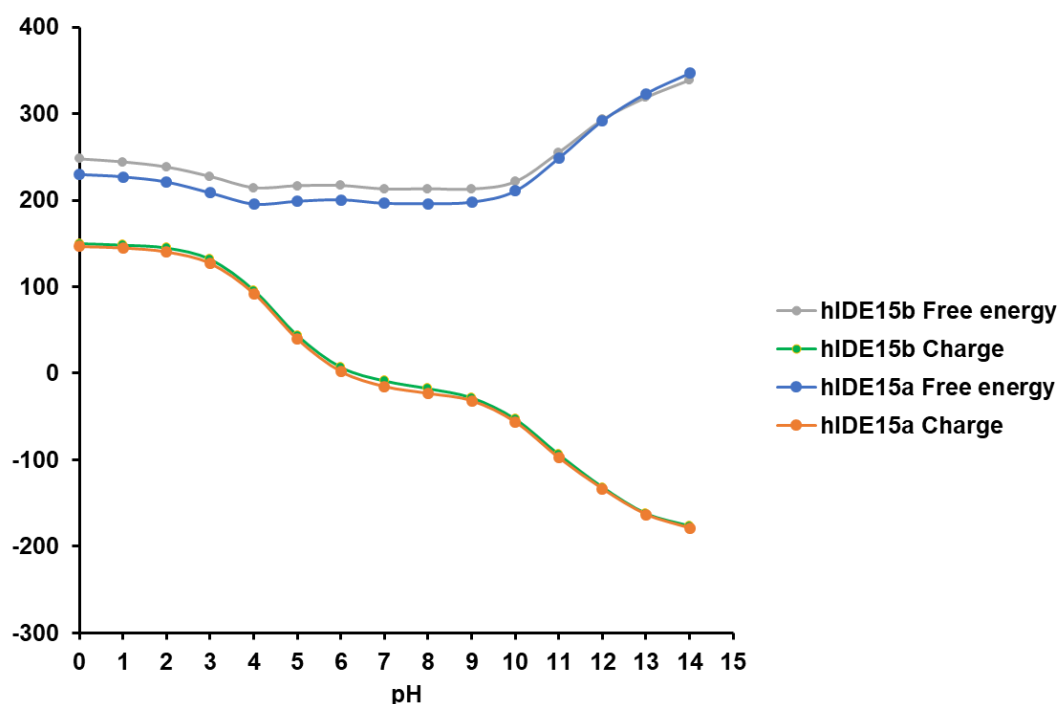
Figure 40: Denaturation energy and net charge as a function of pH, according to PropKa. In a representative manner, the values depicted are from humans IDE-15a and IDE-15b models.

FoldX tool execution on each model allowed us to evaluate free energy after the minimization with the MM procedure performed by Modeller during homology modeling and to compare stabilities within all 3D structures (**Fig. 41**).
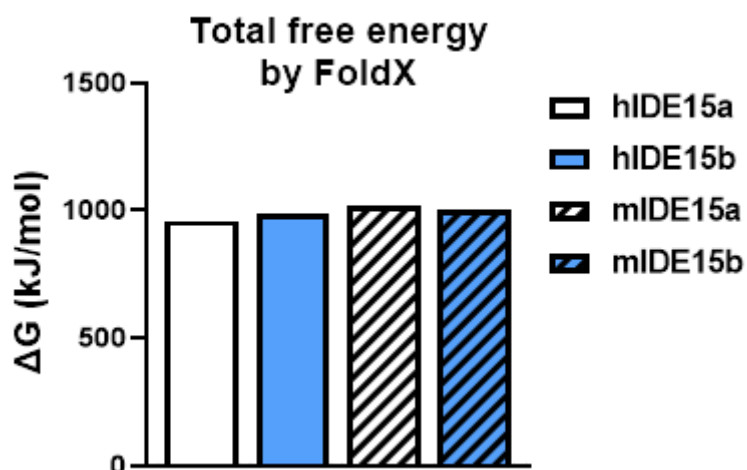
Figure 41: Gibbs free energy (ΔG) calculated with the FoldX tool. The total ΔG value calculated for each IDE isoform is represented.

In addition to the predicted overall stability, the contributions and penalties for specific interactions were estimated. In this way, it was possible to verify with FoldX that the major contributions to the increase in free energy are due to the solvation energy of the polar groups and the entropy of the peptide backbone (**Fig. 42**). The main contributions to its decrease were due to the solvation of the hydrophobic groups and van der Waals interactions (**Fig. 43**).
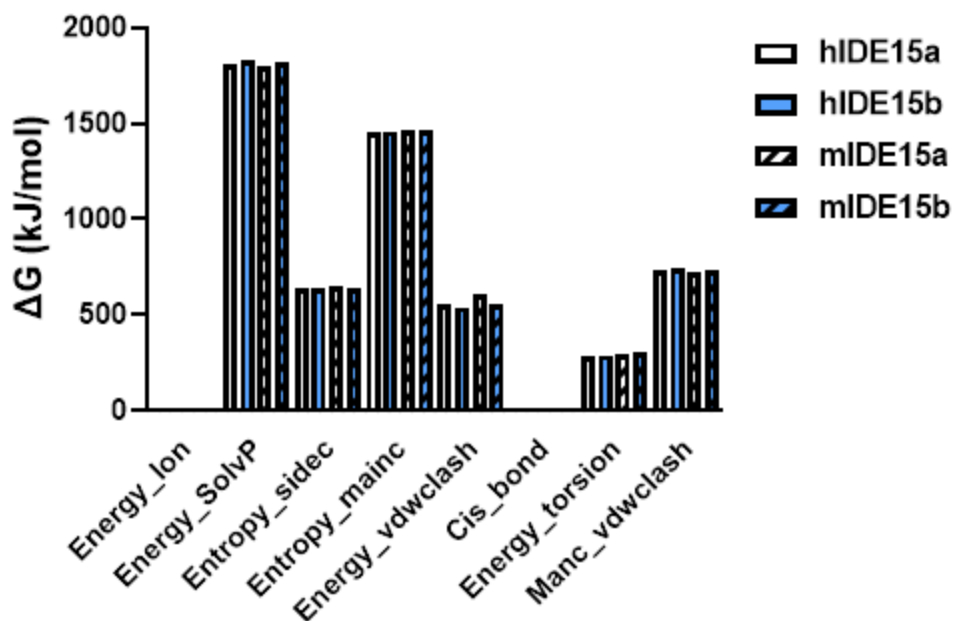
Figure 42. Contributions to the increase in Gibbs free energy (ΔG), calculated using the FoldX tool. The definition of the abbreviations, due to their length, can be found at the end of the glossary of abbreviations.
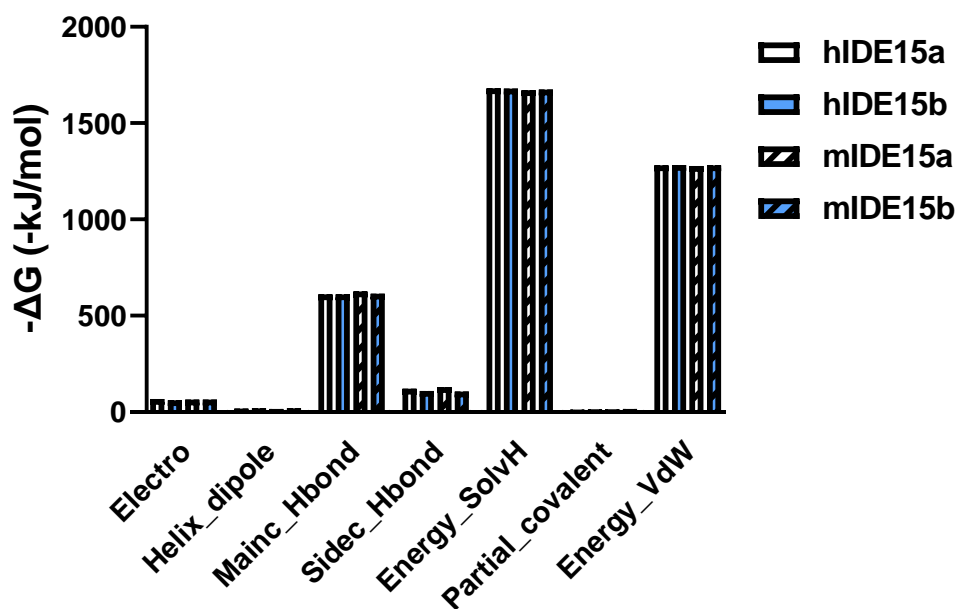
Figure 43. Contributions to the decrease in Gibbs free energy (ΔG), calculated using the FoldX tool. The definition of the abbreviations, due to their length, can be found at the end of the glossary of abbreviations.

IV.4.7. Section summary

In summary, below we present the main findings of this section:

-     In this work we successfully generated, using homology modeling and satisfaction of spatial restrains techniques, complete 3D structures of human and murine IDE isoforms with 15a and 15b exons.

-     We evaluated the quality of our models using diverse parameters of structural validation obtaining scores under expected ranges, indicating good quality of models generated.

-     Then, we calculated free energy and stability of this models finding that they need to be improved by molecular dynamic minimization, but they are suitable to use in further studies and there was no significant difference in this matter between all generated structures.

V. Discussion

V.1. Effects of fasting and refeeding on transcriptional and post-transcriptional regulation of insulin-degrading enzyme in mice

In this study, we provide a detailed description of the transcriptional and posttranscriptional regulation of hepatic IDE in response to fasting and refeeding under normal and high-caloric food consumption. Our study reveals an unexpected complex regulation of IDE, that depends on circulating levels of hormones and metabolites.

We show that in response to fasting, circulating glucagon levels were lower in mice fed a HFD compared to control mice. Different studies have reported disparate results regarding plasma glucagon levels in mice fed a HFD, being either decreased or elevated in different studies [125-130]. Thus, Merino and colleagues reported that high-fat feeding for 12-weeks in mice resulted in hypoglucagonemia compared to control animals, despite hyperinsulinemia and normoglycemia [128]. Interestingly, Merino and colleagues hypothesized that this metabolic phenotype may be an early adaptive response to the eventual progression to T2DM, allowing normoglycemia not only due to the compensatory hyperinsulinemia produced by β-cells, but also by lowering α-cells-mediated glucagon secretion. These findings resembled our data, where mice fed HFD for 8-weeks exhibited lower circulating glucagon levels compared to control mice. We anticipate that longer exposure to a HFD feeding (e.g., 24-weeks) will result in hyperglucagonemia, but in our experimental setting (8-weeks) resulted in hypoglucagonemia.

In the liver, major factors associated with IDE regulation are NEFA (during fasting), and glucose, lactate, and insulin (during refeeding). Transcriptional regulation of *Ide* expression did not translate into protein changes, most likely due to a high sensitivity of the PCR compared to western blot technique. Likewise, changes in activity did not mirror changes in protein levels, suggesting posttranscriptional modifications in the protein. *In silico* web-based analyses identified potential posttranslational modifications, such as phosphorylation and SUMOylation, in the primary structure of IDE, which could be responsible for

changes in activity independently of protein levels. Clearly, this facet of IDE regulation is an under-researched field of study that deserves further investigations.

Exposure to increasing amounts of NEFA released from adipose tissue promotes de development of hepatic insulin resistance [131], and some studies suggest that IDE may be either affected by or involved in this phenomenon. Thus, Hamel and colleagues identified a fatty acid-binding motif within IDE [132] and found that both saturated and unsaturated long-chain free fatty acids (FFA), and the corresponding acyl-coenzyme A thioesters inhibited insulin degradation in a non-competitive manner [132]. Furthermore, FFA decreased insulin degradation in isolated hepatocytes [133] and inhibited the proteolytic activity of IDE released from adipocytes [134]. We recently hypothesized that increasing amounts of saturated FFA released from adipose tissue via the portal system would inhibit both proteolytic and non-proteolytic functions of IDE, in turn decreasing insulin clearance, whether directly by reducing IDE levels and/or activity or indirectly via mechanisms involving insulin receptor internalization and/or recycling. This mechanism may help explain the insulin resistance and hyperinsulinemia seen in obesity [17]. In this study, we found that NEFA levels correlated inversely with hepatic IDE protein levels and activity, being the most relevant physiological variable found to regulate IDE in the liver. Our findings lend support to the notion that IDE represents a mechanistic link between elevated circulating FFA and hepatic insulin resistance, but further research is needed to confirm this hypothesis.

As was reported previously, genetic depletion of hepatic *Ide* in mice fed standard diet or HFD caused insulin resistance or its exacerbation, respectively [70,71]. Unfortunately, this loss-of-function approach cannot discriminate between the effects of the non-proteolytic functions (protein lost) versus proteolytic functions (activity lost). Here, we showed that HFD caused a significant reduction of hepatic IDE levels (~30%) during the fasting state in both liver and skeletal muscle tissues. A remarkable finding of this study is that with a surrogate assessment of insulin resistance (HOMA index) correlated inversely with hepatic IDE protein levels, but not with its activity, lending support to the notion that the non-proteolytic functions of IDE are related to insulin sensitivity in the liver, rather

than proteolytic functions. These findings open the question whether targeting IDE protein levels independently of its activity is a useful approach for treating insulin resistance. Evidence in the literature suggest that this might be the case, because hepatic IDE overexpression in mice fed a HFD improved insulin sensitivity [71], and taurine conjugated bile acid treatment, which augmented hepatic IDE levels without changes in its activity, improved insulin sensitivity in mice fed a HFD [135].

Early reports identified insulin and glucose as modulators of hepatic IDE activity *in vitro*. Thus, Pivovarova and colleagues showed that insulin stimulated and increase in hepatic IDE activity, but this insulin-mediated effect was abolished in the presence of high-glucose levels in hepatocellular carcinoma HepG2 cells [136]. Although the underlying mechanism(s) by which insulin regulated IDE activity was not stablished, they showed that the relative proportion of the more proteolytically active 15a splice isoform was increased after insulin treatment, independently of glucose levels [136]. In this thesis, we found that both insulin and glucose levels correlated directly with hepatic IDE activity *in vivo*. However, the augmented IDE activity seen during refeeding cannot be explained, neither to reduced expression of the less proteolytically active 15b isoform, nor to augmented expression of the more proteolytically active 15a isoform. Our results suggest that the splice isoforms seem not to be an important mechanism by which insulin and glucose regulate hepatic IDE activity in mice. Nonetheless, our studies highlight the relevance of glucose and insulin during refeeding as modulators of hepatic IDE activity. We anticipate that augmented hepatic IDE activity in response to glucose and insulin serve as a mechanism that preserves hepatocytes from being expose to high levels of portal insulin, resulting in downregulation of the insulin receptor and appearance of insulin resistance.

In addition to glucose and insulin, we unexpectedly found that circulating lactate levels are able to predict hepatic IDE activity. Lactate correlated directly with hepatic IDE activity and protein levels. Even more interesting, we found a cause-effect relationship between lactate and the regulation of hepatic IDE activity. In a concentration-dependent manner, lactate levels augmented IDE activity in lysates from livers of mice. Lactate effect on IDE seems not to be due a direct interaction between IDE and lactate, but to an indirect way, most likely

by metabolites and/or other factors related to intracellular lactate metabolism. To our best knowledge, this is the first time that is reported the lactate-mediated regulation of IDE activity in mice. In any case, further research is warranted to decipher molecular mechanism(s) by which lactate regulates hepatic IDE activity.

In humans, skeletal muscle is a major contributor of circulating lactate (~40 %) in the postabsorptive state [137,138]. Lactate is produced from glucose through glycolysis and the conversion of pyruvate by lactate dehydrogenase [139]. Because lactate production depends on insulin-stimulated glucose uptake this metabolic pathway is regulated by insulin´s action in skeletal muscle [140]. After its synthesis in muscle, lactate is released into the systemic circulation, and mostly cycled to the liver rather than oxidized in the muscle [138,141,142], where lactate is used as a gluconeogenic substrate for hepatic glucose production [143]. Interestingly, the skeletal muscle exhibits a high capacity to switch from fat to glucose oxidation in the fasting to postprandial transition, a term coined as "metabolic flexibility" [144-147]. After a glucose load, glucose is quickly extracted from circulation (15-30 min), allowing its oxidation rather than NEFA oxidation, the energy source used during the precedent fast [148-150].

In this line of thinking, it is plausible to hypothesized that lactate is an inter-organ substrate which is produced in muscle and regulates hepatic IDE activity in response to skeletal muscle insulin sensitivity. Our data are consistent with the notion that under insulin sensitivity conditions, such as standard diet feeding, insulin-stimulated glucose uptake is increased in skeletal muscle (data not shown in this thesis, see reference [151]), allowing a quick switch from fat to glucose oxidation in the fasting to postprandial transition. When glycogen stores are replete in muscle, glucose is oxidized through glycolysis raising circulating levels of lactate, which in turn activate hepatic IDE. Conversely, under the insulin resistant conditions, such as those caused by high-caloric intake, insulin-stimulated glucose uptake is reduced, lowering the rate of lactate production, and leading to reduced hepatic IDE activity [151]. Thus, the loss of metabolic flexibility in skeletal muscle is translated into reduced hepatic IDE activation through circulating levels of lactate (**Fig. 44**).
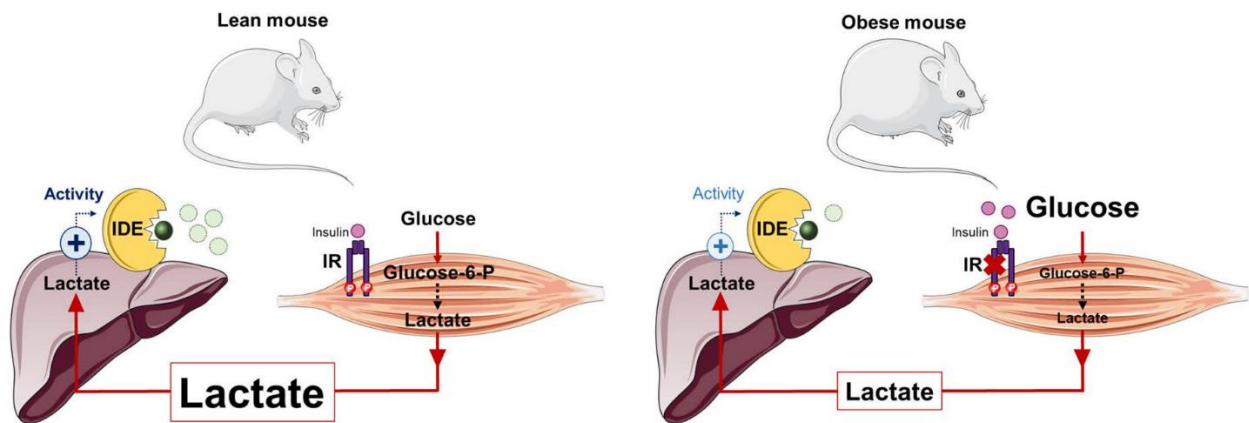
Figure 44. Lactate could act as an inter-organ communicator regulating liver IDE activity. It would activate IDE under physiological conditions of normal muscular insulin sensitivity (insulin stimulates muscle lactate production). In a muscular insulin resistance scenario, lower lactate production would lead to decreased liver IDE activity. Taken from ref [151].

Previous studies of fasting and refeeding on hepatic IDE levels in rodent´ models have yielded contradictory results that are difficult to interpret due to variability in the length and composition of diets, strains, and sex of animals. Nonetheless, the majority of the studies conducted in mice show that high-caloric feeding for 8-16 weeks results in reduced hepatic IDE levels [135,152-154]. We observed similar findings in mice fed a HFD under fasting conditions. Interestingly, longer exposure to a high-caloric intake (6 months) results in higher hepatic IDE levels [155], suggesting that modulation of IDE protein levels in response to diet is time-dependent.

In summary, this study reveals that the effects of fasting and refeeding and SD versus HFD on IDE in mice are more complex than previously expected. In the liver, protein and activity levels are differentially regulated under fasting and refeeding conditions, whereas in skeletal muscle IDE protein levels, but not its activity, participate in the fasting-to-postprandial transition. Changes in circulating levels of insulin, glucose, NEFA, and lactate might be principal determinants in regulating IDE in liver and muscle tissues. Moreover, IDE protein levels in liver and muscle tissues, but not its activity, strongly correlates with a surrogate assessment of insulin resistance, placing the spotlight on IDE protein levels as a pharmacological target for the insulin resistance treatment.

V.2. Pharmacological activation of IDE for treating hepatic insulin resistance

In this thesis, we have investigated the potential pharmacological use of sPIF for treating T2DM in cultured hepatocytes and islets from diabetic mice. Because historically has existed an interest in IDE as pharmacological target in T2DM, efforts in the development of inhibitors as therapeutics in diabetic patients has attracted attention during the last decades. However, inhibitors have produced controversial results regarding their application as modulators of glucose homeostasis and insulin proteostasis, reviewed in [18]. Furthermore, activators are also foreseen but few of them have been disclosed, such as **suramin** [156], **Ia1** and **Ia2** [157], polyaromatic compounds [158], **rat-7** [159], and **BMD 43079** [160], and **hit 1** [161], but none of them have been proven to be effective.

Tissue-specific knockout mouse models in the liver (IDE-KO and L-IDE-KO) have provided important knowledge regarding to proteolytic and non-proteolytic functions of IDE [17]. A constraint of these models is that genetic manipulations of IDE have been limited to deletion or overexpression in the liver (L-IDE-KO) or pancellular deletion (IDE-KO), which modifies not just the activity but also the protein itself. However, studies conducted with the pharmacological activator sPIF would permit the proteolytic activity of IDE to be interrogated while leaving the protein itself unperturbed, which may yield insights into IDE's function on hepatic insulin sensitivity.

In the liver, neither loss nor gain of IDE function (L-IDE-KO mouse and adenoviral delivery, respectively) affected plasma insulin levels or insulin clearance [70,71]. However, loss of hepatic IDE function (L-IDE-KO) resulted in insulin resistance, whereas its overexpression in livers of mice fed a HFD led to improved insulin sensitivity and glucose homeostasis [70,71]. To further investigate the role of the proteolytic activity of IDE on the regulation of hepatic insulin sensitivity, we have treated mouse and human hepatocytes with sPIF. As demonstrate in this thesis, sPIF augmented the proteolytic activity of IDE in both mouse and human hepatocytes. Furthermore, sPIF was able to restore IDE activity in two different scenarios where IDE protein levels were diminished, such as genetic knockdown and HFD feeding, independently of its protein levels.

However, restoring the proteolytic activity of IDE was not sufficient for insulin sensitivity recovery. These data highlight the relevance of IDE protein itself in the regulation of hepatic insulin sensitivity and tease apart proteolytic and non-proteolytic functions. Additionally, our results agree with those presented in this thesis, where hepatic IDE protein levels, but not its proteolytic activity, inversely correlated with insulin resistance in response to the fasting-to-postprandial transition in mice fed SD and HFD [151]. Furthermore, in light of these results, the recovery of insulin sensitivity seen in mice fed a HFD, where IDE was overexpressed in the liver, most likely was due to higher protein levels rather than to increased proteolytic activity [71].

Because reduced IDE function has been implicated in the pathogenesis of both T2DM and Alzheimer's Disease [162], our work does not lend support the notion that pharmacological upregulation of IDE activity by sPIF might represent viable therapeutic strategies for the treatment of diabetes. However, given that hepatic *Ide* expression is reduced in subjects with T2DM [136], it is tentative to hypothesize that therapeutic strategies aimed to restore IDE protein levels itself would be of significance in T2DM. The use of sPIF as a potential treatment for Alzheimer's Disease has been proposed by Hayrabedyan and collaborators, and further research is warranted [68].

V.3. Role of hepatic IDE on glucagon signaling.

V.3.1. Hepatic glucagon signaling in hepatocytes.

As demonstrated in this thesis, IDE is necessary for proper activation of glucagon signaling in mouse liver cells, primary mouse hepatocytes, and immortalized hepatocytes. These results suggest that loss of IDE expression is involved in the pathogenesis of hyperglycemia in T2DM through regulation of hepatic glucagon action.

Studies performed in this thesis and others showed that hepatic IDE levels are diminished in preclinical models and diabetic patients [46-49,151]. Our in vitro model (AML12-shRNA-IDE) mimics the reduced IDE expression levels seen in diabetic patients and mouse models of obesity and diabetes. Furthermore, in a

similar way to the IR, IDE lost leads to lower GCGR levels in hepatocytes. Importantly, this feature is not dependent on transcriptional regulation, but rather post-transcriptionally. In rodents, conditions leading to a sustained elevation of plasma glucagon concentration are generally associated with a decrease in GCGR number in hepatocytes, suggesting that glucagon is negative regulator of the expression of the GCGR protein in liver [163]. In the L-IDE-KO mouse model, glucagon levels were not elevated as compared to control mice [70,71], avoiding pointing the finger at hyperglucagonemia as the culprit for downregulation of GCGR.

In primary cultured rat hepatocytes, glucose, cAMP and glucagon (via cAMP) have been identified as major regulators of GCGR mRNA level [164,165]. In this study we identified, for the first time, IDE as a major regulator of GCGR levels in hepatocytes independently of mRNA expression. Glucagon exposure often affect total number of GCGR in rat and chicken hepatocytes [166,167]. In chicken hepatocytes, the glucagon-induced decrease in GCGR number is partially reversible in the absence of new protein synthesis, suggesting that receptors lost from the cell surface are largely stored within the cells rather than degraded [167]. In this regard, the literature has reported evidence of IDE-mediated regulation of proteasome [168-176]. Interestingly, Sbardella and collaborators reported that the 26S proteasome activity is significantly affected by variations in the intracellular distribution of IDE [177]. IDE-downregulation in SHSY5Y cells bring about an increase in the proteolytic activity of the 26S proteasome, allowing to hypothesize that the IDE-proteasome interaction might represent a novel pathway of regulation of intracellular proteolysis [177]. Because we have seen that loss of IDE in hepatocytes is closely associated with reduced protein levels of GCGR, CREB and FoxO1 (independently of mRNA levels) it is plausible to hypothesized that these effects are proteasome-mediated. Further work is necessary to demonstrate this hypothesis.

Another putative explanation for GCGR lost may be cytoskeleton disarrangement. Recently, we reported that genetic depletion of *Ide* in α-cells (αTC1.9 cell line transfected with an *Ide*-targeting siRNA) resulted in cytoskeleton disarrangement and a significant reduction in the number of primary cilia [15,16]. Classically, IDE has been viewed as a protease of insulin and glucagon, but this

finding points towards non-proteolytic functions (most likely as a scaffold protein) that could be regulating cytoskeleton integrity in pancreatic endocrine cells. Once underappreciated, primary cilium now is thought to efficiently sense external environmental cues and mediate cell-to-cell communication, because many receptors, ion channels, and signaling molecules are highly or differentially expressed. It has previously been reported that cilia are undetectable on hepatocytes [178]. However, recent findings have shown the presence of cilia in hepatocytes [179,180]. Preliminary results obtained during the development of this thesis have identified the presence of primary cilium by immunofluorescence in AML12 and HepG2 cells. Furthermore, loss of IDE significantly alters acetylated-tubulin pattern in the cytoplasm of hepatocytes concomitant with loss of primary cilia (data not shown in this thesis). Because tubulin acetylation is a post-translational modification with emerging roles in intracellular trafficking and signaling [181], further work is warranted to elucidate the contribution of cytoskeleton and primary cilia to number of GCGRs and glucagon signal transduction in hepatocytes.

V.3.2. Hyperglucagonemia and regulation of GCGR.

Clinical data have shown that patients with T1DM or T2DM exhibited elevated circulating glucagon levels, correlating with the pathogenesis of hyperglycemia [182,183]. The contribution of glucagon to hyperglycemia in diabetes was supported by studies showing lower blood glucose levels in mice with deletion of the GCGR, and in humans treated with GCGR antagonist [184-186]. In addition, it was shown that in animal models of endogenous hyperglucagonemia by intrinsic activation of mTORC1 in α-cells, chronic high-glucagon levels induce downregulation of hepatic *Gcgr* gene expression and glucagon signaling, in parallel with improved glucose tolerance and lower glucose level during fasting [187]. However, the A-IDE-KO mouse model, which also exhibited endogenous hyperglucagonemia and downregulation of hepatic GCGR and signaling did not resulted in improved glucose tolerance [15]. In our L-IDE-KO mouse model, GCGR is downregulated in the absence of endogenous hyperglucagonemia, concomitant with augmented expression of gluconeogenic genes and impaired glucose tolerance in SD and HFD feeding [70,71].

V.3.3. IDE-mediated regulation of hepatic gluconeogenesis.

An intriguing finding in this thesis is that despite reduced glucagon signal transduction in hepatocytes with lower levels of IDE, the transcriptional regulation of gluconeogenic genes is upregulated. Thus, our in vivo (L-IDE-KO mice) and in vitro (primary mouse hepatocytes and shRNA-AML12-IDE cells) observations for hepatic glucagon signaling reveal uncovered novel aspects of glucagon biology in unique models of study.

Gluconeogenesis is nutritionally and hormonally regulated, particularly by insulin, glucagon, and glucocorticoids. Cellular signaling upon binding of these hormones to their receptors transduces the signal either through some metabolites, intermediates, protein phosphatases, or kinases [8,188-190]. This modulation often leads to the modification of transcription factors, promoting or preventing them to translocate to the nucleus where they bind and activate transcription of their target genes. In general, during starvation conditions, glucagon stimulates gluconeogenesis through three pathways: (1) CREB/CRTC2/CBP/p300 axis, (2) FoxO1 in association with the peroxisome proliferator-activated receptor γ coactivator 1-α (PGC-1α), and (3) nuclear receptor(s) and its coactivators. On the other hand, under fed conditions, insulin represses gluconeogenesis by inactivating above mentioned transcription factors via PKB2 phosphorylation [8,188-190]. Insulin also stimulates the expression or activity of other groups of transcription factor, such as SREBPs and ChREBP, which upregulates genes involved in glycogen synthesis [8,188-192].

In response to glucagon, activation of adenylyl cyclase results in the conversion of ATP to cAMP. Binding of cAMP to the regulatory subunits of PKA results in dissociation of catalytic subunits from the heterotetrameric PKA. The released catalytic subunits enter the nucleus where they phosphorylate CREB. This cAMP-induced transcriptional response is rapid and sustained for a few hours before returning to the basal state when CREB is dephosphorylated by PP1 or 2A. Our results showed that CREB total protein levels are reduced in livers and primary mouse hepatocytes from L-IDE-KO mice and shRNA-AML12-Ide cells. Interestingly, pCREB levels are elevated at 1h of glucagon stimulation, despite lower GCGR levels and cAMP. Coinciding with this activation, transcription of gluconeogenesis genes is enhanced in hepatocytes. These

results suggest that in conditions of reduced IDE levels, other mechanisms independently of glucagon signaling activate CREB. Because phosphorylation of PKA-dependent substrates is augmented in AML12-shRNA-IDE cells, we hypothesize that PKA is activated independently of glucagon signaling, resulting in elevated levels of pCREB, leading to activation of gluconeogenesis. In support of this notion, several works have described cAMP-independent activation of PKA [193-195].

CREB on its own is not sufficient for efficiently turn on gluconeogenic genes and requires transcriptional coactivators. Phosphorylated CREB by PKA recruits binding of coactivators CREB-binding protein (CBP), CREB regulated transcription coactivator 2 (CRTC2, a.k.a. TORC2), and histone acetyltransferase p300 (p300) [196-198]. During early and late fasting periods functional interactions between each of these coactivators control hepatic gluconeogenesis. At early stage, p300 acetylates lysine 628 of CRTC2 protecting this residue from being degraded by the proteasome. At late stage, when glucagon signal is attenuated, CRCT2 is deacetylated by sirtuin-1 (SIRT1), allowing its ubiquitin and proteasomal degradation [199]. In view of evidence that IDE-mediated regulation of proteasome, we hypothesize that in conditions of reduced IDE levels, there is a protection of CRTC2 at early and late stages from being degraded by the proteasome leading to efficiently sustain gluconeogenic genes expression. In addition, signaling via CREB/CRTC2 promotes the recruitment of lysine acetyltransferase 2B (KAT2B) during starvation, which increases H3K4 acetylation. The increased H3K9 acetylation further potentiated CRTC2 occupancy at CREB binding sites [200].

During the early phase CREB/CRTC2 can enhance the expression of PGC-1α and the estrogen-related receptor gamma (ERRγ), which are key transcriptional regulators of hepatic gluconeogenesis during the later phase of fasting. Another potential mechanism by which IDE deficiency augments transcription of gluconeogenic genes may be upregulation of PGC-1α.

Gluconeogenesis at this late stage of fasting is maintained due to the action of FoxO1. We have observed a significant reduction in FoxO1 levels in shRNA-IDE cells due to posttranslational regulation. Zhou and collaborators demonstrated that the X-box binding protein 1 (XBP-1) interacts with FoxO1 and targets it to the

proteasome-mediated proteolytic pathway [201]. Thus, deletion of XBP-1 increases the abundance of FoxO1, whereas its overexpression decreases the abundance of FoxO1. Furthermore, this XBP-1-mediated proteolysis is regulated independently of insulin signaling via PKB2 [201]. It would be very interesting to investigate if XBP-1 levels mediate proteolytic regulation of FoxO1 in AML12-shRNA-IDE cells. On the other hand, acetylation of FoxO1 at Lys-242, Lys-245, and Lys-262 by CBP and p300 attenuates FoxO1's transcriptional activity and phosphorylation [202,203]. However, deacetylation of FoxO1 by SIRT1 promotes its binding to the promoters of gluconeogenic genes. This modification also desensitizes proteasome-mediated degradation of FoxO1, resulting in constitutive activation of FoxO1 leading to overstimulation of gluconeogenic genes [204]. Impaired deacetylation of FoxO1 by SIRT1 may also contribute to lower abundance of FoxO1 in the setting of reduced IDE levels.

In summary, multiple mechanisms altering transcriptional and post-transcriptional regulation of nuclear factors and co-activators may explain the observed effects on gluconeogenesis in conditions of lower hepatic IDE levels. Among them, IDE-mediated regulation of SIRT1 may account for effects seen on gluconeogenesis. In fact, it has been described that SIRT1 overexpression enhanced expression of IDE in cultures of neurons [205]. Thus, in the hypothetical case that lower abundance of IDE would result in reduced cellular levels of SIRT1, the abundance of acetylated-CRTC2 and -FoxO1 would be increased. Acetylation of CRTC2 would protect it from being degraded by the proteasome at early and late stages of fasting leading to efficiently sustain gluconeogenic genes expression. Conversely, acetylation of FoxO1 would sensitize the transcriptional factor for proteasome-mediated degradation contributing to lower abundance of FoxO1 (**Fig. 45**).

Figure 45: Diagram illustrating hypothetical SIRT1-mediated regulatory mechanisms of gluconeogenesis in hepatocytes with low abundancy of IDE. A. In the presence of IDE at early stage of fasting, p300 acetylates CRTC2 protecting it from being degraded by the proteasome and leading to transcription of gluconeogenic genes and PGC-1α. At the same time, CBP and p300 acetylated FoxO1 favoring its proteasomal degradation and attenuating its transcriptional activity. At late stage SIRT1 deacetylates CRTC2 allowing its degradation by the proteasome. On the other hand, at late-stage deacetylation of FoxO1 by SIRT1 protects it from being degraded by the proteasome and leading to transcription of gluconeogenic genes and ERRγ. **B.** Under conditions of low abundance of IDE (e.g., HFD) the abundance of SIRT1 protein levels is significantly reduced, leading to higher levels of acetylated CRCT2 and FoxO1. Acetylation of CRTC2 efficiently sustain gluconeogenic genes transcription, whereas acetylation of FoxO1 its degradation by the proteasome.

On the other hand, the nuclear receptors are a superfamily of transcription factors including homodimeric nuclear receptors, heterodimeric nuclear receptors, and monomeric nuclear receptors that regulates hepatic gluconeogenesis at later stages of fasting [189]. Homodimeric nuclear receptors normally reside in the cytosol by interacting with molecular chaperones such as heat shock proteins (HSPs). Upon the binding of steroid-derived ligands, such as glucocorticoid or estrogen), glucocorticoid receptor (GR) or ERRγ translocate to the nucleus and bind to promoters of gluconeogenic genes. Full transcriptional activation of these nuclear receptors requires an association with transcriptional co-activator PGC1α. Because IDE has been proposed to act as an HSP [168], another potential mechanism by which regulates gluconeogenesis is through this non-proteolytic function. In this case, reduced abundance of cytoplasmatic IDE

would result in augmented nuclear translocation of GR and ERRγ leading to constitutive transcription of gluconeogenic genes (**Fig. 46**).
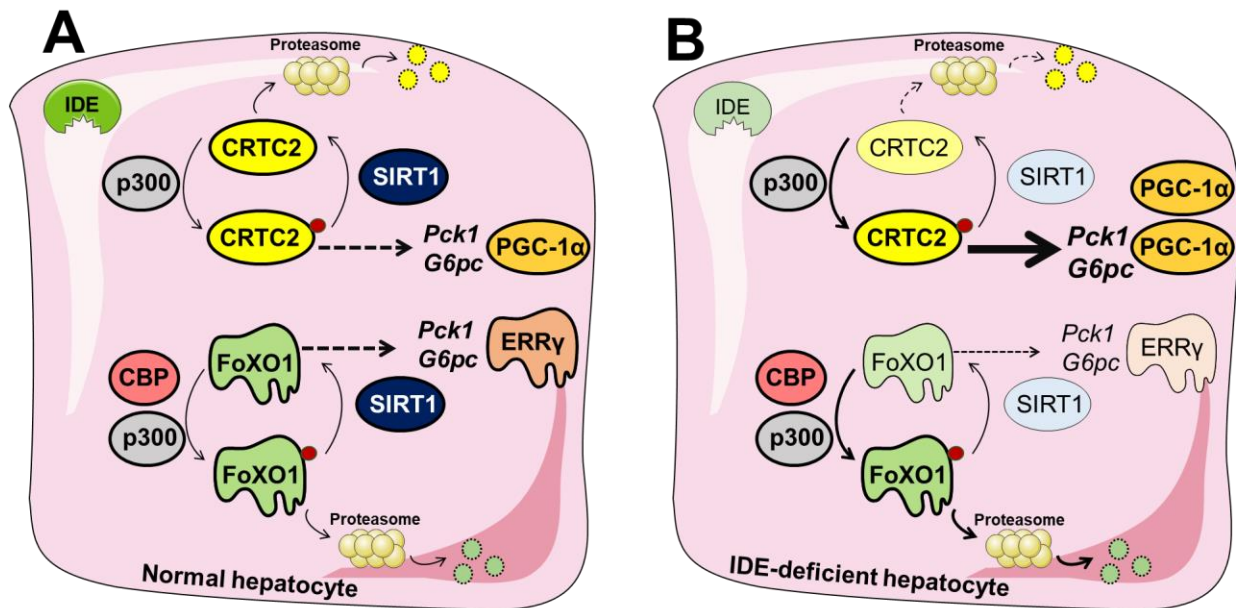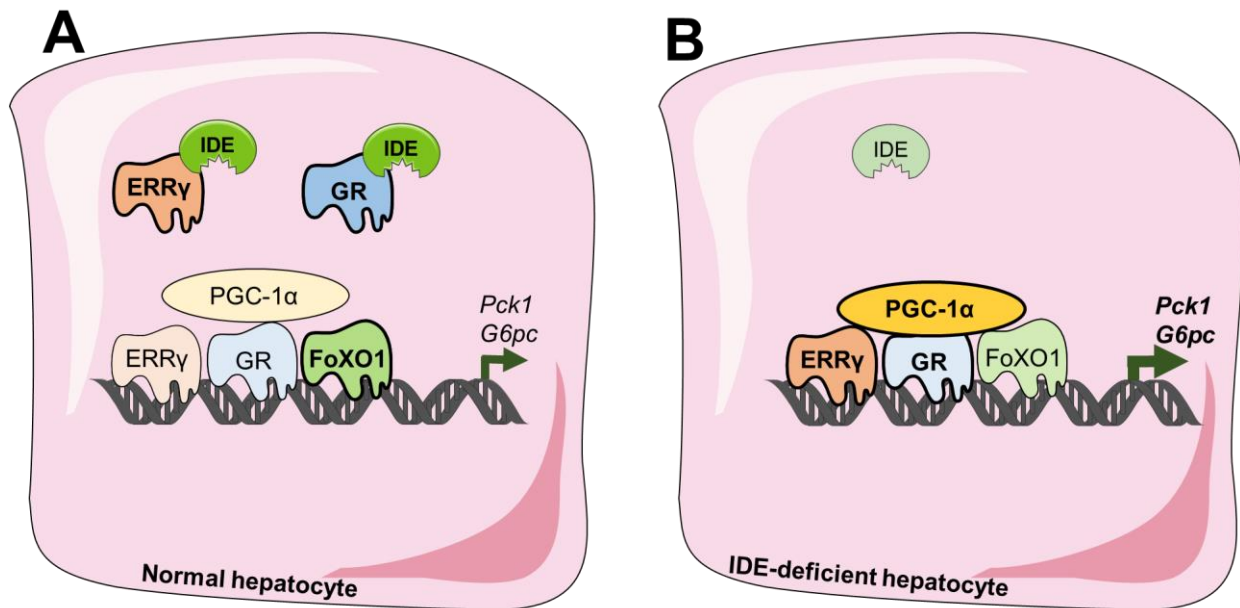

Figure 46: Diagram illustrating hypothetical nuclear receptors-mediated regulatory mechanisms of gluconeogenesis in hepatocytes with low abundancy of IDE. A. At late phase of fasting, transcriptional activation of hepatic gluconeogenesis is driven by PGC-1α and FoxO1. Most of ERRγ and GR transcription factors reside in the cytosol by interacting with IDE, which is acting as an HSP or chaperone. **B.** Under conditions of low abundance of IDE, the early phase triggers higher PCC-1α levels and lower abundance of FoxO1, but the majority of ERRγ and GR translocate to the nucleus increasing gluconeogenic genes expression.

Finally, our findings support coining the term "selective hepatic glucagon resistance" as it was proposed by Brown MS and Goldstein JL for "selective hepatic insulin resistance" [206]. Although IDE partially abolished glucagon-mediated signaling in hepatocytes, the net effect is to enhance expression of gluconeogenic genes.

From an integrated physiological perspective, we must consider the intricate signaling effectors that carry out the cell-autonomous response to glucagon in the context of tissue-specific metabolism that coordinates gluconeogenic response. Thus, the relative contribution of glucagon to glucose production varies depending on glycogen content and the availability of gluconeogenic substrates in the circulation, particularly, the adipocyte-hepatocyte axis. In this line of thinking, glucagon stimulates hepatic amino acid metabolism [207] and turnover through cAMP-PKA-CREB signaling [208,209], resulting in an increased flux of

amino acids into the hepatocytes and is thereby also able to provide substrates in the form of gluconeogenic amino acids. Finally, hepatic elimination of GCGR is sufficient to induce an increased α-cell mas [210]. When glucagon signaling is inhibited, hyperaminoacidemia occurs, which has been suggested as the factor leading to α-cell hyperplasia. The impact of "selective hepatic glucagon resistance"- mediated by IDE on hepatic amino acid metabolism and the liver-alpha cells axis is currently completely unknown, and further studies are warranted.

V.3.4 Hepatic insulin signaling in AML12-shRNA-IDE cells

We have previously shown that hepatic *Ide* deletion results in insulin resistance in livers from L-IDE-KO mice [70,71]. Unexpectedly, insulin signaling was significantly improved in AML12-shRNA-IDE cells. These contradictory results may be explained in two ways: (1) Culture media for AML12 contains high levels of insulin and dexamethasone which can be confounded variables altering the insulin signaling in these cells. (2) shRNA-mediated ablation of *Ide* resulted in a reduction of IDE levels by ~50%, whereas in livers from L-IDE-KO the expression of IDE was completely abolished. Thus, an expression-dependent effect may explain the observed phenotype on insulin signaling in AML12 cells. On the other hand, these are immortalized cells, which substantially differs from hepatocytes from livers of L-IDE-KO mice. Interestingly, we have developed a cell line in which *Ide* was ablated in HepG2 using the CRISPER/Cas9 system, resulting in impaired insulin signaling as seen in livers from L-IDE-KO mice (data in progress, not shown in this thesis). Nonetheless, it would be worthy to investigate the expression-dependent impact on insulin signaling in heterozygous L-IDE-KO mice as compared to homozygous controls.

V.4. Role of hepatic IDE on mitochondrial function and biogenesis.

Mitochondria are dynamically cellular organelles that constantly undergo morphological changes such as fusion (elongation) or fission (fragmentation), which are associated with maintenance of mitochondrial function and meeting bioenergetic demands for hepatocyte polarization [211]. On the other hand,

hepatocytes have a well-defined polarized morphology, which includes apical and basolateral membrane domains that are segregated for tight junctions [212]. Polarization is an energy-dependent process essential for hepatocyte function, metabolism, excretion, and detoxification [213]. Further studies are warranted to demonstrate whether IDE regulates hepatocyte polarization.

Since we have demonstrated that IDE upregulates mitochondrial respiration and energy production from both glycolytic and mitochondrial ATP production rates, we demonstrate that IDE regulates mitochondrial function. Our studies have not identified at what level IDE regulates mitochondrial respiration, but considering that FoxO1 levels are diminished, most likely, IDE regulates mitochondrial biogenesis through a FoxO1-dependent mechanism. It would be of relevance to understand whether fusion or fission are altered in shRNA-AML12-IDE cells.

On the other hand, the cellular energy sensor AMPK, which senses the cellular ratio AMP/ATP, plays a crucial role in coordinating multiple cellular process to maintain energy homeostasis [214] for hepatocytes to polarize, including mitochondrial biogenesis [214]. The impact of IDE on AMPK has not been addressed in this work but is a worth avenue to explore if IDE regulates mitochondrial respiration and possibly biogenesis through AMPK.

As we mentioned above, IDE regulates cytoskeleton integrity in pancreatic endocrine cells and loss of IDE in AML12 cells leads to alterations in acetylated tubulin. Organelle organization and transport rely on the dynamics and organization of cytoskeletal components such as microtubules and actin [215,216]. The main role of actin in mitochondrial dynamics is closely linked to the formation of endoplasmic reticulum contacts, known as ERMES (ER-mitochondria encounter structures), which are involved in mitochondrial fission and fusion [217,218]. Thus, the study of ERMES and the interaction of microtubules and/or microtubules-associated proteins (kinesis and dyneins) may open a new avenue to investigate non-proteolytic IDE functions.

In summary, the impact of IDE on hepatic mitochondrial function and biogenesis opens novel research lines of investigation which may led to uncover

new molecular and cellular mechanisms involving the cytoskeleton and the nutritional sensor AMPK.

As mentioned above, mitochondrial homeostasis is controlled by different processes, such as fusion, fission and autophagy (mitophagy). Different studies have underscore FoxO transcription factors as key mitochondrial regulator. Specifically, FoxOs regulate mitochondrial biogenesis by dampening the nuclear respiratory factor 1 - mitochondrial transcription factor A (NRF1-Tfam) and the proto-oncogene c-Myc - mitochondrial transcription factor A (c-Myc-Tfam) cascades directly, and inhibiting NAD-SIRT1-PGC-1α cascade indirectly by inducing heme oxygenase 1 gene (*Hmox1*) and repressing frataxin (*Fxn*) and uroporphyrinogen III decarboxylase (*Urod*). In addition, FoxOs mediate mitochondrial fusion, via mitofusin-1 (*Mfn1*) and mitofusin-2 (*Mfn2*), and fission, via dynamin-1-like protein (*Drp1*), mitochondrial fission 1 protein (*Fis1*), and mitochondrial elongation factor 2 (*Mief2*). FoxOs control mitophagy in the stages of autophagosome formation and maturation as reviewed in [219].

Yang and collaborators have described that glucagon regulates hepatic mitochondrial function and biogenesis through FoxO1 in HepG2 cells [118]. Glucagon decreased the heme production in a FoxO1-dependent manner, suppressed heme-dependent complex III (UQCRC1) and complex IV (MT-CO1) and inhibited hepatic mitochondrial function. In addition, glucagon tends to reduce hepatic mitochondrial biogenesis by attenuating the expression of NRF1, TFAM and MFN2, which is mediated by FoxO1. Importantly, the suppression of mitochondrial function by glucagon was largely rescued by deleting the FoxO1 gene in hepatocytes [118].

Since hepatic depletion of IDE in AML12 cells significantly reduces FoxO1 levels, we anticipate that genes controlling mitochondrial biogenesis (NRF1, TFAM and MFN2) and mitochondrial function (UQCRC1, MT-CO1) are upregulated in these cells, contributing to the observed mitochondrial phenotype. Finally, the axis IDE-FoxO1 in regulating mitochondrial function and biogenesis in hepatocytes deserves further research (**Fig. 47**).
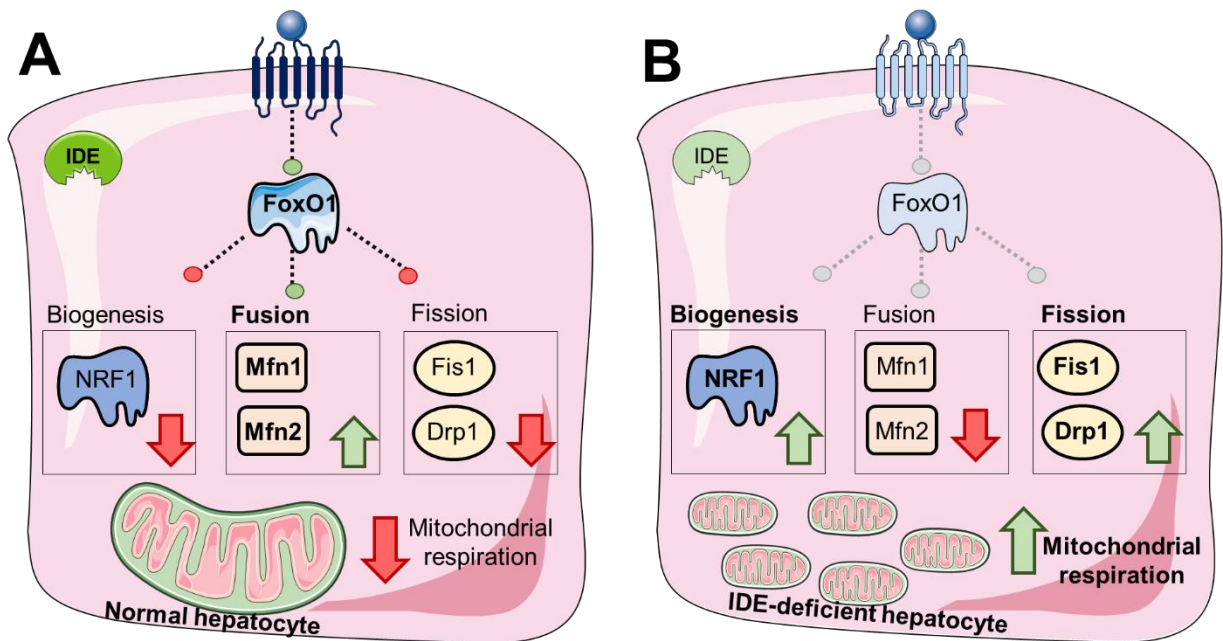
Figure 47: Illustration depicting FoxO1 regulation of mitochondrial dynamics in response to glucagon in AML12 cells. **A.** In hepatocytes, FoxO1 upregulates fusion proteins (Mfn1 and Mfn2), downregulates fission proteins (Drp1 and Fis1), and downregulates biogenesis (NRF1, Tfam) leading to enlarged mitochondria. **B.** In hepatocytes with low abundance of IDE, glucagon signaling is reduced in parallel with lower abundance of FoxO1 levels. In this scenario is favored mitochondrial biogenesis and fission leading to increased mitochondrial number and function.

V.5. Homology modelling-generated IDE structures.

As in most enzymes, the three-dimensional structure of IDE is closely linked to its function [19,21,28,220,221]. The ability to establish specific interactions with other proteins and substrates also requires a complex conformational configuration [19,21,28,220,221]. Therefore, in order to study IDE *in silico* and obtain results that are as representative of reality as possible, it is necessary to robustly generate a model of the structure of the enzyme. Structures reported by means of classical techniques as X-ray diffraction, magnetic resonance or more recently CryoEM; contain gaps and mutations typical of the methodology used to obtain them. These structures surely can be useful for many applications, but they offer limitations in a precise simulation of molecular dynamics. That is why in this thesis we decided to use experimentally obtained structures as templates for homology modeling of complete IDE structures, both human and murine, because mice are a frequently used animal model in the study of this protein, and with which the comparison of structural characteristics is mandatory. Recently, Ghoula and

103

collaborators have already produced a 3D model of the human IDE structure using the homology modeling methodology [222], although they focus only on the canonical sequence of the human IDE and they used that system to evaluate the mechanistic of closed to opened state conformational changes [222]. However, in our case, in addition to the model with the canonical human IDE with exon 15a translated, we have also generated the human IDE with exon 15b translated and both isoforms of the murine sequences. Furthermore, with our models generated with multiple template alignments using several experimental 3D structures to fill the gaps in the better selected one (PDB code: 2JG4) [84], we have obtained lower DOPE-HR scores than when using 2JG4 as single template and de novo modeling of the loops not contained in the template. In addition, our models have obtained good structural quality control scores, so they are suitable and will be useful for future molecular dynamics and docking simulation approaches.

It is of interest, even when not significant difference on free energy were calculated for each of our models, that when we quantified the number of potential hydrogen bonds, we found that this kind of non-covalent interaction is more abundant in the 15a isoforms of both species studied compared to the 15b ones. That is understandable being 15b isoform previously described as less active [117] and taking into consideration the role of hydrogen bonding in the mechanistic of IDE activity [19,223,224].

V.6. Acknowledge of limitations.

Our studies present some limitations that could be improved and need to be addressed in future studies. For example: preferred use of primary hepatocytes over immortalized cell lines, phenotypic characterization of female mice, use of an inducible liver specific *Ide* knock-out mouse model, and, the use of human hepatocytes. *In silico*-generated models should be refined before being used in molecular dynamic simulations.

VI. Conclusions

I. Our results highlight that the regulation of hepatic IDE in response to the fasting-to-postprandial transition is more complex than previously expected in mice. In addition to insulin, glucose and NEFA, we have identified circulating lactate levels as principal determinants in regulating hepatic IDE. Finally, we propose lactate as an inter-organ metabolite produced in skeletal muscle that regulates hepatic IDE activation in response to changes in the nutritional status.

II. Hepatic IDE protein levels, but not its activity, strongly correlate with a surrogate assessment of insulin resistance. sPIF-mediated recovery of IDE activity does not counteract insulin resistance in hepatocytes. These findings indicate that pharmacological approaches aimed at targeting IDE protein levels, rather than its enzymatic activity, would be a better approach for treating hepatic insulin resistance.

III. For the first time, we demonstrate a cause-effect relationship between IDE and impaired hepatic glucagon signal transduction through a mechanism that, at least in part, involves posttranscriptional down-regulation of glucagon receptors. Unexpectedly, hepatic IDE loss of expression leads to upregulation of gluconeogenic genes in a time-dependent manner. Our findings challenge the current notion that hepatic glucagon resistance in mice is beneficial for maintaining glucose homeostasis and lend support to the notion that IDE is involved in the pathophysiology of hepatic-mediated hyperglycemia in type 2 diabetes.

IV. We demonstrate that IDE regulates mitochondrial function by increasing glycolytic and mitochondrial ATP production rates, which results in a high-energetic cell status, at least in part, through FoxO1-dependent mechanism(s). These findings lend support to novel non-proteolytic IDE functions in regulating energy homeostasis in hepatocytes.

V. In this work, we generated *in silico* models of complete human and murine IDE structures of both 15a and 15b isoforms; being the 15b ones, to our knowledge, the first complete structures generated for those isoforms. All our models were of good quality and will be useful to perform molecular dynamics simulations and docking.

VII. References

1. International Diabetes Federation. IDF Diabetes Atlas, 10th edn. Brussels, Belgium. 2021. Available online: https://www.diabetesatlas.org (accessed on May, 2022).

2. O'Sullivan, J.B. Gestational diabetes. Unsuspected, asymptomatic diabetes in pregnancy. *N Engl J Med* **1961**, *264*, 1082-1085, doi:10.1056/nejm196105252642104.

3. Pinés Corrales, P.J.; Villodre Lozano, P.; Quílez Toboso, R.P.; Moya Moya, A.J.; López García, M.D.C. Prevalence of gestational diabetes with a 2-step strategy and cut-off values from the 1979 National Diabetes Data Group. Are we applying the best strategy for our patients? *Endocrinol Diabetes Nutr (Engl Ed)* **2022**, doi:10.1016/j.endien.2022.06.006.

4. Garvick, S.; Altenburg, L.; Dunlap, B.; Fisher, A.; Watson, A.; Gregory, T. Diagnosis and management of type 2 diabetes in children. *Jaapa* **2022**, *35*, 16-22, doi:10.1097/01.JAA.0000832648.15129.b8.

5. Shibib, L.; Al-Qaisi, M.; Ahmed, A.; Miras, A.D.; Nott, D.; Pelling, M.; Greenwald, S.E.; Guess, N. Reversal and Remission of T2DM - An Update for Practitioners. *Vasc Health Risk Manag* **2022**, *18*, 417-443, doi:10.2147/vhrm.S345810.

6. Idrees, T.; Castro-Revoredo, I.A.; Migdal, A.L.; Moreno, E.M.; Umpierrez, G.E. Update on the management of diabetes in long-term care facilities. *BMJ Open Diabetes Res Care* **2022**, *10*, doi:10.1136/bmjdrc-2021-002705.

7. Janah, L.; Kjeldsen, S.; Galsgaard, K.D.; Winther-Sørensen, M.; Stojanovska, E.; Pedersen, J.; Knop, F.K.; Holst, J.J.; Wewer Albrechtsen, N.J. Glucagon Receptor Signaling and Glucagon Resistance. *Int J Mol Sci* **2019**, *20*, doi:10.3390/ijms20133314.

8. Rodgers, R.L. Glucagon, cyclic AMP, and hepatic glucose mobilization: A half-century of uncertainty. *Physiol Rep* **2022**, *10*, e15263, doi:10.14814/phy2.15263.

9. Wakelam, M.J.; Murphy, G.J.; Hruby, V.J.; Houslay, M.D. Activation of two signal-transduction systems in hepatocytes by glucagon. *Nature* **1986**, *323*, 68-71, doi:10.1038/323068a0.

10. Sinclair, E.M.; Yusta, B.; Streutker, C.; Baggio, L.L.; Koehler, J.; Charron, M.J.; Drucker, D.J. Glucagon receptor signaling is essential for control of murine hepatocyte survival. *Gastroenterology* **2008**, *135*, 2096-2106, doi:10.1053/j.gastro.2008.07.075.

11. Gilon, P. The Role of α-Cells in Islet Function and Glucose Homeostasis in Health and Type 2 Diabetes. *J Mol Biol* **2020**, *432*, 1367-1394, doi:10.1016/j.jmb.2020.01.004.

12. Baron, A.D.; Schaeffer, L.; Shragg, P.; Kolterman, O.G. Role of hyperglucagonemia in maintenance of increased rates of hepatic glucose output in type II diabetics. *Diabetes* **1987**, *36*, 274-283, doi:10.2337/diab.36.3.274.

13. Asadi, F.; Dhanvantari, S. Pathways of Glucagon Secretion and Trafficking in the Pancreatic Alpha Cell: Novel Pathways, Proteins, and Targets for

Hyperglucagonemia. *Front Endocrinol (Lausanne)* **2021**, *12*, 726368, doi:10.3389/fendo.2021.726368.

14. Ye, J. Mechanism of insulin resistance in obesity: a role of ATP. *Front Med* **2021**, *15*, 372-382, doi:10.1007/s11684-021-0862-5.

15. Merino, B.; Casanueva-Álvarez, E.; Quesada, I.; González-Casimiro, C.M.; Fernández-Díaz, C.M.; Postigo-Casado, T.; Leissring, M.A.; Kaestner, K.H.; Perdomo, G.; Cózar-Castellano, I. Insulin-degrading enzyme ablation in mouse pancreatic alpha cells triggers cell proliferation, hyperplasia and glucagon secretion dysregulation. *Diabetologia* **2022**, doi:10.1007/s00125-022-05729-y.

16. Pablos, M.; Casanueva-Álvarez, E.; González-Casimiro, C.M.; Merino, B.; Perdomo, G.; Cózar-Castellano, I. Primary Cilia in Pancreatic β- and α-Cells: Time to Revisit the Role of Insulin-Degrading Enzyme. *Front Endocrinol (Lausanne)* **2022**, *13*, 922825, doi:10.3389/fendo.2022.922825.

17. González-Casimiro, C.M.; Merino, B.; Casanueva-Álvarez, E.; Postigo-Casado, T.; Cámara-Torres, P.; Fernández-Díaz, C.M.; Leissring, M.A.; Cózar-Castellano, I.; Perdomo, G. Modulation of Insulin Sensitivity by Insulin-Degrading Enzyme. *Biomedicines* **2021**, *9*, doi:10.3390/biomedicines9010086.

18. Leissring, M.A.; González-Casimiro, C.M.; Merino, B.; Suire, C.N.; Perdomo, G. Targeting Insulin-Degrading Enzyme in Insulin Clearance. *Int J Mol Sci* **2021**, *22*, doi:10.3390/ijms22052235.

19. Shen, Y.; Joachimiak, A.; Rosner, M.R.; Tang, W.J. Structures of human insulin-degrading enzyme reveal a new substrate recognition mechanism. *Nature* **2006**, *443*, 870-874, doi:10.1038/nature05143.

20. Stefanidis, L.; Fusco, N.D.; Cooper, S.E.; Smith-Carpenter, J.E.; Alper, B.J. Molecular Determinants of Substrate Specificity in Human Insulin-Degrading Enzyme. *Biochemistry* **2018**, *57*, 4903-4914, doi:10.1021/acs.biochem.8b00474.

21. Affholter, J.A.; Cascieri, M.A.; Bayne, M.L.; Brange, J.; Casaretto, M.; Roth, R.A. Identification of residues in the insulin molecule important for binding to insulin-degrading enzyme. *Biochemistry* **1990**, *29*, 7727-7733, doi:10.1021/bi00485a022.

22. Schäffer, L. A model for insulin binding to the insulin receptor. *European journal of biochemistry* **1994**, *221*, 1127-1132, doi:10.1111/j.1432-1033.1994.tb18833.x.

23. Kristensen, C.; Kjeldsen, T.; Wiberg, F.C.; Schäffer, L.; Hach, M.; Havelund, S.; Bass, J.; Steiner, D.F.; Andersen, A.S. Alanine scanning mutagenesis of insulin. *J Biol Chem* **1997**, *272*, 12978-12983, doi:10.1074/jbc.272.20.12978.

24. De Meyts, P. Insulin/receptor binding: the last piece of the puzzle? What recent progress on the structure of the insulin/receptor complex tells us (or not) about negative cooperativity and activation. *BioEssays : news and*

reviews in molecular, cellular and developmental biology **2015**, *37*, 389-397, doi:10.1002/bies.201400190.

25. Macháčková, K.; Mlčochová, K.; Potalitsyn, P.; Hanková, K.; Socha, O.; Buděšínský, M.; Muždalo, A.; Lepšík, M.; Černeková, M.; Radosavljević, J.; et al. Mutations at hypothetical binding site 2 in insulin and insulin-like growth factors 1 and 2 result in receptor- and hormone-specific responses. *J Biol Chem* **2019**, *294*, 17371-17382, doi:10.1074/jbc.RA119.010072.

26. Manolopoulou, M.; Guo, Q.; Malito, E.; Schilling, A.B.; Tang, W.J. Molecular basis of catalytic chamber-assisted unfolding and cleavage of human insulin by human insulin-degrading enzyme. *J Biol Chem* **2009**, *284*, 14177-14188, doi:10.1074/jbc.M900068200.

27. Fagan, J.M.; Waxman, L. Purification of a protease in red blood cells that degrades oxidatively damaged haemoglobin. *Biochem J* **1991**, *277 (Pt 3)*, 779-786, doi:10.1042/bj2770779.

28. Zhang, Z.; Liang, W.G.; Bailey, L.J.; Tan, Y.Z.; Wei, H.; Wang, A.; Farcasanu, M.; Woods, V.A.; McCord, L.A.; Lee, D.; et al. Ensemble cryoEM elucidates the mechanism of insulin capture and degradation by human insulin degrading enzyme. *Elife* **2018**, *7*, doi:10.7554/eLife.33572.

29. Humphrey, W.; Dalke, A.; Schulten, K. VMD: visual molecular dynamics. *Journal of molecular graphics* **1996**, *14*, 33-38, 27-38, doi:10.1016/0263-7855(96)00018-5.

30. Elbein, S.C.; Hoffman, M.D.; Teng, K.; Leppert, M.F.; Hasstedt, S.J. A genome-wide search for type 2 diabetes susceptibility genes in Utah Caucasians. *Diabetes* **1999**, *48*, 1175-1182, doi:10.2337/diabetes.48.5.1175.

31. Groves, C.J.; Wiltshire, S.; Smedley, D.; Owen, K.R.; Frayling, T.M.; Walker, M.; Hitman, G.A.; Levy, J.C.; O'Rahilly, S.; Menzel, S.; et al. Association and haplotype analysis of the insulin-degrading enzyme (IDE) gene, a strong positional and biological candidate for type 2 diabetes susceptibility. *Diabetes* **2003**, *52*, 1300-1305, doi:10.2337/diabetes.52.5.1300.

32. Karamohamed, S.; Demissie, S.; Volcjak, J.; Liu, C.; Heard-Costa, N.; Liu, J.; Shoemaker, C.M.; Panhuysen, C.I.; Meigs, J.B.; Wilson, P.; et al. Polymorphisms in the insulin-degrading enzyme gene are associated with type 2 diabetes in men from the NHLBI Framingham Heart Study. *Diabetes* **2003**, *52*, 1562-1567, doi:10.2337/diabetes.52.6.1562.

33. Gu, H.F.; Efendic, S.; Nordman, S.; Ostenson, C.G.; Brismar, K.; Brookes, A.J.; Prince, J.A. Quantitative trait loci near the insulin-degrading enzyme (IDE) gene contribute to variation in plasma insulin levels. *Diabetes* **2004**, *53*, 2137-2142, doi:10.2337/diabetes.53.8.2137.

34. Sladek, R.; Rocheleau, G.; Rung, J.; Dina, C.; Shen, L.; Serre, D.; Boutin, P.; Vincent, D.; Belisle, A.; Hadjadj, S.; et al. A genome-wide association study identifies novel risk loci for type 2 diabetes. *Nature* **2007**, *445*, 881-885, doi:10.1038/nature05616.

35. Kwak, S.H.; Cho, Y.M.; Moon, M.K.; Kim, J.H.; Park, B.L.; Cheong, H.S.; Shin, H.D.; Jang, H.C.; Kim, S.Y.; Lee, H.K.; et al. Association of polymorphisms in the insulin-degrading enzyme gene with type 2 diabetes in the Korean population. *Diabetes research and clinical practice* **2008**, *79*, 284-290, doi:10.1016/j.diabres.2007.08.017.

36. Furukawa, Y.; Shimada, T.; Furuta, H.; Matsuno, S.; Kusuyama, A.; Doi, A.; Nishi, M.; Sasaki, H.; Sanke, T.; Nanjo, K. Polymorphisms in the IDE-KIF11-HHEX gene locus are reproducibly associated with type 2 diabetes in a Japanese population. *The Journal of clinical endocrinology and metabolism* **2008**, *93*, 310-314, doi:10.1210/jc.2007-1029.

37. Nordman, S.; Ostenson, C.G.; Efendic, S.; Gu, H.F. Loci of TCF7L2, HHEX and IDE on chromosome 10q and the susceptibility of their genetic polymorphisms to type 2 diabetes. *Experimental and clinical endocrinology & diabetes : official journal, German Society of Endocrinology [and] German Diabetes Association* **2009**, *117*, 186-190, doi:10.1055/s-0028-1100419.

38. Slominskiĭ, P.A.; Pivovarova, O.V.; Shadrina, M.I.; Artem'eva, A.V.; Pfaipffer, F.G.; Rudovich, N.N.; Agadzhanian, S.E.; Pronin, V.S.; Limborskaia, S.A. Association of insulinase gene polymorphisms with type 2 diabetes mellitus in patients from the Moscow population. *Genetika* **2009**, *45*, 113-117, doi:10.1134/S1022795409010165.

39. Rudovich, N.; Pivovarova, O.; Fisher, E.; Fischer-Rosinsky, A.; Spranger, J.; Möhlig, M.; Schulze, M.B.; Boeing, H.; Pfeiffer, A.F. Polymorphisms within insulin-degrading enzyme (IDE) gene determine insulin metabolism and risk of type 2 diabetes. *Journal of molecular medicine (Berlin, Germany)* **2009**, *87*, 1145-1151, doi:10.1007/s00109-009-0540-6.

40. Hu, C.; Zhang, R.; Wang, C.; Wang, J.; Ma, X.; Lu, J.; Qin, W.; Hou, X.; Wang, C.; Bao, Y.; et al. PPARG, KCNJ11, CDKAL1, CDKN2A-CDKN2B, IDE-KIF11-HHEX, IGF2BP2 and SLC30A8 are associated with type 2 diabetes in a Chinese population. *PloS one* **2009**, *4*, e7643, doi:10.1371/journal.pone.0007643.

41. Zhao, J.; Bradfield, J.P.; Zhang, H.; Annaiah, K.; Wang, K.; Kim, C.E.; Glessner, J.T.; Frackelton, E.C.; Otieno, F.G.; Doran, J.; et al. Examination of all type 2 diabetes GWAS loci reveals HHEX-IDE as a locus influencing pediatric BMI. *Diabetes* **2010**, *59*, 751-755, doi:10.2337/db09-0972.

42. Cotsapas, C.; Prokunina-Olsson, L.; Welch, C.; Saxena, R.; Weaver, C.; Usher, N.; Guiducci, C.; Bonakdar, S.; Turner, N.; LaCroix, B.; et al. Expression analysis of loci associated with type 2 diabetes in human tissues. *Diabetologia* **2010**, *53*, 2334-2339, doi:10.1007/s00125-010-1861-2.

43. McFall, G.P.; Wiebe, S.A.; Vergote, D.; Westaway, D.; Jhamandas, J.; Dixon, R.A. IDE (rs6583817) polymorphism and type 2 diabetes differentially modify executive function in older adults. *Neurobiology of aging* **2013**, *34*, 2208-2216, doi:10.1016/j.neurobiolaging.2013.03.010.

44. Xu, W.L.; Pedersen, N.L.; Keller, L.; Kalpouzos, G.; Wang, H.X.; Graff, C.; Winblad, B.; Bäckman, L.; Fratiglioni, L. HHEX_23 AA Genotype

Exacerbates Effect of Diabetes on Dementia and Alzheimer Disease: A Population-Based Longitudinal Study. *PLoS medicine* **2015**, *12*, e1001853, doi:10.1371/journal.pmed.1001853.

45.   Lu, X.; Huang, Y.; Liu, Y.; Wu, X.; Shi, X. Variants in the insulin-degrading enzyme gene are associated with metabolic syndrome in Chinese elders. *Metabolism: clinical and experimental* **2009**, *58*, 1465-1469, doi:10.1016/j.metabol.2009.04.027.

46.   Fosam, A.; Sikder, S.; Abel, B.S.; Tella, S.H.; Walter, M.F.; Mari, A.; Muniyappa, R. Reduced Insulin Clearance and Insulin-Degrading Enzyme Activity Contribute to Hyperinsulinemia in African Americans. *The Journal of clinical endocrinology and metabolism* **2020**, *105*, doi:10.1210/clinem/dgaa070.

47.   Sofer, Y.; Nash, Y.; Osher, E.; Fursht, O.; Goldsmith, G.; Nahary, L.; Shaklai, S.; Tordjman, K.M.; Serebro, M.; Touati, E.B.; et al. Insulin-degrading enzyme higher in subjects with metabolic syndrome. *Endocrine* **2021**, doi:10.1007/s12020-020-02548-2.

48.   Pivovarova, O.; von Loeffelholz, C.; Ilkavets, I.; Sticht, C.; Zhuk, S.; Murahovschi, V.; Lukowski, S.; Döcke, S.; Kriebel, J.; de las Heras Gala, T.; et al. Modulation of insulin degrading enzyme activity and liver cell proliferation. *Cell cycle (Georgetown, Tex.)* **2015**, *14*, 2293-2300, doi:10.1080/15384101.2015.1046647.

49.   Fawcett, J.; Sang, H.; Permana, P.A.; Levy, J.L.; Duckworth, W.C. Insulin metabolism in human adipocytes from subcutaneous and visceral depots. *Biochemical and biophysical research communications* **2010**, *402*, 762-766, doi:10.1016/j.bbrc.2010.10.104.

50.   Bojsen-Møller, K.N.; Lundsgaard, A.M.; Madsbad, S.; Kiens, B.; Holst, J.J. Hepatic Insulin Clearance in Regulation of Systemic Insulin Concentrations-Role of Carbohydrate and Energy Availability. *Diabetes* **2018**, *67*, 2129-2136, doi:10.2337/db18-0539.

51.   Farris, W.; Mansourian, S.; Chang, Y.; Lindsley, L.; Eckman, E.A.; Frosch, M.P.; Eckman, C.B.; Tanzi, R.E.; Selkoe, D.J.; Guenette, S. Insulin-degrading enzyme regulates the levels of insulin, amyloid beta-protein, and the beta-amyloid precursor protein intracellular domain in vivo. *Proceedings of the National Academy of Sciences of the United States of America* **2003**, *100*, 4162-4167, doi:10.1073/pnas.0230450100.

52.   Abdul-Hay, S.O.; Kang, D.; McBride, M.; Li, L.; Zhao, J.; Leissring, M.A. Deletion of insulin-degrading enzyme elicits antipodal, age-dependent effects on glucose and insulin tolerance. *PloS one* **2011**, *6*, e20818, doi:10.1371/journal.pone.0020818

PONE-D-10-05674 [pii].

53.   Steneberg, P.; Bernardo, L.; Edfalk, S.; Lundberg, L.; Backlund, F.; Ostenson, C.G.; Edlund, H. The type 2 diabetes-associated gene ide is required for insulin secretion and suppression of alpha-synuclein levels in beta-cells. *Diabetes* **2013**, *62*, 2004-2014, doi:db12-1045 [pii]

10.2337/db12-1045.

54.   Villa-Pérez, P.; Merino, B.; Fernandez-Diaz, C.M.; Cidad, P.; Lobaton, C.D.; Moreno, A.; Muturi, H.T.; Ghadieh, H.E.; Najjar, S.M.; Leissring, M.A.; et al. Liver-specific ablation of insulin-degrading enzyme causes hepatic insulin resistance and glucose intolerance, without affecting insulin clearance in mice. *Metabolism: clinical and experimental* **2018**, doi:10.1016/j.metabol.2018.08.001.

55.   Najjar, S.M. Regulation of insulin action by CEACAM1. *Trends in endocrinology and metabolism: TEM* **2002**, *13*, 240-245, doi:10.1016/s1043-2760(02)00608-2.

56.   Merino, B.; Fernández-Díaz, C.M.; Parrado-Fernández, C.; González-Casimiro, C.M.; Postigo-Casado, T.; Lobaton, C.D.; Leissring, M.A.; Cózar-Castellano, I.; Perdomo, G. Hepatic insulin-degrading enzyme regulates glucose and insulin homeostasis in diet-induced obese mice. *Metabolism: clinical and experimental* **2020**, 154352, doi:10.1016/j.metabol.2020.154352.

57.   Ramu, S.; Stamatkin, C.; Timms, L.; Ruble, M.; Roussev, R.G.; Barnea, E.R. PreImplantation factor (PIF) detection in maternal circulation in early pregnancy correlates with live birth (bovine model). *Reprod Biol Endocrinol* **2013**, *11*, 105, doi:10.1186/1477-7827-11-105.

58.   Stamatkin, C.W.; Roussev, R.G.; Stout, M.; Absalon-Medina, V.; Ramu, S.; Goodman, C.; Coulam, C.B.; Gilbert, R.O.; Godke, R.A.; Barnea, E.R. PreImplantation Factor (PIF) correlates with early mammalian embryo development-bovine and murine models. *Reprod Biol Endocrinol* **2011**, *9*, 63, doi:10.1186/1477-7827-9-63.

59.   Barnea, E.R.; Kirk, D.; Paidas, M.J. Preimplantation factor (PIF) promoting role in embryo implantation: increases endometrial integrin-α2β3, amphiregulin and epiregulin while reducing betacellulin expression via MAPK in decidua. *Reprod Biol Endocrinol* **2012**, *10*, 50, doi:10.1186/1477-7827-10-50.

60.   Barnea, E.R. Applying embryo-derived immune tolerance to the treatment of immune disorders. *Ann N Y Acad Sci* **2007**, *1110*, 602-618, doi:10.1196/annals.1423.064.

61.   Coulam, C.B.; Roussev, R.G.; Thomason, E.J.; Barnea, E.R. Preimplantation factor (PIF) predicts subsequent pregnancy loss. *Am J Reprod Immunol* **1995**, *34*, 88-92, doi:10.1111/j.1600-0897.1995.tb00923.x.

62.   Zare, F.; Seifati, S.M.; Dehghan-Manshadi, M.; Fesahat, F. Preimplantation Factor (PIF): a peptide with various functions. *JBRA Assist Reprod* **2020**, *24*, 214-218, doi:10.5935/1518-0557.20190082.

63.   Duzyj, C.M.; Barnea, E.R.; Li, M.; Huang, S.J.; Krikun, G.; Paidas, M.J. Preimplantation factor promotes first trimester trophoblast invasion. *Am J Obstet Gynecol* **2010**, *203*, 402.e401-404, doi:10.1016/j.ajog.2010.06.060.

64.   O'Brien, C.B.; Barnea, E.R.; Martin, P.; Levy, C.; Sharabi, E.; Bhamidimarri, K.R.; Martin, E.; Arosemena, L.; Schiff, E.R. Randomized, Double-Blind, Placebo-Controlled, Single Ascending Dose Trial of

Synthetic Preimplantation Factor in Autoimmune Hepatitis. *Hepatol Commun* **2018**, *2*, 1235-1246, doi:10.1002/hep4.1239.

65. Weiss, L.; Bernstein, S.; Jones, R.; Amunugama, R.; Krizman, D.; Jebailey, L.; Almogi-Hazan, O.; Yekhtin, Z.; Shiner, R.; Reibstein, I.; et al. Preimplantation factor (PIF) analog prevents type I diabetes mellitus (TIDM) development by preserving pancreatic function in NOD mice. *Endocrine* **2011**, *40*, 41-54, doi:10.1007/s12020-011-9438-5.

66. Chen, Y.C.; Rivera, J.; Fitzgerald, M.; Hausding, C.; Ying, Y.L.; Wang, X.; Todorova, K.; Hayrabedyan, S.; Barnea, E.R.; Peter, K. PreImplantation factor prevents atherosclerosis via its immunomodulatory effects without affecting serum lipids. *Thromb Haemost* **2016**, *115*, 1010-1024, doi:10.1160/th15-08-0640.

67. Paidas, M.J.; Krikun, G.; Huang, S.J.; Jones, R.; Romano, M.; Annunziato, J.; Barnea, E.R. A genomic and proteomic investigation of the impact of preimplantation factor on human decidual cells. *Am J Obstet Gynecol* **2010**, *202*, 459.e451-458, doi:10.1016/j.ajog.2010.03.024.

68. Hayrabedyan, S.; Todorova, K.; Spinelli, M.; Barnea, E.R.; Mueller, M. The core sequence of PIF competes for insulin/amyloid β in insulin degrading enzyme: potential treatment for Alzheimer's disease. *Oncotarget* **2018**, *9*, 33884-33895, doi:10.18632/oncotarget.26057.

69. Cózar-Castellano, I.; Perdomo, G. Assessment of Insulin Tolerance In Vivo in Mice. *Methods Mol Biol* **2020**, *2128*, 217-224, doi:10.1007/978-1-0716-0385-7_15.

70. Villa-Pérez, P.; Merino, B.; Fernández-Díaz, C.M.; Cidad, P.; Lobatón, C.D.; Moreno, A.; Muturi, H.T.; Ghadieh, H.E.; Najjar, S.M.; Leissring, M.A.; et al. Liver-specific ablation of insulin-degrading enzyme causes hepatic insulin resistance and glucose intolerance, without affecting insulin clearance in mice. *Metabolism: clinical and experimental* **2018**, *88*, 1-11, doi:10.1016/j.metabol.2018.08.001.

71. Merino, B.; Fernández-Díaz, C.M.; Parrado-Fernández, C.; González-Casimiro, C.M.; Postigo-Casado, T.; Lobatón, C.D.; Leissring, M.A.; Cózar-Castellano, I.; Perdomo, G. Hepatic insulin-degrading enzyme regulates glucose and insulin homeostasis in diet-induced obese mice. *Metabolism: clinical and experimental* **2020**, *113*, 154352, doi:10.1016/j.metabol.2020.154352.

72. Matthews, D.R.; Hosker, J.P.; Rudenski, A.S.; Naylor, B.A.; Treacher, D.F.; Turner, R.C. Homeostasis model assessment: insulin resistance and beta-cell function from fasting plasma glucose and insulin concentrations in man. *Diabetologia* **1985**, *28*, 412-419, doi:10.1007/bf00280883.

73. Pilar Valdecantos, M.; Prieto-Hontoria, P.L.; Pardo, V.; Módol, T.; Santamaría, B.; Weber, M.; Herrero, L.; Serra, D.; Muntané, J.; Cuadrado, A.; et al. Essential role of Nrf2 in the protective effect of lipoic acid against lipoapoptosis in hepatocytes. *Free radical biology & medicine* **2015**, *84*, 263-278, doi:10.1016/j.freeradbiomed.2015.03.019.

74. Livak, K.J.; Schmittgen, T.D. Analysis of relative gene expression data using real-time quantitative PCR and the 2(-Delta Delta C(T)) Method.

Methods (San Diego, Calif.) **2001**, *25*, 402-408, doi:10.1006/meth.2001.1262.

75. Fernández-Díaz, C.M.; Escobar-Curbelo, L.; López-Acosta, J.F.; Lobatón, C.D.; Moreno, A.; Sanz-Ortega, J.; Perdomo, G.; Cózar-Castellano, I. Insulin degrading enzyme is up-regulated in pancreatic β cells by insulin treatment. *Histology and histopathology* **2018**, *33*, 1167-1180, doi:10.14670/hh-11-997.

76. InterPro: Protein sequence, analysis & classification. Available online: http://www.ebi.ac.uk/interpro/ (accessed on May, 2022).

77. Mitchell, A.; Chang, H.-Y.; Daugherty, L.; Fraser, M.; Hunter, S.; Lopez, R.; McAnulla, C.; McMenamin, C.; Nuka, G.; Pesseat, S.; et al. The InterPro protein families database: the classification resource after 15 years. *Nucleic Acids Research* **2015**, *43*, D213-D221, doi:10.1093/nar/gku1243.

78. UniProt. Available online: http://www.uniprot.org/ (accessed on May, 2022).

79. McGinnis, S.; Madden, T.L. BLAST: at the core of a powerful and diverse set of sequence analysis tools. *Nucleic Acids Research* **2004**, *32*, W20-W25, doi:10.1093/nar/gkh435.

80. Protein Data Bank. Available online: http://www.rcsb.org/pdb/home/home.do (accessed on May 2022).

81. Velankar, S.; Ginkel, G.v.; Alhroub, Y.; Battle, G.; Berrisford, J.; Conroy, M.; Dana, J.; Gore, S.; Gutmanas, A.; Haslam, P.; et al. PDBe: improved accessibility of macromolecular structure data from PDB and EMDB. *Nucleic Acids Res* **2016**, *44*, d385-395.

82. Higgins, D.G.; Sharp, P.M. CLUSTAL: a package for performing multiple sequence alignment on a microcomputer. *Gene* **1988**, *73*, 237-244.

83. Thompson, J.D.; Gibson, T.J.; Higgins, D.G. Multiple sequence alignment using ClustalW and ClustalX. In *Curr Protoc Bioinformatics*; 2002.

84. Im, H.; Manolopoulou, M.; Malito, E.; Shen, Y.; Zhao, J.; Neant-Fery, M.; Sun, C.Y.; Meredith, S.C.; Sisodia, S.S.; Leissring, M.A.; et al. Structure of substrate-free human insulin-degrading enzyme (IDE) and biophysical analysis of ATP-induced conformational switch of IDE. *J Biol Chem* **2007**, *282*, 25453-25463, doi:10.1074/jbc.M701590200.

85. Dolan, M.; Noah, J.; Hurt, D. Comparison of Common Homology Modeling Algorithms: Application of User-Defined Alignments. In *Homology Modeling*, Orry, A.J.W., Abagyan, R., Eds.; Methods in Molecular Biology; Humana Press: 2012; Volume 857, pp. 399-414.

86. Fiser, A.; Šali, A. Modeller: Generation and Refinement of Homology-Based Protein Structure Models. In *Methods in Enzymology*; Academic Press: 2003; Volume Volume 374, pp. 461-491.

87. Webb, B.; Sali, A. Protein structure modeling with MODELLER. In *Protein Structure Prediction*; Springer: 2014; pp. 1-15.

88. Lopes, P.E.; Guvench, O.; MacKerell Jr, A.D. Current Status of Protein Force Fields for Molecular Dynamics Simulations. In *Molecular Modeling of Proteins*; Springer: 2015; pp. 47-71.

89. Monticelli, L.; Tieleman, D.P. Force Fields for Classical Molecular Dynamics. In *Biomolecular Simulations*, Monticelli, L., Salonen, E., Eds.; Methods in Molecular Biology; Humana Press: 2013; Volume 924, pp. 197-213.

90. Zhu, X.; Lopes, P.E.M.; MacKerell, A.D. Recent developments and applications of the CHARMM force fields. *Wiley Interdisciplinary Reviews: Computational Molecular Science* **2012**, *2*, 167-185, doi:10.1002/wcms.74.

91. Zhang, L.; Hermans, J. Hydrophilicity of cavities in proteins. *Proteins: Structure, Function, and Bioinformatics* **1996**, *24*, 433-438.

92. Damjanović, A.; Schlessman, J.L.; Fitch, C.A.; Garca, A.E.; García-Moreno E, B. MD study of water penetration in SNase. *Biophys. J.* **2007**, *93*, 2791-2804.

93. Damjanović, A.; Brooks, B.R.; García-Moreno E, B. Conformational Relaxation and Water Penetration Coupled to Ionization of Internal Groups in Proteins. *The Journal of Physical Chemistry A* **2011**, *115*, 4042-4053, doi:10.1021/jp110373f.

94. Li, H.; Robertson, A.D.; Jensen, J.H. Very fast empirical prediction and rationalization of protein pKa values. *Proteins: Structure, Function, and Bioinformatics* **2005**, *61*, 704-721, doi:10.1002/prot.20660.

95. Bas, D.C.; Rogers, D.M.; Jensen, J.H. Very fast prediction and rationalization of pKa values for protein–ligand complexes. *Proteins: Structure, Function, and Bioinformatics* **2008**, *73*, 765-783, doi:10.1002/prot.22102.

96. Rostkowski, M.; Olsson, M.H.; Søndergaard, C.R.; Jensen, J.H. Graphical analysis of pH-dependent properties of proteins predicted using PROPKA. *BMC structural biology* **2011**, *11*, 6.

97. Gleeson, D.; Smith, N.D.; Boyer, J.L. Bicarbonate-dependent and -independent intracellular pH regulatory mechanisms in rat hepatocytes. Evidence for Na+-HCO3- cotransport. *The Journal of clinical investigation* **1989**, *84*, 312-321, doi:10.1172/jci114156.

98. Schulze, R.J.; Schott, M.B.; Casey, C.A.; Tuma, P.L.; McNiven, M.A. The cell biology of the hepatocyte: A membrane trafficking machine. *J Cell Biol* **2019**, *218*, 2096-2112, doi:10.1083/jcb.201903090.

99. Rougée, L.R.; Mohutsky, M.A.; Bedwell, D.W.; Ruterbories, K.J.; Hall, S.D. The Impact of the Hepatocyte-to-Plasma pH Gradient on the Prediction of Hepatic Clearance and Drug-Drug Interactions for CYP2D6 Substrates. *Drug Metab Dispos* **2016**, *44*, 1819-1827, doi:10.1124/dmd.116.071761.

100. Imberti, R.; Ferrigno, A.; Tartaglia, A.; Rizzo, V.; Richelmi, P.; Vairetti, M. Changes in extra- and intracellular pH in hepatocytes exposed to gabexate mesilate. *Int J Immunopathol Pharmacol* **2014**, *27*, 365-370, doi:10.1177/039463201402700306.

101. Eisenberg, D.; Lüthy, R.; Bowie, J.U. VERIFY3D: assessment of protein models with three-dimensional profiles. *Methods in enzymology* **1997**, 396-404.

102. Laskowski, R.; Furnham, N.; Thornton, J. The Ramachandran Plot and Protein Structure Validation. *Biomolecular Forms and Functions A Celebration of* **2013**, *50*, 62-75.

103. Laskowski, R.; MacArthur, M.; Moss, D.; Thornton, J.; Aaron, W. PROCHECK: a program to check the stereochemical quality of protein structures. *J. Appl. Cryst.* **1993**, 283-291.

104. Laskowski, R.; MacArthur, M.; Thornton, J. PROCHECK: validation of protein structure coordinates. In *International Tables of Crystallography*, E, R.M.A., Ed.; Dordrecht, Kluwer Academic Publishers: The Netherlands, 2001; Volume F. Crystallography of Biological Macromolecules, pp. 722-725.

105. Rodriguez, R.; Chinea, G.; Lopez, N.; Pons, T.; Vriend, G. Homology modeling, model and software evaluation: three related resources. *Bioinformatics* **1998**, *14*, 523-528, doi:10.1093/bioinformatics/14.6.523.

106. Colovos, C.; Yeates, T.O. Verification of protein structures: Patterns of nonbonded atomic interactions. *Protein Science* **1993**, *2*, 1511-1519, doi:10.1002/pro.5560020916.

107. Wiederstein, M.; Sippl, M.J. ProSA-web: interactive web service for the recognition of errors in three-dimensional structures of proteins. *Nucleic Acids Research* **2007**, *35*, W407-W410, doi:10.1093/nar/gkm290.

108. Sippl, M.J. Recognition of errors in three-dimensional structures of proteins. *Proteins* **1993**, *17*, 355–362.

109. The Structure Analysis and Verification Server. Version 4. University of California in Los Angeles. Available online: http://services.mbi.ucla.edu/SAVES/ (accessed on May, 2022).

110. Wiederstein, M. ProSA-web. Protein Structure Analysis. Available online: https://prosa.services.came.sbg.ac.at (accessed on May, 2022).

111. Humphrey, W.; Dalke, A.; Schulten, K. VMD: visual molecular dynamics. *Journal of molecular graphics* **1996**, *14*, 33-38.

112. Liu, Y.; Stone, J.E.; Cai, E.; Fei, J.; Lee, S.H.; Park, S.; Ha, T.; Selvin, P.R.; Schulten, K. VMD as a Software for Visualization and Quantitative Analysis of Super Resolution Imaging and Single Particle Tracking. *Biophysical Journal* **2014**, *106*, 202a, doi:10.1016/j.bpj.2013.11.1187.

113. Schulten, K. *Computational Biophysics: Methods, and applications with VMD and NAMD*; Newnes: 2014.

114. Voet, D.; Voet, J.G.; Pratt, C.W. *Fundamentals of Biochemistry: Life at the Molecular Level: Life at the Molecular Level*; Wiley Global Education: 2011.

115. Cox, M.M. *Lehninger principles of biochemistry*; Freeman: 2013.

116. Berg, J.M.; Deis, F.H.; Tymoczko, J.L.; Stryer, L.; Gerber, N.C.; Gumport, R.; Koeppe, R.E. *Biochemistry student companion*; Macmillan: 2011.

117. Farris, W.; Leissring, M.A.; Hemming, M.L.; Chang, A.Y.; Selkoe, D.J. Alternative splicing of human insulin-degrading enzyme yields a novel isoform with a decreased ability to degrade insulin and amyloid beta-protein. *Biochemistry* **2005**, *44*, 6513-6525, doi:10.1021/bi0476578.

118. Yang, W.; Yan, H.; Pan, Q.; Shen, J.Z.; Zhou, F.; Wu, C.; Sun, Y.; Guo, S. Glucagon regulates hepatic mitochondrial function and biogenesis through FOXO1. *J Endocrinol* **2019**, *241*, 265-278, doi:10.1530/joe-19-0081.

119. Hernández Rodríguez, E.W. Modelación molecular de rodopsinas humanas mutantes asociadas a retinosis pigmentaria. Universidad de Ciencias Médicas de La Habana. Universidad Autónoma de Madrid, 2014.

120. Hernández-Rodríguez, E.W.; Sánchez-García, E.; Crespo-Otero, R.; Montero-Alejo, A.L.; Montero, L.A.; Thiel, W. Understanding rhodopsin mutations linked to the retinitis pigmentosa disease: a QM/MM and DFT/MRCI study. *The Journal of Physical Chemistry B* **2012**, *116*, 1060-1076.

121. Colovos, C.; Yeates, T.O. Verification of protein structures: patterns of nonbonded atomic interactions. *Protein Sci* **1993**, *2*, 1511-1519, doi:10.1002/pro.5560020916.

122. Hooft, R.W.; Vriend, G.; Sander, C.; Abola, E.E. Errors in protein structures. *Nature* **1996**, *381*, 272, doi:10.1038/381272a0.

123. Lüthy, R.; Bowie, J.U.; Eisenberg, D. Assessment of protein models with three-dimensional profiles. *Nature* **1992**, *356*, 83-85, doi:10.1038/356083a0.

124. Bowie, J.U.; Lüthy, R.; Eisenberg, D. A method to identify protein sequences that fold into a known three-dimensional structure. *Science* **1991**, *253*, 164-170, doi:10.1126/science.1853201.

125. Ahrén, B.; Simonsson, E.; Scheurink, A.J.; Mulder, H.; Myrsén, U.; Sundler, F. Dissociated insulinotropic sensitivity to glucose and carbachol in high-fat diet-induced insulin resistance in C57BL/6J mice. *Metabolism* **1997**, *46*, 97-106, doi:10.1016/s0026-0495(97)90175-x.

126. Conarello, S.L.; Jiang, G.; Mu, J.; Li, Z.; Woods, J.; Zycband, E.; Ronan, J.; Liu, F.; Roy, R.S.; Zhu, L.; et al. Glucagon receptor knockout mice are resistant to diet-induced obesity and streptozotocin-mediated beta cell loss and hyperglycaemia. *Diabetologia* **2007**, *50*, 142-150, doi:10.1007/s00125-006-0481-3.

127. Ellingsgaard, H.; Ehses, J.A.; Hammar, E.B.; Van Lommel, L.; Quintens, R.; Martens, G.; Kerr-Conte, J.; Pattou, F.; Berney, T.; Pipeleers, D.; et al. Interleukin-6 regulates pancreatic alpha-cell mass expansion. *Proceedings of the National Academy of Sciences of the United States of America* **2008**, *105*, 13163-13168, doi:10.1073/pnas.0801059105.

128. Merino, B.; Alonso-Magdalena, P.; Lluesma, M.; Ñeco, P.; Gonzalez, A.; Marroquí, L.; García-Arévalo, M.; Nadal, A.; Quesada, I. Pancreatic alpha-cells from female mice undergo morphofunctional changes during

compensatory adaptations of the endocrine pancreas to diet-induced obesity. *Scientific reports* **2015**, *5*, 11622, doi:10.1038/srep11622.

129. Mu, J.; Jiang, G.; Brady, E.; Dallas-Yang, Q.; Liu, F.; Woods, J.; Zycband, E.; Wright, M.; Li, Z.; Lu, K.; et al. Chronic treatment with a glucagon receptor antagonist lowers glucose and moderately raises circulating glucagon and glucagon-like peptide 1 without severe alpha cell hypertrophy in diet-induced obese mice. *Diabetologia* **2011**, *54*, 2381-2391, doi:10.1007/s00125-011-2217-2.

130. Winzell, M.S.; Brand, C.L.; Wierup, N.; Sidelmann, U.G.; Sundler, F.; Nishimura, E.; Ahrén, B. Glucagon receptor antagonism improves islet function in mice with insulin resistance induced by a high-fat diet. *Diabetologia* **2007**, *50*, 1453-1462, doi:10.1007/s00125-007-0675-3.

131. Item, F.; Konrad, D. Visceral fat and metabolic inflammation: the portal theory revisited. *Obesity reviews : an official journal of the International Association for the Study of Obesity* **2012**, *13 Suppl 2*, 30-39, doi:10.1111/j.1467-789X.2012.01035.x.

132. Hamel, F.G.; Upward, J.L.; Bennett, R.G. In vitro inhibition of insulin-degrading enzyme by long-chain fatty acids and their coenzyme A thioesters. *Endocrinology* **2003**, *144*, 2404-2408, doi:10.1210/en.2002-0007.

133. Svedberg, J.; Björntorp, P.; Smith, U.; Lönnroth, P. Free-fatty acid inhibition of insulin binding, degradation, and action in isolated rat hepatocytes. *Diabetes* **1990**, *39*, 570-574, doi:10.2337/diab.39.5.570.

134. Sonne, O. Increased inhibitory potency of free fatty acid-poor albumin on the released and activity of insulin-degrading enzymes from isolated rat adipocytes and hepatocytes. *Analytical biochemistry* **1985**, *151*, 109-117, doi:10.1016/0003-2697(85)90059-4.

135. Vettorazzi, J.F.; Kurauti, M.A.; Soares, G.M.; Borck, P.C.; Ferreira, S.M.; Branco, R.C.S.; Michelone, L.S.L.; Boschero, A.C.; Junior, J.M.C.; Carneiro, E.M. Bile acid TUDCA improves insulin clearance by increasing the expression of insulin-degrading enzyme in the liver of obese mice. *Scientific reports* **2017**, *7*, 14876, doi:10.1038/s41598-017-13974-0.

136. Pivovarova, O.; Gögebakan, O.; Pfeiffer, A.F.; Rudovich, N. Glucose inhibits the insulin-induced activation of the insulin-degrading enzyme in HepG2 cells. *Diabetologia* **2009**, *52*, 1656-1664, doi:10.1007/s00125-009-1350-7.

137. Consoli, A.; Nurjahan, N.; Gerich, J.E.; Mandarino, L.J. Skeletal muscle is a major site of lactate uptake and release during hyperinsulinemia. *Metabolism: clinical and experimental* **1992**, *41*, 176-179, doi:10.1016/0026-0495(92)90148-4.

138. Consoli, A.; Nurjhan, N.; Reilly, J.J., Jr.; Bier, D.M.; Gerich, J.E. Contribution of liver and skeletal muscle to alanine and lactate metabolism in humans. *The American journal of physiology* **1990**, *259*, E677-684, doi:10.1152/ajpendo.1990.259.5.E677.

139. van Hall, G. Lactate kinetics in human tissues at rest and during exercise. *Acta physiologica (Oxford, England)* **2010**, *199*, 499-508, doi:10.1111/j.1748-1716.2010.02122.x.

140. Newsholme, E.; Leech, T. Carbohydrate metabolism. In *Functional Biochemistry in Health and Disease*; Wiley-Blackwell: Oxford, UK, 2009; pp. 97-127.

141. Kreisberg, R.A.; Pennington, L.F.; Boshell, B.R. Lactate turnover and gluconeogenesis in normal and obese humans. Effect of starvation. *Diabetes* **1970**, *19*, 53-63, doi:10.2337/diab.19.1.53.

142. Andres, R.; Cader, G.; Zierler, K.L. The quantitatively minor role of carbohydrate in oxidative metabolism by skeletal muscle in intact man in the basal state; measurements of oxygen and glucose uptake and carbon dioxide and lactate production in the forearm. *The Journal of clinical investigation* **1956**, *35*, 671-682, doi:10.1172/jci103324.

143. Shulman, G.I.; Rossetti, L.; Rothman, D.L.; Blair, J.B.; Smith, D. Quantitative analysis of glycogen repletion by nuclear magnetic resonance spectroscopy in the conscious rat. *The Journal of clinical investigation* **1987**, *80*, 387-393, doi:10.1172/jci113084.

144. Kelley, D.E.; Mokan, M.; Simoneau, J.A.; Mandarino, L.J. Interaction between glucose and free fatty acid metabolism in human skeletal muscle. *The Journal of clinical investigation* **1993**, *92*, 91-98, doi:10.1172/jci116603.

145. Kelley, D.E.; Mandarino, L.J. Fuel selection in human skeletal muscle in insulin resistance: a reexamination. *Diabetes* **2000**, *49*, 677-683, doi:10.2337/diabetes.49.5.677.

146. Storlien, L.; Oakes, N.D.; Kelley, D.E. Metabolic flexibility. *The Proceedings of the Nutrition Society* **2004**, *63*, 363-368, doi:10.1079/pns2004349.

147. Kelley, D.E. Skeletal muscle fat oxidation: timing and flexibility are everything. *The Journal of clinical investigation* **2005**, *115*, 1699-1702, doi:10.1172/jci25758.

148. Kelley, D.; Mitrakou, A.; Marsh, H.; Schwenk, F.; Benn, J.; Sonnenberg, G.; Arcangeli, M.; Aoki, T.; Sorensen, J.; Berger, M.; et al. Skeletal muscle glycolysis, oxidation, and storage of an oral glucose load. *The Journal of clinical investigation* **1988**, *81*, 1563-1571, doi:10.1172/jci113489.

149. Sidossis, L.S.; Wolfe, R.R. Glucose and insulin-induced inhibition of fatty acid oxidation: the glucose-fatty acid cycle reversed. *The American journal of physiology* **1996**, *270*, E733-738, doi:10.1152/ajpendo.1996.270.4.E733.

150. Hue, L.; Taegtmeyer, H. The Randle cycle revisited: a new head for an old hat. *American journal of physiology. Endocrinology and metabolism* **2009**, *297*, E578-591, doi:10.1152/ajpendo.00093.2009.

151. González-Casimiro, C.M.; Cámara-Torres, P.; Merino, B.; Diez-Hermano, S.; Postigo-Casado, T.; Leissring, M.A.; Cózar-Castellano, I.; Perdomo, G. Effects of Fasting and Feeding on Transcriptional and Posttranscriptional

Regulation of Insulin-Degrading Enzyme in Mice. *Cells* **2021**, *10*, doi:10.3390/cells10092446.

152. Brandimarti, P.; Costa-Júnior, J.M.; Ferreira, S.M.; Protzek, A.O.; Santos, G.J.; Carneiro, E.M.; Boschero, A.C.; Rezende, L.F. Cafeteria diet inhibits insulin clearance by reduced insulin-degrading enzyme expression and mRNA splicing. *The Journal of endocrinology* **2013**, *219*, 173-182, doi:10.1530/joe-13-0177.

153. Kurauti, M.A.; Costa-Júnior, J.M.; Ferreira, S.M.; Dos Santos, G.J.; Protzek, A.O.; Nardelli, T.R.; de Rezende, L.F.; Boschero, A.C. Acute exercise restores insulin clearance in diet-induced obese mice. *The Journal of endocrinology* **2016**, *229*, 221-232, doi:10.1530/joe-15-0483.

154. Kim, Y.; Rouse, M.; González-Mariscal, I.; Egan, J.M.; O'Connell, J.F. Dietary curcumin enhances insulin clearance in diet-induced obese mice via regulation of hepatic PI3K-AKT axis and IDE, and preservation of islet integrity. *Nutrition & metabolism* **2019**, *16*, 48, doi:10.1186/s12986-019-0377-0.

155. Wei, X.; Ke, B.; Zhao, Z.; Ye, X.; Gao, Z.; Ye, J. Regulation of insulin degrading enzyme activity by obesity-associated factors and pioglitazone in liver of diet-induced obese mice. *PloS one* **2014**, *9*, e95399, doi:10.1371/journal.pone.0095399.

156. Adessi, C.; Enderle, T.; Grueninger, F.; Roth, D. Activator for Insulin Degrading Enzyme. 2006.

157. Cabrol, C.; Huzarska, M.A.; Dinolfo, C.; Rodriguez, M.C.; Reinstatler, L.; Ni, J.; Yeh, L.A.; Cuny, G.D.; Stein, R.L.; Selkoe, D.J.; et al. Small-molecule activators of insulin-degrading enzyme discovered through high-throughput compound screening. *PloS one* **2009**, *4*, e5274, doi:10.1371/journal.pone.0005274.

158. Çakir, B.; Dağliyan, O.; Dağyildiz, E.; Bariş, İ.; Kavakli, I.H.; Kizilel, S.; Türkay, M. Structure based discovery of small molecules to regulate the activity of human insulin degrading enzyme. *PloS one* **2012**, *7*, e31787, doi:10.1371/journal.pone.0031787.

159. Kukday, S.S.; Manandhar, S.P.; Ludley, M.C.; Burriss, M.E.; Alper, B.J.; Schmidt, W.K. Cell-permeable, small-molecule activators of the insulin-degrading enzyme. *J Biomol Screen* **2012**, *17*, 1348-1361, doi:10.1177/1087057112451921.

160. Deprez-Poulain, R.; Charton, J.; Deprez, B.; Leroux, F.; Gauriot, M.; Tang, W.-J.; Totobenazara, J. Ligands of Insulin Degrading Enzyme and Their Uses. 2011.

161. Kraupner, N.; Dinh, C.P.; Wen, X.; Landry, V.; Herledan, A.; Leroux, F.; Bosc, D.; Charton, J.; Maillard, C.; Warenghem, S.; et al. Identification of indole-based activators of insulin degrading enzyme. *Eur J Med Chem* **2022**, *228*, 113982, doi:10.1016/j.ejmech.2021.113982.

162. Farris, W.; Mansourian, S.; Leissring, M.A.; Eckman, E.A.; Bertram, L.; Eckman, C.B.; Tanzi, R.E.; Selkoe, D.J. Partial loss-of-function mutations in insulin-degrading enzyme that induce diabetes also impair degradation

of amyloid beta-protein. *Am J Pathol* **2004**, *164*, 1425-1434, doi:10.1016/s0002-9440(10)63229-4.

163. Desbuquois, B. Glucagon receptors and glucagon sensitive adenylate cyclase In *Polypeptide Hormone Receptors*; Posner B. I.: Marcel Dekker, New York, 1983; pp. 345-417.

164. Burcelin, R.; Mrejen, C.; Decaux, J.F.; De Mouzon, S.H.; Girard, J.; Charron, M.J. In vivo and in vitro regulation of hepatic glucagon receptor mRNA concentration by glucose metabolism. *J Biol Chem* **1998**, *273*, 8088-8093, doi:10.1074/jbc.273.14.8088.

165. Abrahamsen, N.; Lundgren, K.; Nishimura, E. Regulation of glucagon receptor mRNA in cultured primary rat hepatocytes by glucose and cAMP. *J Biol Chem* **1995**, *270*, 15853-15857, doi:10.1074/jbc.270.26.15853.

166. Noda, C.; Shinjyo, F.; Tomomura, A.; Kato, S.; Nakamura, T.; Ichihara, A. Mechanism of heterologous desensitization of the adenylate cyclase system by glucagon in primary cultures of adult rat hepatocytes. *J Biol Chem* **1984**, *259*, 7747-7754.

167. Premont, R.T.; Iyengar, R. Glucagon-induced desensitization of adenylyl cyclase in primary cultures of chick hepatocytes. Evidence for multiple pathways. *J Biol Chem* **1988**, *263*, 16087-16095.

168. Tundo, G.R.; Sbardella, D.; Ciaccio, C.; Bianculli, A.; Orlandi, A.; Desimio, M.G.; Arcuri, G.; Coletta, M.; Marini, S. Insulin-degrading enzyme (IDE): a novel heat shock-like protein. *J Biol Chem* **2013**, *288*, 2281-2289, doi:10.1074/jbc.M112.393108.

169. Hamel, F.G. Preliminary report: inhibition of cellular proteasome activity by free fatty acids. *Metabolism* **2009**, *58*, 1047-1049, doi:10.1016/j.metabol.2009.04.005.

170. Fawcett, J.; Permana, P.A.; Levy, J.L.; Duckworth, W.C. Regulation of protein degradation by insulin-degrading enzyme: analysis by small interfering RNA-mediated gene silencing. *Arch Biochem Biophys* **2007**, *468*, 128-133, doi:10.1016/j.abb.2007.09.019.

171. Bennett, R.G.; Fawcett, J.; Kruer, M.C.; Duckworth, W.C.; Hamel, F.G. Insulin inhibition of the proteasome is dependent on degradation of insulin by insulin-degrading enzyme. *J Endocrinol* **2003**, *177*, 399-405, doi:10.1677/joe.0.1770399.

172. Bennett, R.G.; Hamel, F.G.; Duckworth, W.C. Insulin inhibits the ubiquitin-dependent degrading activity of the 26S proteasome. *Endocrinology* **2000**, *141*, 2508-2517, doi:10.1210/endo.141.7.7575.

173. Duckworth, W.C.; Bennett, R.G.; Hamel, F.G. Insulin acts intracellularly on proteasomes through insulin-degrading enzyme. *Biochem Biophys Res Commun* **1998**, *244*, 390-394, doi:10.1006/bbrc.1998.8276.

174. Bennett, R.G.; Hamel, F.G.; Duckworth, W.C. Characterization of the insulin inhibition of the peptidolytic activities of the insulin-degrading enzyme-proteasome complex. *Diabetes* **1997**, *46*, 197-203, doi:10.2337/diab.46.2.197.

175. Duckworth, W.C.; Bennett, R.G.; Hamel, F.G. A direct inhibitory effect of insulin on a cytosolic proteolytic complex containing insulin-degrading enzyme and multicatalytic proteinase. *J Biol Chem* **1994**, *269*, 24575-24580.

176. Bennett, R.G.; Hamel, F.G.; Duckworth, W.C. Identification and isolation of a cytosolic proteolytic complex containing insulin degrading enzyme and the multicatalytic proteinase. *Biochem Biophys Res Commun* **1994**, *202*, 1047-1053, doi:10.1006/bbrc.1994.2034.

177. Sbardella, D.; Tundo, G.R.; Sciandra, F.; Bozzi, M.; Gioia, M.; Ciaccio, C.; Tarantino, U.; Brancaccio, A.; Coletta, M.; Marini, S. Proteasome Activity Is Affected by Fluctuations in Insulin-Degrading Enzyme Distribution. *PloS one* **2015**, *10*, e0132455, doi:10.1371/journal.pone.0132455.

178. Mansini, A.P.; Peixoto, E.; Thelen, K.M.; Gaspari, C.; Jin, S.; Gradilone, S.A. The cholangiocyte primary cilium in health and disease. *Biochim Biophys Acta Mol Basis Dis* **2018**, *1864*, 1245-1253, doi:10.1016/j.bbadis.2017.06.006.

179. Liu, L.; Sheng, J.Q.; Wang, M.R.; Gan, Y.; Wu, X.L.; Liao, J.Z.; Tian, D.A.; He, X.X.; Li, P.Y. Primary Cilia Blockage Promotes the Malignant Behaviors of Hepatocellular Carcinoma via Induction of Autophagy. *Biomed Res Int* **2019**, *2019*, 5202750, doi:10.1155/2019/5202750.

180. Li, X.; Yang, S.; Deepak, V.; Chinipardaz, Z.; Yang, S. Identification of Cilia in Different Mouse Tissues. *Cells* **2021**, *10*, doi:10.3390/cells10071623.

181. Perdiz, D.; Mackeh, R.; Poüs, C.; Baillet, A. The ins and outs of tubulin acetylation: more than just a post-translational modification? *Cell Signal* **2011**, *23*, 763-771, doi:10.1016/j.cellsig.2010.10.014.

182. Wewer Albrechtsen, N.J.; Hartmann, B.; Veedfald, S.; Windeløv, J.A.; Plamboeck, A.; Bojsen-Møller, K.N.; Idorn, T.; Feldt-Rasmussen, B.; Knop, F.K.; Vilsbøll, T.; et al. Hyperglucagonaemia analysed by glucagon sandwich ELISA: nonspecific interference or truly elevated levels? *Diabetologia* **2014**, *57*, 1919-1926, doi:10.1007/s00125-014-3283-z.

183. Müller, W.A.; Faloona, G.R.; Aguilar-Parada, E.; Unger, R.H. Abnormal alpha-cell function in diabetes. Response to carbohydrate and protein ingestion. *N Engl J Med* **1970**, *283*, 109-115, doi:10.1056/nejm197007162830301.

184. Johnson, D.G.; Goebel, C.U.; Hruby, V.J.; Bregman, M.D.; Trivedi, D. Hyperglycemia of diabetic rats decreased by a glucagon receptor antagonist. *Science* **1982**, *215*, 1115-1116, doi:10.1126/science.6278587.

185. Gelling, R.W.; Du, X.Q.; Dichmann, D.S.; Romer, J.; Huang, H.; Cui, L.; Obici, S.; Tang, B.; Holst, J.J.; Fledelius, C.; et al. Lower blood glucose, hyperglucagonemia, and pancreatic alpha cell hyperplasia in glucagon receptor knockout mice. *Proceedings of the National Academy of Sciences of the United States of America* **2003**, *100*, 1438-1443, doi:10.1073/pnas.0237106100.

186. Kazda, C.M.; Ding, Y.; Kelly, R.P.; Garhyan, P.; Shi, C.; Lim, C.N.; Fu, H.; Watson, D.E.; Lewin, A.J.; Landschulz, W.H.; et al. Evaluation of Efficacy

and Safety of the Glucagon Receptor Antagonist LY2409021 in Patients With Type 2 Diabetes: 12- and 24-Week Phase 2 Studies. *Diabetes Care* **2016**, *39*, 1241-1249, doi:10.2337/dc15-1643.

187. Bozadjieva Kramer, N.; Lubaczeuski, C.; Blandino-Rosano, M.; Barker, G.; Gittes, G.K.; Caicedo, A.; Bernal-Mizrachi, E. Glucagon Resistance and Decreased Susceptibility to Diabetes in a Model of Chronic Hyperglucagonemia. *Diabetes* **2021**, *70*, 477-491, doi:10.2337/db20-0440.

188. Oh, K.J.; Han, H.S.; Kim, M.J.; Koo, S.H. Transcriptional regulators of hepatic gluconeogenesis. *Arch Pharm Res* **2013**, *36*, 189-200, doi:10.1007/s12272-013-0018-5.

189. Oh, K.J.; Han, H.S.; Kim, M.J.; Koo, S.H. CREB and FoxO1: two transcription factors for the regulation of hepatic gluconeogenesis. *BMB Rep* **2013**, *46*, 567-574, doi:10.5483/bmbrep.2013.46.12.248.

190. Goldstein, I.; Hager, G.L. The Three Ds of Transcription Activation by Glucagon: Direct, Delayed, and Dynamic. *Endocrinology* **2018**, *159*, 206-216, doi:10.1210/en.2017-00521.

191. Chakravarty, K.; Cassuto, H.; Reshef, L.; Hanson, R.W. Factors that control the tissue-specific transcription of the gene for phosphoenolpyruvate carboxykinase-C. *Crit Rev Biochem Mol Biol* **2005**, *40*, 129-154, doi:10.1080/10409230590935479.

192. Anyamaneeratch, K.; Rojvirat, P.; Sukjoi, W.; Jitrapakdee, S. Insights into Transcriptional Regulation of Hepatic Glucose Production. *Int Rev Cell Mol Biol* **2015**, *318*, 203-253, doi:10.1016/bs.ircmb.2015.05.004.

193. Niu, J.; Vaiskunaite, R.; Suzuki, N.; Kozasa, T.; Carr, D.W.; Dulin, N.; Voyno-Yasenetskaya, T.A. Interaction of heterotrimeric G13 protein with an A-kinase-anchoring protein 110 (AKAP110) mediates cAMP-independent PKA activation. *Curr Biol* **2001**, *11*, 1686-1690, doi:10.1016/s0960-9822(01)00530-9.

194. Melville, Z.; Hernández-Ochoa, E.O.; Pratt, S.J.P.; Liu, Y.; Pierce, A.D.; Wilder, P.T.; Adipietro, K.A.; Breysse, D.H.; Varney, K.M.; Schneider, M.F.; et al. The Activation of Protein Kinase A by the Calcium-Binding Protein S100A1 Is Independent of Cyclic AMP. *Biochemistry* **2017**, *56*, 2328-2337, doi:10.1021/acs.biochem.7b00117.

195. Søberg, K.; Skålhegg, B.S. The Molecular Basis for Specificity at the Level of the Protein Kinase a Catalytic Subunit. *Front Endocrinol (Lausanne)* **2018**, *9*, 538, doi:10.3389/fendo.2018.00538.

196. Kwok, R.P.; Lundblad, J.R.; Chrivia, J.C.; Richards, J.P.; Bächinger, H.P.; Brennan, R.G.; Roberts, S.G.; Green, M.R.; Goodman, R.H. Nuclear protein CBP is a coactivator for the transcription factor CREB. *Nature* **1994**, *370*, 223-226, doi:10.1038/370223a0.

197. Xu, W.; Kasper, L.H.; Lerach, S.; Jeevan, T.; Brindle, P.K. Individual CREB-target genes dictate usage of distinct cAMP-responsive coactivation mechanisms. *Embo j* **2007**, *26*, 2890-2903, doi:10.1038/sj.emboj.7601734.

198. Luo, Q.; Viste, K.; Urday-Zaa, J.C.; Senthil Kumar, G.; Tsai, W.W.; Talai, A.; Mayo, K.E.; Montminy, M.; Radhakrishnan, I. Mechanism of CREB recognition and coactivation by the CREB-regulated transcriptional coactivator CRTC2. *Proceedings of the National Academy of Sciences of the United States of America* **2012**, *109*, 20865-20870, doi:10.1073/pnas.1219028109.

199. Liu, Y.; Dentin, R.; Chen, D.; Hedrick, S.; Ravnskjaer, K.; Schenk, S.; Milne, J.; Meyers, D.J.; Cole, P.; Yates, J., 3rd; et al. A fasting inducible switch modulates gluconeogenesis via activator/coactivator exchange. *Nature* **2008**, *456*, 269-273, doi:10.1038/nature07349.

200. Ravnskjaer, K.; Hogan, M.F.; Lackey, D.; Tora, L.; Dent, S.Y.; Olefsky, J.; Montminy, M. Glucagon regulates gluconeogenesis through KAT2B- and WDR5-mediated epigenetic effects. *The Journal of clinical investigation* **2013**, *123*, 4318-4328, doi:10.1172/jci69035.

201. Zhou, Y.; Lee, J.; Reno, C.M.; Sun, C.; Park, S.W.; Chung, J.; Lee, J.; Fisher, S.J.; White, M.F.; Biddinger, S.B.; et al. Regulation of glucose homeostasis through a XBP-1-FoxO1 interaction. *Nat Med* **2011**, *17*, 356-365, doi:10.1038/nm.2293.

202. Perrot, V.; Rechler, M.M. The coactivator p300 directly acetylates the forkhead transcription factor Foxo1 and stimulates Foxo1-induced transcription. *Mol Endocrinol* **2005**, *19*, 2283-2298, doi:10.1210/me.2004-0292.

203. Matsuzaki, H.; Daitoku, H.; Hatta, M.; Aoyama, H.; Yoshimochi, K.; Fukamizu, A. Acetylation of Foxo1 alters its DNA-binding ability and sensitivity to phosphorylation. *Proceedings of the National Academy of Sciences of the United States of America* **2005**, *102*, 11278-11283, doi:10.1073/pnas.0502738102.

204. Frescas, D.; Valenti, L.; Accili, D. Nuclear trapping of the forkhead transcription factor FoxO1 via Sirt-dependent deacetylation promotes expression of glucogenetic genes. *J Biol Chem* **2005**, *280*, 20589-20595, doi:10.1074/jbc.M412357200.

205. Corpas, R.; Revilla, S.; Ursulet, S.; Castro-Freire, M.; Kaliman, P.; Petegnief, V.; Giménez-Llort, L.; Sarkis, C.; Pallàs, M.; Sanfeliu, C. SIRT1 Overexpression in Mouse Hippocampus Induces Cognitive Enhancement Through Proteostatic and Neurotrophic Mechanisms. *Mol Neurobiol* **2017**, *54*, 5604-5619, doi:10.1007/s12035-016-0087-9.

206. Brown, M.S.; Goldstein, J.L. Selective versus total insulin resistance: a pathogenic paradox. *Cell Metab* **2008**, *7*, 95-96, doi:10.1016/j.cmet.2007.12.009.

207. Schmid, R.; Schusdziarra, V.; Schulte-Frohlinde, E.; Maier, V.; Classen, M. Role of amino acids in stimulation of postprandial insulin, glucagon, and pancreatic polypeptide in humans. *Pancreas* **1989**, *4*, 305-314, doi:10.1097/00006676-198906000-00006.

208. Snodgrass, P.J.; Lin, R.C.; Müller, W.A.; Aoki, T.T. Induction of urea cycle enzymes of rat liver by glucagon. *J Biol Chem* **1978**, *253*, 2748-2753.

209. Heibel, S.K.; Lopez, G.Y.; Panglao, M.; Sodha, S.; Mariño-Ramírez, L.; Tuchman, M.; Caldovic, L. Transcriptional regulation of N-acetylglutamate synthase. *PloS one* **2012**, *7*, e29527, doi:10.1371/journal.pone.0029527.

210. Longuet, C.; Robledo, A.M.; Dean, E.D.; Dai, C.; Ali, S.; McGuinness, I.; de Chavez, V.; Vuguin, P.M.; Charron, M.J.; Powers, A.C.; et al. Liver-specific disruption of the murine glucagon receptor produces α-cell hyperplasia: evidence for a circulating α-cell growth factor. *Diabetes* **2013**, *62*, 1196-1205, doi:10.2337/db11-1605.

211. Fu, D.; Lippincott-Schwartz, J.; Arias, I.M. Increased mitochondrial fusion and autophagy help isolated hepatocytes repolarize in collagen sandwich cultures. *Autophagy* **2013**, *9*, 2154-2155, doi:10.4161/auto.26167.

212. Bryant, D.M.; Mostov, K.E. From cells to organs: building polarized tissue. *Nat Rev Mol Cell Biol* **2008**, *9*, 887-901, doi:10.1038/nrm2523.

213. Gissen, P.; Arias, I.M. Structural and functional hepatocyte polarity and liver disease. *J Hepatol* **2015**, *63*, 1023-1037, doi:10.1016/j.jhep.2015.06.015.

214. Hardie, D.G.; Ross, F.A.; Hawley, S.A. AMPK: a nutrient and energy sensor that maintains energy homeostasis. *Nat Rev Mol Cell Biol* **2012**, *13*, 251-262, doi:10.1038/nrm3311.

215. Illescas, M.; Peñas, A.; Arenas, J.; Martín, M.A.; Ugalde, C. Regulation of Mitochondrial Function by the Actin Cytoskeleton. *Front Cell Dev Biol* **2021**, *9*, 795838, doi:10.3389/fcell.2021.795838.

216. Anesti, V.; Scorrano, L. The relationship between mitochondrial shape and function and the cytoskeleton. *Biochim Biophys Acta* **2006**, *1757*, 692-699, doi:10.1016/j.bbabio.2006.04.013.

217. Guo, Y.; Li, D.; Zhang, S.; Yang, Y.; Liu, J.J.; Wang, X.; Liu, C.; Milkie, D.E.; Moore, R.P.; Tulu, U.S.; et al. Visualizing Intracellular Organelle and Cytoskeletal Interactions at Nanoscale Resolution on Millisecond Timescales. *Cell* **2018**, *175*, 1430-1442.e1417, doi:10.1016/j.cell.2018.09.057.

218. Abrisch, R.G.; Gumbin, S.C.; Wisniewski, B.T.; Lackner, L.L.; Voeltz, G.K. Fission and fusion machineries converge at ER contact sites to regulate mitochondrial morphology. *J Cell Biol* **2020**, *219*, doi:10.1083/jcb.201911122.

219. Cheng, Z. FoxO transcription factors in mitochondrial homeostasis. *Biochem J* **2022**, *479*, 525-536, doi:10.1042/bcj20210777.

220. Guo, Q.; Manolopoulou, M.; Bian, Y.; Schilling, A.B.; Tang, W.J. Molecular basis for the recognition and cleavages of IGF-II, TGF-alpha, and amylin by human insulin-degrading enzyme. *J Mol Biol* **2010**, *395*, 430-443, doi:10.1016/j.jmb.2009.10.072.

221. Fernández-Gamba, A.; Leal, M.C.; Morelli, L.; Castaño, E.M. Insulin-degrading enzyme: structure-function relationship and its possible roles in health and disease. *Curr Pharm Des* **2009**, *15*, 3644-3655, doi:10.2174/138161209789271799.

222. Ghoula, M.; Janel, N.; Camproux, A.C.; Moroy, G. Exploring the Structural Rearrangements of the Human Insulin-Degrading Enzyme through Molecular Dynamics Simulations. *Int J Mol Sci* **2022**, *23*, doi:10.3390/ijms23031746.

223. Leissring, M.A.; Selkoe, D.J. Structural biology: enzyme target to latch on to. *Nature* **2006**, *443*, 761-762, doi:10.1038/nature05210.

224. McCord, L.A.; Liang, W.G.; Dowdell, E.; Kalas, V.; Hoey, R.J.; Koide, A.; Koide, S.; Tang, W.J. Conformational states and recognition of amyloidogenic peptides of human insulin-degrading enzyme. *Proceedings of the National Academy of Sciences of the United States of America* **2013**, *110*, 13827-13832, doi:10.1073/pnas.1304575110.

VIII. Annexes

VIII.1. List of publications authored by the PhD candidate during his doctorate period.

I. Merino, B.; Fernández-Díaz, C.M.; Parrado-Fernández, C.; **González-Casimiro, C.M.**; Postigo-Casado, T.; Lobatón, C.D.; Leissring, M.A.; Cózar-Castellano, I.; Perdomo, G. Hepatic insulin-degrading enzyme regulates glucose and insulin homeostasis in diet-induced obese mice. *Metabolism* **2020**, *113*, 154352, doi:10.1016/j.metabol.2020.154352.

II. **González-Casimiro, C.M**.; Cámara-Torres, P.; Merino, B.; Diez-Hermano, S.; Postigo-Casado, T.; Leissring, M.A.; Cózar-Castellano, I.; Perdomo, G. Effects of Fasting and Feeding on Transcriptional and Posttranscriptional Regulation of Insulin-Degrading Enzyme in Mice. *Cells* **2021**, *10*, doi:10.3390/cells10092446.

III. **González-Casimiro, C.M**.; Merino, B.; Casanueva-Álvarez, E.; Postigo-Casado, T.; Cámara-Torres, P.; Fernández-Díaz, C.M.; Leissring, M.A.; Cózar-Castellano, I.; Perdomo, G. Modulation of Insulin Sensitivity by Insulin-Degrading Enzyme. *Biomedicines* **2021**, *9*, doi:10.3390/biomedicines9010086.

IV. Leissring, M.A.; **González-Casimiro, C.M.**; Merino, B.; Suire, C.N.; Perdomo, G. Targeting Insulin-Degrading Enzyme in Insulin Clearance. *Int J Mol Sci* **2021**, *22*, doi:10.3390/ijms22052235.

V. Merino, B.; Casanueva-Álvarez, E.; Quesada, I.; **González-Casimiro, C.M.**; Fernández-Díaz, C.M.; Postigo-Casado, T.; Leissring, M.A.; Kaestner, K.H.; Perdomo, G.; Cózar-Castellano, I. Insulin-degrading enzyme ablation in mouse pancreatic alpha cells triggers cell proliferation, hyperplasia and glucagon secretion dysregulation. *Diabetologia* **2022**, doi:10.1007/s00125-022-05729-y.

VI. Pablos, M.; Casanueva-Álvarez, E.; **González-Casimiro, C.M**.; Merino, B.; Perdomo, G.; Cózar-Castellano, I. Primary Cilia in Pancreatic β- and α-Cells: Time to Revisit the Role of Insulin-Degrading Enzyme. *Front Endocrinol (Lausanne)* **2022**, *13*, 922825, doi:10.3389/fendo.2022.922825.

VII. **González-Casimiro, C.M.**; Arribas-Rodriguez, E.; Fiz-López, A.; Casas, J.; Gutierrez, S.; Tellería, P.; Novoa, C.; Rojo-Rello, S.; Tamayo, E.; Orduña, A.; Dueñas, C.; Bernardo, D. and Perdomo G. Altered Surface Expression of Insulin-Degrading Enzyme on Monocytes and Lymphocytes from COVID-19 Patients Both at Diagnosis and after Hospital Discharge. *Int J Mol Sci* **2022**, *23*, doi:10.3390/ijms231911070.